Effective Date: April 22, 2011
Revision -

GSFC JPSS CMO
08/06/2011
Released

Joint Polar Satellite System (JPSS) Ground Project
Code 474
474-00049

Joint Polar Satellite System (JPSS) VIIRS Aerosol Optical Thickness (AOT) and Particle Size Parameter Algorithm Theoretical Basis Document (ATBD)

For Public Release

The information provided herein does not contain technical data as defined in the International Traffic in Arms Regulations (ITAR) 22 CFC 120.10. This document has been approved For Public Release.

National Aeronautics and Space Administration

Goddard Space Flight Center
Greenbelt, Maryland

This page intentionally left blank.

Joint Polar Satellite System (JPSS)
VIIRS Aerosol Optical Thickness (AOT)
and Particle Size Parameter
Algorithm Theoretical Basis Document (ATBD)

Prepared By:

Neal Baker
JPSS Data Products and Algorithms, Senior Engineering Advisor
(Electronic Approvals available online at https://jpssmis.gsfc.nasa.gov/mainmenu_dsp.cfm)

Approved By:

Heather Kilcoyne
DPA Manager
(Electronic Approvals available online at https://jpssmis.gsfc.nasa.gov/mainmenu_dsp.cfm)

Goddard Space Flight Center
Greenbelt, Maryland

This page intentionally left blank.

Preface

This document is under JPSS Ground Algorithm configuration control. Once this document is approved, JPSS approved changes are handled in accordance with Class I and Class II change control requirements as described in the JPSS Configuration Management Procedures, and changes to this document shall be made by complete revision.

Any questions should be addressed to:

JPSS Ground Project Configuration Management Office
NASA/GSFC
Code 474
Greenbelt, MD 20771

This page intentionally left blank.

Change History Log

Revision	Effective Date	Description of Changes (Reference the CCR & CCB/ERB Approve Date)
Original	04/22/2011	**474-CCR-11-0064:** This version baselines D43313, VIIRS Aerosol Optical Thickness (AOT) and Particle Size Parameter Algorithm Theoretical Basis Document (ATBD), Rev F dated 02/16/2010 as a JPSS document, version Rev –. This is the version that was approved for NPP launch. Per NPOESS CDFCB - External, Volume V – Metadata, doc number D34862-05, this has been approved for Public Release into CLASS. This CCR was approved by the JPSS Ground Algorithm ERB on April 22, 2011**.**

This page intentionally left blank.

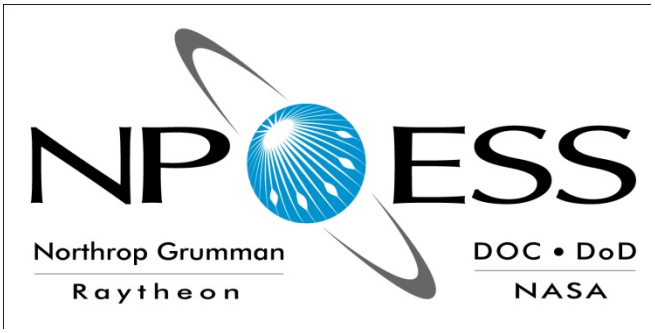

NATIONAL POLAR-ORBITING OPERATIONAL ENVIRONMENTAL SATELLITE SYSTEM (NPOESS)

VIIRS AEROSOL OPTICAL THICKNESS (AOT) AND PARTICLE SIZE PARAMETER ALGORITHM THEORETICAL BASIS DOCUMENT (ATBD) (D43313 Rev F)

CDRL No. A032

Northrop Grumman Space & Mission Systems Corporation
One Space Park
Redondo Beach, California 90278

This documentation/technical data was developed pursuant to Contract Number F04701-02-C-0502 with the US Government. The US Government's rights in and to this copyrighted data are as specified in DFAR 252.227-7013, which was made part of the above contract.

This document has been identified per the NPOESS Common Data Format Control Book – External Volume 5 Metadata, D34862-05, Appendix B as a document to be provided to the NOAA Comprehensive Large Array-data Stewardship System (CLASS) via the delivery of NPOESS Document Release Packages to CLASS.

The information provided herein does not contain technical data as defined in the International Traffic in Arms Regulations (ITAR) 22 CFR 120.10.

This document has been approved by the Unites States Government for public release in accordance with NOAA NPOESS Integrated Program Office.

Distribution: Statement A: Approved for public release; distribution is unlimited.

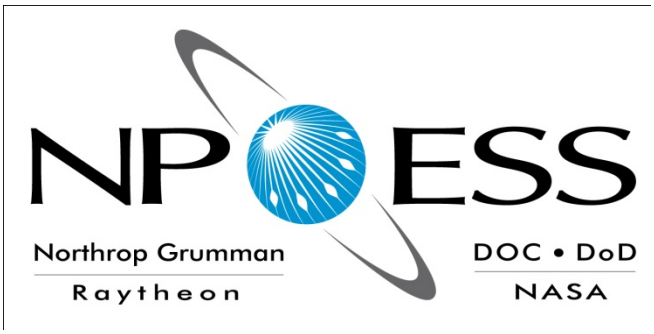

NATIONAL POLAR-ORBITING OPERATIONAL ENVIRONMENTAL SATELLITE SYSTEM (NPOESS)

VIIRS AEROSOL OPTICAL THICKNESS (AOT) AND PARTICLE SIZE PARAMETER ALGORITHM THEORETICAL BASIS DOCUMENT (ATBD) (D43313 Rev F)

ELECTRONIC APPROVAL SIGNATURES:

_____

Roy Tsugawa Date
Algorithm & Data Processing IPT Lead &
Algorithm Change Control Board Chairperson

_____

Ben James Date
Operations & Support IPT Lead

The following individuals are recognized for their contributions to the current or previous versions of this document.

Doug Hoyt
Sid Jackson
Heather Kilcoyne
Richard Slonaker
Scott Vibert
Eric Vermote
Xuepeng (Tom) Zhao

Revision/Change Record

Document Number D43313

Revision	Document Date	Revision/Change Description	Pages Affected
---	1/18/2007	Initial PCIM Release to bring document into Matrix Accountability. Reference original document number: Y2388 delivered in 2006	All
A	8/14/2007	Updated for changes to the science code baseline implemented by SPCR ALG00001205	All
B	9/17/2007	Updated for changes to the science code baseline implemented by SPCR ALG00001222	55-58
C	3/11/2008	Updated for changes to the science code baseline implemented by SPCR ALG00001279	21-22
D	11/18/2008	Updated for changes to the science code baseline implemented by SPCR ALG00001358	i-iii, x, 1, 3, 6, 9, 11, 13-17, 27, 29, 31-35, 40, 42, 47, 58, 59
E	12/10/2008	Updated for changes to the science code baseline implemented by SPCR ALG00001387	71-74
F	2/16/2010	In preparation for Public Release of this ATBD, the following administrative changes were made: all ITAR markings were removed, and Distribution Statement F added. ECR A-184A. Approved for Public Release per Contracts Letter 100610-02.	All

TABLE OF CONTENTS

LIST OF FIGURES

LIST OF TABLES

GLOSSARY OF ACRONYMS

6S	Second Simulation of the Satellite Signal in the Solar Spectrum
AeroNet	Aerosol Robotic Network
AGI	Advanced Global Imager
AOT	Aerosol Optical Thickness
ATBD	Algorithm Theoretical Basis Document
AVHRR	Advanced Very High Resolution Radiometer
CMIS	Conical Scanning Microwave Imager/Scanner
DAO	Data Assimilation Office
DEM	Digital Evaluation Model
EDR	Environmental Data Record
EVI	Enhanced Vegetation Index
FNMOC	Fleet Numerical Meteorology and Oceanography Center
FOV	Field of View
GACP	Global Aerosol Climatology Program
GSFC	Goddard Space Flight Center
IPO	Integrated Program Office
IPT	Integrated Product Team
IR	InfraRed
ITSS	Information Technology and Scientific Services (Raytheon)
LUT	Look-up Table
MAS	MODIS Airborne Simulator
MERIS	Medium Resolution Imaging Spectroradiometer
MODIS	Moderate Resolution Imaging Spectroradiometer
MODTRAN	Moderate Resolution Transmission Model
NCEP	National Center for Environmental Prediction
NOGAPS	Navy Operational Global Atmospheric Prediction System
NPOESS	National Polar-orbiting Operational Environmental Satellite System
OMPS	Ozone Mapping Profiling Suite
QA	Quality Assurance
RGB	Red Green Blue
RTM	Radiative Transfer Model

SBRS	Santa Barbara Remote Sensing
SeaWiFS	Sea-viewing, Wide Field-of-view Sensor
SNR	Signal-to-Noise Ratio
SRD	Sensor Requirements Document
SWIR	Short Wave InfraRed
TOA	Top of the Atmosphere
TOMS	Total Ozone Mapping Spectrometer

ABSTRACT

Atmospheric aerosol plays a role in the Earth's radiation budget through radiative forcing and chemical reactions. Quantifying this forcing requires accurate information on the global distribution of aerosol optical thickness, size distribution, and single scattering albedo. Aerosols play an important role in global warming by affecting the rate at which warming occurs, as the aerosols effectively cool the atmosphere by influencing the reflective and absorbing properties of clouds. Aerosol information is also vital to the atmospheric correction for the Sea Surface Temperature and Vegetation Index, climate modeling, and battlefield visibility modeling. Due to the high spatial and temporal variability of the aerosol particles, the satellite approach is the only feasible choice for global aerosol characterization.

This document describes the operational retrieval algorithm of the Visible/Infrared Imager/Radiometer Suite (VIIRS) aerosol optical thickness and particle size parameter products. The aerosol optical thickness product consists of the vertical column total extinction for a range of wavelengths from .4 to 2.25 microns. The particle size parameter product consists of the angstrom exponent computed from the optical thicknesses at two separate wavelengths. Retrieval of these products will be performed globally in daylight except over bright surfaces and under cloudy conditions. The aerosol optical thickness is calculated over both land and ocean using a look-up table (LUT) of pre-computed values for several atmospheric parameters in order to simplify the radiative transfer calculations. The aerosol LUT is computed for multiple aerosol types, optical thickness values, and sun-sensor viewing geometries. The LUT accounts for multiple scattering in the atmosphere by molecules and aerosol particles. A separate set of LUTs is used to compute the coupling of the surface BRDF with the atmosphere. Because the reflective properties of ocean and land are very different, separate retrieval approaches are used over the land and the ocean. Over the ocean, the surface BRDF is computed based on wind speed and the BRDF-atmosphere coupling is included in the radiative transfer calculations. Over the land, a dark pixel method introduced by Kaufman *et al*. (1997) for the Moderate Resolution Imaging Spectroradiometer (MODIS) is adopted to identify areas where dense vegetation allows retrieval. The VIIRS sensor design includes a band at 2.25μm to detect the dark pixels required for retrieval of optical thickness over land. The aerosol retrieval over land uses a Lambertian surface reflectance assumption in the radiative transfer calculations. Modifications to use the BRDF-atmosphere coupling are discussed in this document but have not yet been implemented in the code. The aerosol particle size parameter is computed from the aerosol optical thickness values at two different wavelengths.

1.0 INTRODUCTION

It is well known that atmospheric aerosols play an important role in the Earth's radiative budget (Charlson *et al*., 1992) and affects the global climate through radiative forcing and chemical reactions. Aerosols are also related to the cloud albedo effect through microphysical interactions with cloud particles. Aerosol information is critical for atmospheric correction algorithms and military operations. The climate effects of atmospheric aerosols may be comparable to CO_2 greenhouse effects, but with opposite sign and larger uncertainty (Hansen and Lacis, 1990; IPCC, 1994). To quantify the aerosol radiative forcing, which will be used by the atmosphere correction for the land products, and narrow down its uncertainty, information about global distributions of aerosol optical thickness (AOT) and size distribution is necessary. Due to the high spatial and temporal variability of the aerosol particles, only space based measurements can provide global coverage.

1.1 Purpose

This Algorithm Theoretical Basis Document (ATBD) describes the algorithms used to retrieve the Aerosol Optical Thickness and Particle Size Parameter Environmental Data Records (EDRs) for the Visible/Infrared Imager/Radiometer Suite (VIIRS) instrument on the National Polar-orbiting Operational Environmental Satellite System (NPOESS). These products are summarized in Table 1. Specifically, this document identifies the sources of input data, both VIIRS and non-VIIRS, required for retrieval; provides the physical theory and mathematical background underlying the use of this information in the retrievals; includes implementation details; and describes assumptions and limitations of the proposed approach.

TABLE 1. SUMMARY OF AEROSOL OPTICAL THICKNESS AND PARTICLE SIZE PARAMETER PRODUCT

Parameter Name	Units	Horizontal Cell Size	Comments
Aerosol Optical Depth	Dimensionless	6 km (Nadir)	Retrieved globally during daylight except areas of clouds and bright surfaces Reported at several wavelengths between 0.4 and 4.0 μm
Aerosol Particle Size Parameter	Ångström Wavelength Exponent:	6 km (Nadir)	Threshold: Ångström Wavelength Exponent, uses optical depth at pairs of wavelengths

Parameter Name	Units	Horizontal Cell Size	Comments
	Dimensionless Effective Radius: μm		Objective: Effective radius determination

1.2 SCOPE

This document covers the algorithm theoretical basis for the retrieval of the aerosol optical thickness and size distribution products of VIIRS on NPOESS. The VIIRS aerosol solution was developed using the MODIS and AVHRR aerosol algorithm heritages.

Section 1 describes the purpose and scope of this document. Section 2 is an overview of the aerosol retrievals. The theoretical description and implementation of the algorithm are described in Section 3. Assumptions and limitations of the approach are summarized in Section 4. References for citations in the text are listed in Section 5.

1.3 VIIRS DOCUMENTS

Reference to VIIRS project or reference documents is indicated by a number in italicized brackets (e.g., *[Y-1]).*

[Y-1] Visible/Infrared Imager/Radiometer Suite (VIIRS) Sensor Requirements Document (SRD) for National Polar-orbiting Operational Environmental Satellite System (NPOESS) Spacecraft and Sensors

[Y-2] NEDL/NEDT Sensor Requirements Flowdown Memo, Aerosol Optical Thickness and Size Parameter, document number RAD.NEDL.AOT.

[Y-3] VIIRS System Specification Document. SS154640.

[Y-2390] VIIRS Suspended Matter Algorithm Theoretical Basis Document. Vermote, E., R. Slonaker, S. Vibert, H. Kilcoyne, D. Hoyt and T. Zhao, Version 5, Rev.2, May 2002.

[Y-2412] VIIRS Cloud Mask Algorithm Theoretical Basis Document. Reed, B., Version 5, Rev.2, December 2002.

[Y-3249] VIIRS Error Budget, Version 3, April 2000.

[AL60822-VIR-005] VIIRS Aerosol Algorithm BRDF and Adjacency Report. Slonaker, R. and E. Vermote, Version 1, November 2003.

2.0 EXPERIMENT OVERVIEW

2.1 Objectives of VIIRS Aerosol Optical Thickness and Size Parameter Retrievals

The objective of this algorithm is to calculate the aerosol optical thickness, proportional to the total aerosol loading of the ambient aerosol, over both land and ocean globally on a daily basis. Because the reflective properties of the Earth's surface under an aerosol layer vary significantly from land type to land type, different methods are used over the land and the ocean. As clouds block the surface reflectance, the aerosol optical thickness cannot be found for cloudy pixels. Retrievals are only performed during the daytime due to the lack of light in the visible channels during the nighttime.

The overall objectives of the VIIRS aerosol retrievals are:

1. To determine the aerosol optical thickness, which is an indicator of the amount of direct aerosol radiative forcing on the climate, an input to radiative transfer models used to calculate this forcing, a critical military operations planning tool, and a required input to atmospheric correction algorithms. The aerosol optical thickness is defined in the VIIRS SRD [Y-1] as the "extinction (scattering + absorption) vertical optical thickness of aerosols at multiple wavelengths within the 0.4 – 2.4 μm spectral range based on narrow band (bandwidth < 0.05 μm) measurements. Optical thickness (τ) is related to transmission (t) by t=exp(-τ)."

2. To determine the aerosol model, which is an indicator of the particle size distribution and the chemical composition of the predominant aerosol type present.

3. To determine the aerosol particle size parameter, which is an indicator of the importance of the aerosol effect on radiation. The larger the aerosol, the more important the effect on radiation. Radiatively important sizes range from 0.1 to 10.0 microns. Larger sizes are difficult to determine with current space-based remote sensing measurements. More detailed size distribution information enables a more complete determination of the radiative properties of the aerosols. Aerosols have an indirect radiative forcing through their modification of cloud properties. These effects can be monitored through their changes in size distribution in the vicinity of cloud fields. The threshold size parameter is the Ångström wavelength exponent *alpha* (α):

$$\alpha = -\frac{\ln \tau_1 - \ln \tau_2}{\ln \lambda_1 - \ln \lambda_2} \qquad (1)$$

Where τ_1 and τ_2 are optical thickness retrieved a two separate wavelengths λ_1 and λ_2. To determine the Ångström wavelength exponent, optical thickness in two different narrow wavelength bands separated by at least 200 nm is required. If aerosol particle size distribution is given by an inverse power law, such as a Junge distribution, then alpha (α) can be related to the exponent in the power law.

The objective size parameter requirement is their effective radius, which is defined as the area weighted average radius of the aerosol particle size distribution. The effective radius provides another approximate measure of the size of the aerosol.

Optical thickness and size parameter retrievals apply only under clear and daytime conditions.

2.2 Band Characteristics

The narrow band measurements of the VIIRS sensor in the 0.4 to 4.0 μm range are used to derive aerosol optical thickness. The visible and near infrared channels used to derive optical thickness are all within window regions and their bandwidths are narrow. As a result, the contamination of gas (such as O_2, O_3, H_20) absorption is minimized in direct measurements. For the retrieval over land, mid-IR channels (2.25 and 3.7 μm) are correlated to blue and red channels (0.488 and 0.672 μm) for identification of dark pixels for the retrieval. Table 2 summarizes the VIIRS Moderate Resolution Bands.

TABLE 2. VIIRS MODERATE RESOLUTION BAND CHARACTERISTICS

Band Name	Wavelength (□m)	Bandwidth (□m)
M1	0.412	0.0200
M2	0.445	0.0180
M3	0.488	0.0200
M4	0.555	0.0200
M5	0.672	0.0200
M6	0.746	0.0150
M7	0.865	0.0390
M8	1.240	0.0200
M9	1.378	0.0150
M10	1.610	0.0600
M11	2.250	0.0500
M12	3.700	0.1800
M13	4.050	0.1550
M14	8.550	0.3000
M15	10.7625	1.0000
M16	12.0125	0.9500

2.3 AEROSOL RETRIEVAL STRATEGIES

It has been demonstrated that aerosol optical thickness can be retrieved from solar-reflected radiance, and that aerosol size distribution information is carried in the spectral dependence of aerosol optical thickness (e.g., King *et al*., 1978; Tanré *et al*., 1992). Thus, satellite reflectance measurement limited to one (GOES) or two channels (Advanced Very High Resolution Radiometer [AVHRR]) were used first to derive the total aerosol content by assuming a given aerosol model. Iterative methods were introduced by Kaufman (1990) and Ferrare (1990) to retrieve more aerosol parameters simultaneously, such as size, single-scattering albedo, and optical thickness. As pointed out by Tanré *et al*. (1996), the success of these methods was limited by their poor accuracy related to limited spectral resolution, inaccurate calibration, and gas absorption contamination. Currently, multiple-channel measurements (e.g., the Moderate Resolution Imaging Spectroradiometer [MODIS]) are adopted to retrieve aerosol parameters. Retrieval accuracy may be improved significantly by selecting channels carefully (to reduce gas or surface contamination) and by introducing correction schemes based on multiple-channel information.

An approach similar to MODIS, but with a higher spatial resolution product, is proposed for VIIRS on NPOESS. Solar-reflected spectral reflectances measured by a satellite in well-selected multiple channels of visible and near-IR will be used to derive the aerosol optical thickness and size distribution simultaneously over land and ocean. The core of the approach is to use Look-Up Tables (LUTs), which are pre-computed for multiple values of the AOT and multiple aerosol models by using sophisticated radiation transfer models (such as Second Simulation of the Satellite Signal in the Solar Spectrum [6S]). The measured spectral reflectances in several channels are compared with the reflectances computed using the values of atmospheric parameters stored in the LUTs and surface parameters computed within the AOT code to identify the best solution for both AOT and aerosol model.

2.3.1 Aerosol Optical Thickness Retrievals Over Water

The relatively homogeneous surface of the ocean enables the direct application of the LUT approach to find the aerosol optical thickness and size distribution. The observed reflectances at the top of the atmosphere (TOA) are inverted using the LUTs and the surface BRDF computed as a function of wind speed to find a preliminary value of optical thickness for each candidate aerosol model. Ancillary information on the total column water vapor and ozone are input and used to correct for species absorption in the inversion. The model exhibiting minimum residual is the best fit to the observations, and its corresponding AOT is the retrieved value. The aerosol models used over ocean are dynamic. There are separate models for an aerosol fine mode and an aerosol coarse mode. A single fine mode and a single coarse mode may be combined with any relative weight between them to form the dynamic aerosol model. This method is based on MODIS heritage and is a direct adaptation of the algorithm developed by Kaufman and Tanré (1998).

2.3.2 Aerosol Optical Thickness Retrievals Over Land

Over land retrievals are more challenging due to brighter surface conditions (i.e., noisier inversion conditions). Surface reflectance, aerosol optical thickness and aerosol model are solved for simultaneously based on the expected spectral albedo shape of vegetated surfaces derived from atmospheric correction using AERONET data and a limited set of 5 static aerosol models. A priori assumptions of spectral albedo shape and limitations in model freedom are necessary given the number of free parameters and inherently noisier retrieval.

2.3.3 Aerosol Size Parameter Retrievals

The Ångström wavelength exponent can be easily calculated from the optical thicknesses in two channels. The SRD definition of the Ångström requires that these bands be separated by at least 200 nm. The band pairs used for the Ångström exponent retrieval will be determined as the algorithm is validated with MODIS data and with help from the AOT. The retrieved Ångström exponent can be related to an effective radius through a relationship derived from observations at 11 AeroNet sites, and will be determined globally. In case the aerosol model has been successfully inverted the effective radius can also be determined directly for a particular model as a function of optical thickness (see Dubovik *et al.*, 2001).

3.0 ALGORITHM DESCRIPTION

3.1 Algorithm Input

The algorithm requires ancillary information from the VIIRS instrument and from outside sources as explained below.

3.1.1 VIIRS Data

The VIIRS data required by the optical thickness and size parameter algorithm are higher-level VIIRS products and are summarized in Table 3 below.

TABLE 3. ANCILLARY DATA FROM VIIRS PRODUCTS

Input Data	Source of Data
Cloud Information	VIIRS Cloud Mask IP
Land/Water Information	VIIRS Cloud Mask IP
Sunglint Information	Internal, VIIRS Cloud Mask IP
Snow/Ice Information	Internal, VIIRS Cloud Mask IP
Volcanic ash information	VIIRS Cloud Mask IP
Turbid water information	Internal
Bright pixel information	Internal
Fire information	Internal, VIIRS Cloud Mask IP
Calibrated Brightness Temperatures	VIIRS Calibrated TOA Brightness Temperature SDR
Calibrated Reflectances	VIIRS Calibrated TOA Reflectance SDR

3.1.1.1 Cloud Information

The optical thickness and size parameter EDRs are only required for clear or cloud-free conditions; thus, a cloud mask to remove pixels contaminated by cloud cover is needed. A cloud over land will not allow the detection of the dark pixels required for aerosol retrieval, and will cause the optical thickness to be overestimated over the ocean. A quality flag will be included with the Aerosol products to specify areas where clouds may contaminate the retrieval.

Some pixels will be classified as “probably clear” which indicate that there is a possibility of contamination by small clouds. Use of these pixels in the aerosol retrieval will trigger the possible contamination by cloud quality mask. It is anticipated that the fraction of pixels in that category will be high early on in the application of the cloud mask and will decrease as the cloud mask product matures. Those retrievals should definitely be used with caution if at all.

The presence of clouds in adjacent pixels will cause a quality flag to be set. The presence of nearby clouds can generate several artifacts in the retrieval of aerosol: (a) mixed pixels probably exist at the border of the cloud and are not detected, (b) shadows may contaminate the cell and not be properly flagged (c) cloud could generate scattering either by the atmospheric scattering (molecular) or by the instrument.

An additional thin cirrus check using band M9 is performed internally. This allows a more conservative test to be applied for screening thin cirrus than is appropriate for the VCM.

3.1.1.2 Land/Water Information

The algorithm for determining optical thickness uses two different procedures depending on whether the pixel is over land or water. Information on the location of the pixel is required. This information will be included in the packet of information received from the cloud mask.

3.1.1.3 Sunglint Information

Sun glint information is provided by the VIIRS Cloud Mask. The sunglint contribution will also be computed dynamically inside the aerosol retrieval code using the approach described in 6S which can account for wind speed and wind direction, the wind speed and direction will be either read from NCEP data or from a climatology of wind speed and direction. The threshold for sunglint contribution will be fixed to be no greater than 3% of the value of the reflectance corrected for gaseous absorption and molecular scattering observed at 1.24□m, limiting the relative error on the optical thickness to an acceptable level. The theoretical value of the sunglint will be taken into account in the retrieval process up to 3%, above that value no retrieval will be performed. In the case where the VIIRS Cloud Mask identifies a broader sun glint exclusion region than the internal test, this broader exclusion region shall not be processed. This approach could be refined later on by extending the area of retrieval inside the sunglint provided the wind speed and direction could be estimated accurately either by the use of ancillary data or by the satellite data itself in the middle infrared (1.6□m, 2.25□m, 3.75□m) where the aerosol contribution is low except for dust cases.

Sunglint is also detected over land, this is especially important since water bodies not in the land/water mask can be misinterpreted in either fires, clouds or clear lands pixels categories. The sunglint reflectance is computed dynamically over all surfaces (land and ocean), over land when the reflectance of sunglint is over 0.05, the pixels which appears contaminated by sunglint, showing a middle infrared anomaly (MIRA) value above 0.1 but not cold enough to be cloud and not hot enough to be fire are flagged accordingly. The MIRA value is computed as follows:

$$MIRA = \rho_{3.75} - 0.82\rho_{M11} + 0.32\rho_{M10} \quad (2)$$

Where $\rho_{3.75}$ is the estimated reflectance at 3.75 microns and ρ_{M11} and ρ_{M10} are the observed TOA reflectances in bands M11 and M10 respectively. Figure 1 illustrates the effect of sunglint in the middle infrared RGB composite; Figure 2 shows the masking of the sunglint according to the criteria described above.

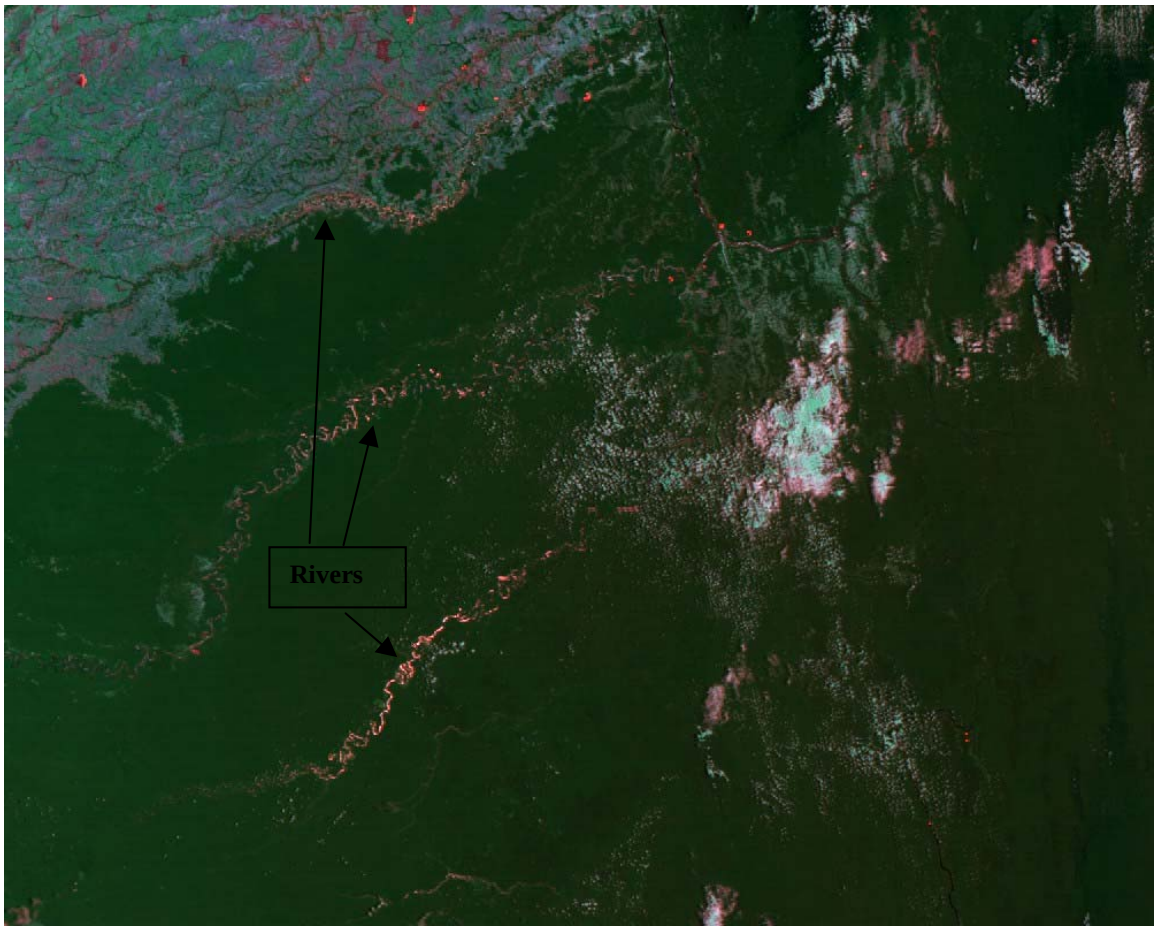

FIGURE 1. DETAILS OF THE SOUTH AMERICA SCENE (THE RIVERS APPEAR REDDISH BECAUSE THEY ARE AFFECTED BY SUNGLINT).

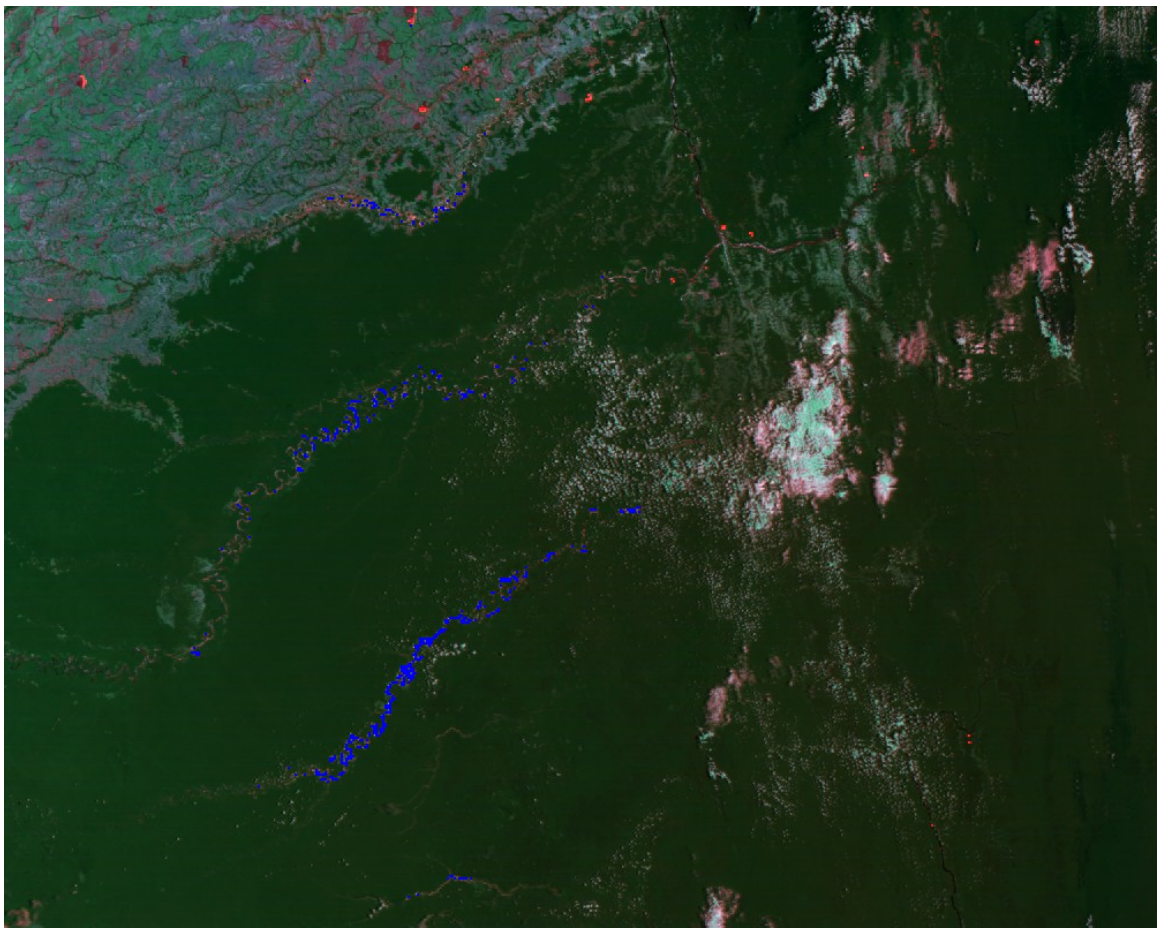

FIGURE 2. SAME AS FIGURE 5, BUT THE SUNGLINT MASK HAS BEEN APPLIED IN BLUE.

3.1.1.4 Snow/Ice Information

Optical thickness in areas of snow and ice cover cannot be accurately retrieved using current algorithms. It is, however, conceivable that further research will lead to a method for its retrieval, in which case the algorithm would be implemented. A very minimal amount of snow can introduce substantial error in the retrieval therefore a very conservative method has to be developed to make sure no snow or mixed snow pixels are used by the algorithm. A specific algorithm based on the MODIS data has been designed to detect snow-contaminated pixels. We have developed some criteria in an effort to discriminate between snow and cloud. When snow is detected, the aerosol algorithm performs an aggressive filtering of the optical thickness values (based on spectral dependence) around the snow covered area to eliminate contamination by sub-pixel snow as much as possible it is therefore important to limit that process as much as possible to optimize processing time and reduce “false” rejection. The internal cloud mask described previously should not

misclassify snow as cloud because it uses quantities that are not sensitive to snow (MIRA and VIIRS band M9) in most conditions. For pixels which have not been classified as cloud, fire or sunglint but still have a high visible reflectance anomaly (blue-red/2), the test using the ratio between band M8 (1.24□m) and M7 (0.87□m) is used classify the pixels as snow or not ($\rho_{M8}/\rho_{M7} < 0.9$). In addition, a condition on the surface temperature (should be <280K) is also required.

Figure 3 shows a true RGB of the scene of interest to demonstrate our snow filtering. The scene is partially covered by snow and cloud. In the visible, it is difficult to clearly discriminate between the two in most cases. Figure 4 shows a false RGB that allows discrimination. In that RGB, the snow appears now as very dark blue, since the reflectance of snow is small at 1.6□m and 4.0□m (or even 2.13□m) but very high in the visible (0.47□m). Low altitude clouds of water droplets are more or less white. Sometimes the higher altitude clouds that contain ice particles are blue but of lighter tint than snow. Qualitatively, this composite gives us a good identification of where snow exists and where clouds may contaminate the scene. Figure 5 shows the internal snow mask. It appears to correctly detect most of the snow without problems. There are a few cases where the cirrus band causes snow to be classified as cloud (on mountains tops). For the intended purposes, the internal snow test is satisfactory.

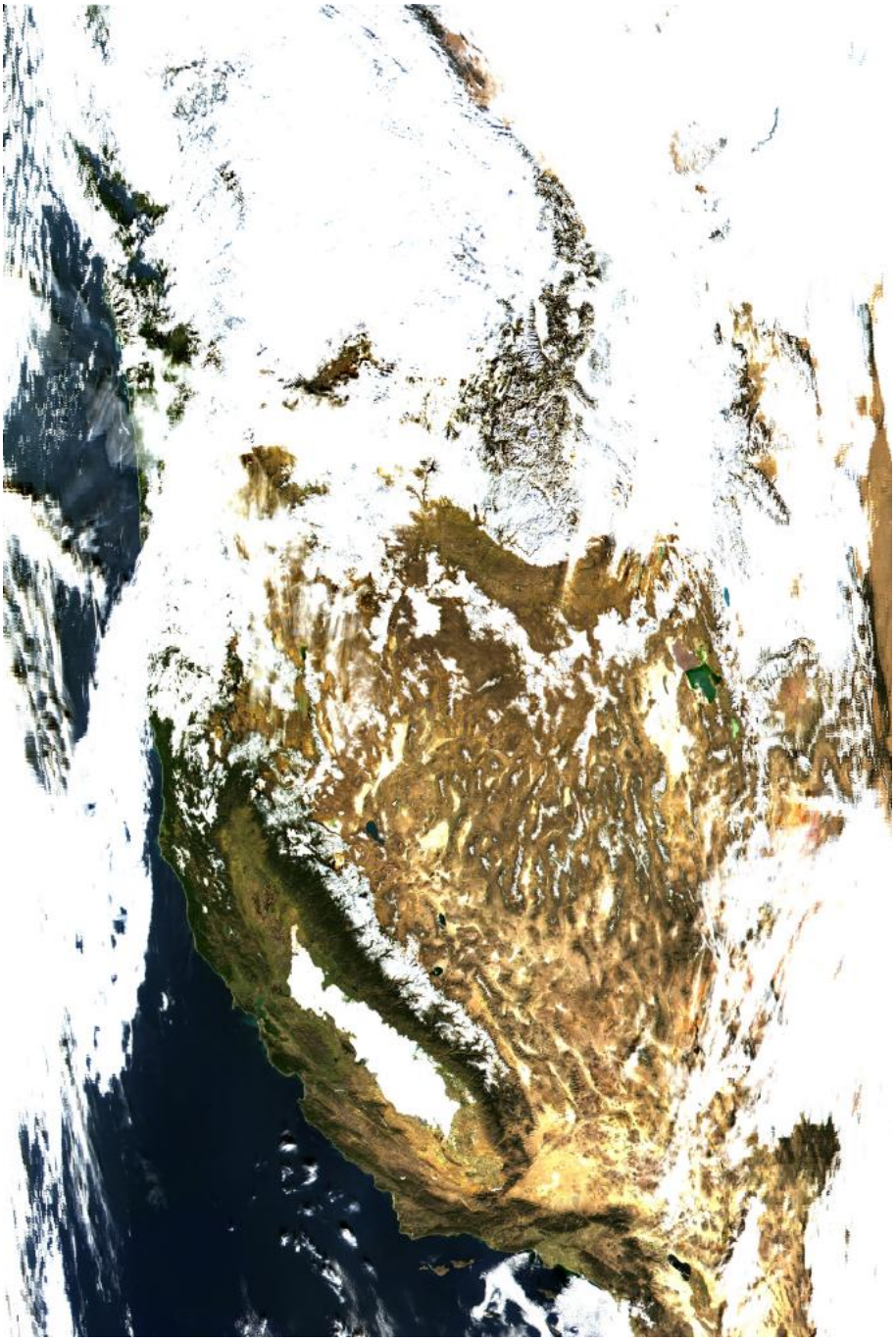

FIGURE 3. TRUE RGB IMAGE OF A MOD09 (MODIS SURFACE REFLECTANCE) GRANULE OVER THE US WEST COAST ON DAY 337 (2000).

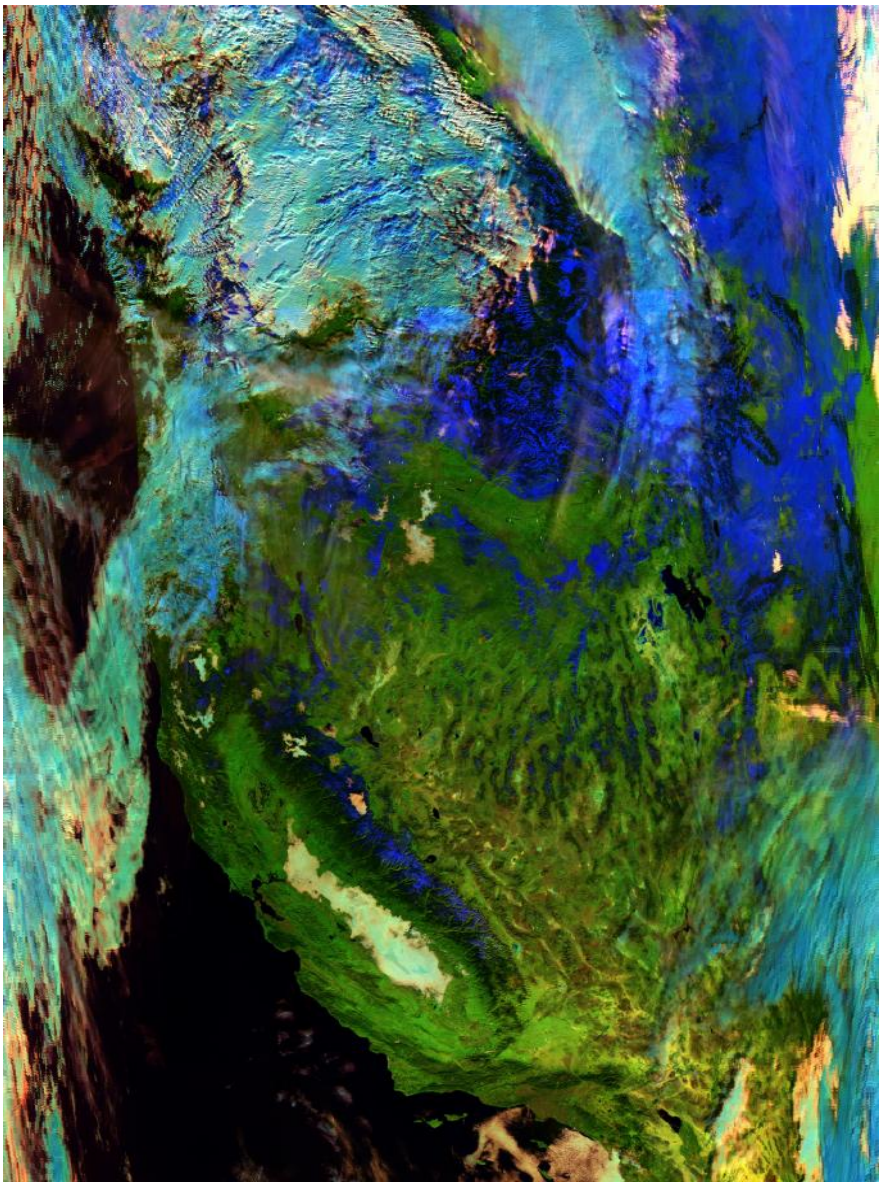

FIGURE 4. FALSE RGB (RED=4.0□M, GREEN=1.6□M, BLUE=0.47□M) CORRESPONDING TO FIGURE 3.

FIGURE 5. RESULTS OF THE INTERNAL SNOW TEST (SNOW IS IN RED), CORRESPONDING TO FIGURES 3 AND 4.

3.1.1.5 Fire Information

An internal fire mask has also been implemented in the Aerosol Optical Thickness algorithm based on the direct application of surface reflectance in the middle-infrared. The fire mask has its own use for aerosol. Big fires can perturb the signal at 2.13□m, which is used to estimate the reflectance in the visible. It is therefore cautious to reject pixels that

may be affected from fire for the aerosol inversion process. Figure 6 gives for the same scene again an illustration of the mechanism used to detect fire in the middle infrared. Figure 7 is an RGB image of a detail of the previous scene; reflectance at 4.0□m (calculated internally) is in the red, 2.1□m in the blue and 1.6□m in the green. Clouds detected previously are the blue features. Fires appear as red spots because the thermal anomaly produced by fires raised significantly the reflectance in the middle infrared (4.0□m) before it affects the shorter wavelengths (2.1□m and 1.6□m). The filtering technique used is the MIRA index. We classified as fires the pixels where MIRA is greater than 0.1, which were not detected as clouds and whose temperatures are greater than the air temperature. The difference between surface temperature and air temperature for fires detection is dependent on the geometry because specular reflectance can also cause elevated values of MIRA. The threshold in temperature difference is dependent on the actual reflectance of the sunglint computed using geometry and NCEP surface winds. In the area where sunglint is significant (reflectance of glint > 0.05 at 2.1□m), fires are required to be at least 7.5K warmer than the air temperature. In other areas, only a –5K difference is required.

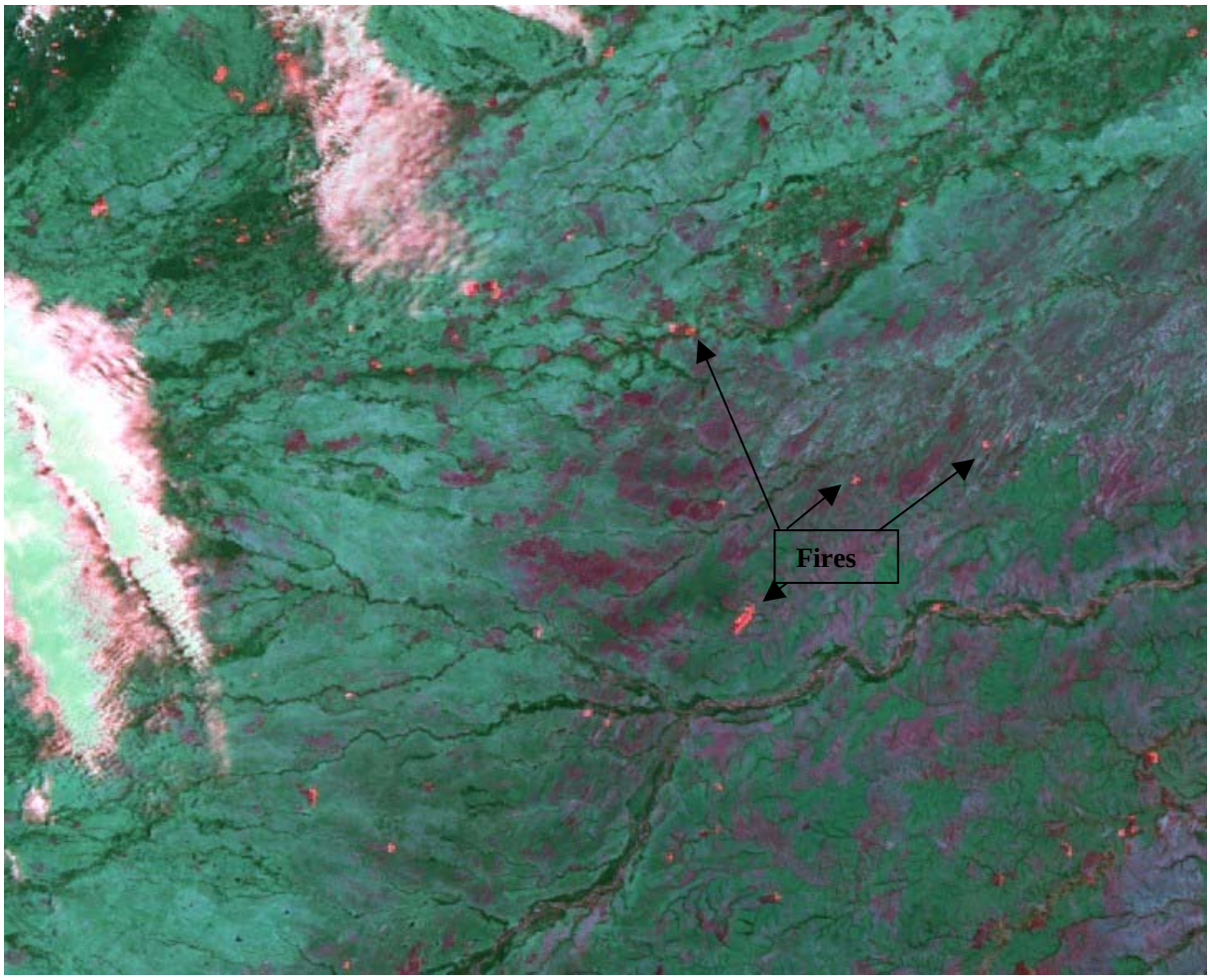

FIGURE 6. MIDDLE INFRARED RGB COMPOSITE SHOWING THE REFLECTANCE OBSERVED AT 4.0□M (RED), 1.6□M (GREEN) AND 2.1□M (BLUE) OF A SOUTH AMERICA SCENE. FIRES APPEAR AS SMALL RED CLUSTERS.

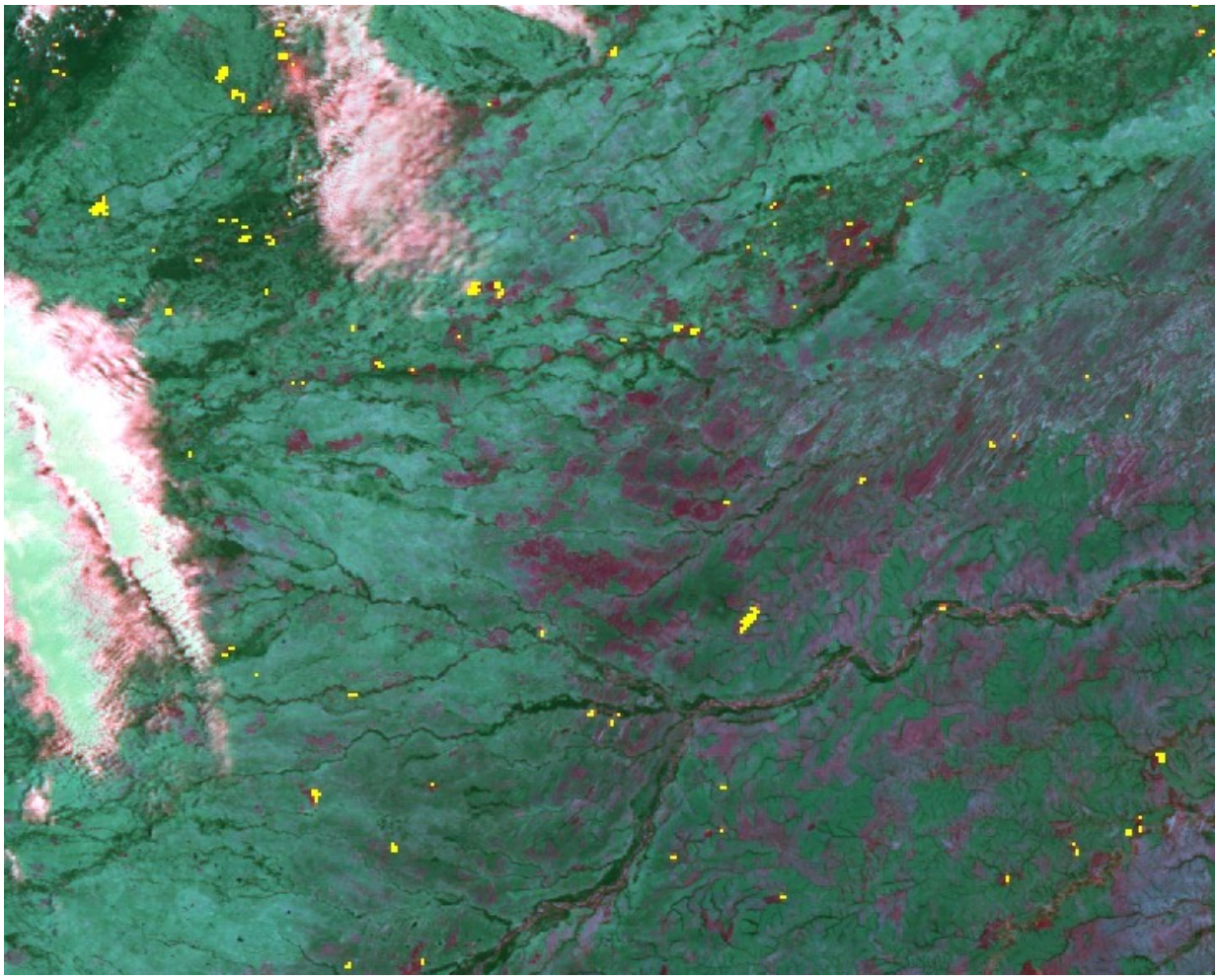

FIGURE 7. SAME AS FIGURE 6 WITH PIXELS DETECTED BY INTERNAL FIRE TEST INDICATED IN YELLOW.

3.1.1.6 Turbid / Shallow Water Information

The MODIS heritage turbid / shallow water test described in Li *et. al.* (2003) is used to identify turbid and/or shallow water. The sediment masking algorithm follows: the observed reflectances at 0.488, 1.24, 1.61, and 2.25 □m are used to derive the power law fit using least squares minimization. Expected reflectances at 0.555, 0.672, and 0.865 □m based on the power law fit are computed. Since a Rayleigh plus aerosol scattering atmosphere is expected to have a path reflectance which is a power law in wavelength, the differences between the observed reflectances and the calculated reflectances in these bands approximately correspond to the water leaving reflectance introduced by sediments. For the clear water areas, the differences are close to zero; while for the turbid water areas, the differences are all greater than 0.01. Significant bottom reflection will also cause a deviation from the expected power law fit.

3.1.1.7 Calibrated TOA Reflectances and Brightness Temperatures

The VIIRS-observed geolocated reflectances and brightness temperatures for some channels are required. These reflectances will be corrected for ozone and water vapor absorption. The solar/viewing angles required for inversion of the corrected reflectances into the aerosol optical thickness LUT will be obtained from these inputs.

3.1.2 Non-VIIRS Data

Ancillary data from other NPOESS instruments and non-NPOESS sources is listed below in Table 4.

TABLE 4. ANCILLARY DATA FROM OTHER SOURCES

Input Data	Source of Data	Units
Ozone Concentration	NCEP	Atm-cm
Total Precipitable Water	NCEP	cm
Surface Air Temperature	NCEP	K
Wind Speed	NCEP	m/s
Wind Direction	NCEP	Degrees from North
Surface Pressure	NCEP	mb
Surface Elevation	NCEP	km
1 km Digital Elevation	VIIRS Calibrated TOA Reflectance SDR	m
AOT Climatology	Internal	□

3.1.2.1 Ozone Concentration

The total column amount of ozone is required by the aerosol EDRs to correct the input VIIRS reflectances for absorption by ozone. This data is obtained from the NCEP model data. The threshold horizontal resolution of the ozone EDR is 50 km. This is much larger than the input reflectance resolution of 1 km and the retrieval resolution of 10 km for VIIRS. However, ozone is slowly varying over distance and this discrepancy in resolutions should not be a problem. A backup for the NCEP model data will be the FNMOC (NOGAPS) model data, and then climatology. An accuracy of 15 *milli-atm-cm* will provide adequate ozone input for the correction.

3.1.2.2 Total Precipitable Water

The total precipitable water amount is required by the aerosol EDRs to correct the input VIIRS reflectances for water vapor absorption. This data will be obtained from the NCEP model data. As the VIIRS bands were chosen to avoid areas of significant water absorption, the error in the input data should be negligible. FNMOC (NOGAPS) model data will be used as a backup data source.

3.1.2.3 Surface Air Temperature

The surface air temperature is used in the internal tests for clouds, sunglint and fire. The surface air temperature will be obtained from the NCEP model data. As a backup data source, FNMOC (NOGAPS) model data will be used.

3.1.2.4 Wind Speed and Direction

The sea surface wind speed and direction is required for the sunglint and whitecap corrections of the water-leaving radiance used in the calculation of the aerosol optical thickness over the ocean. This information will be supplied by NCEP model data. The wind velocity is used to calculate the Fresnel reflection on the sea surface using the Cox and Munk (1954) rough ocean model. This gives the probability distribution of surface slopes as a function of wind speed and direction. The percentage of the sea covered by sea foam depends on wind speed following Koepke's model (1984). This foam affects the reflectance of the ocean, and this effect is assumed to be independent of wavelength. The resulting effect on optical thickness, size distribution, and effective radius is not large; therefore, the inclusion of the whitecap correction is not vital. The use of the wind velocity in the sunglint correction is also not vital, as the pixels affected by sunglint can alternately be removed by not considering pixels within $\pm 30^\circ$ of the solar zenith and azimuth angles. FNMOC (NOGAPS) model data will be used as a backup data sources. A constant wind velocity can be assumed as another alternative.

3.1.2.5 Surface Pressure and Surface Elevation

The surface pressure is used to calculate the Rayleigh, or molecular, scattering correction of the input VIIRS reflectances. The NCEP surface elevation is used in conjunction with the 1 km resolution digital elevation from the VIIRS SDR to compute the 1 km surface pressure. The surface pressure and elevation will be obtained from the NCEP model data. As a backup data source, FNMOC (NOGAPS) model data will be used.

3.1.2.6 1 km Digital Elevation

A digital elevation model is required to calculate the exact surface pressure for a particular location. The pixel resolution (~1 km) elevation is included in the moderate resolution SDR file.

3.1.2.7 Aerosol Climatology

For atmospheric correction over land, aerosol climatology is needed for those cases where no VIIRS aerosol optical thickness measurements exist. Initially, the preliminary aerosol climatology of the Global Aerosol Climatology Program (GACP) will be used (Geogdzhayev and Mishchenko, 1999). This climatology has a 1 by 1 degree spatial resolution and gives monthly means. It is based on NOAA-9 observations and gives the aerosol optical depth and size distribution over oceans. The GACP climatology is not fully satisfactory for our purposes since it does not provide values over land. It is anticipated that improved GACP aerosol climatologies will become available using MODIS, MISR, SeaWiFS, and other sensors. These will be available before the first launch of VIIRS. Eventually, we expect VIIRS itself to generate an aerosol climatology that will be used for VIIRS.

3.2 THEORETICAL DESCRIPTION OF AEROSOL OPTICAL THICKNESS AND SIZE PARAMETER RETRIEVALS

Over both land and ocean, the TOA radiance received by the satellite is a combination of contributions from two sources: the atmospheric path radiance and the contribution from the surface (including coupling between the surface and atmosphere). Over land, the surface reflectance differs significantly depending on surface type. Over the ocean, the surface is relatively homogeneous and the surface reflectance relatively constant. A look-up table accounting for multiple scattering in the atmosphere by molecules and aerosol particles is used along with the known reflectance of the ocean surface to calculate the aerosol optical depth. The water-leaving radiance is dependent upon the chlorophyll content, or ocean color, and the turbidity. In rough seas, sea foam and whitecaps can reflect additional sunlight; therefore, the whitecap coverage is calculated as a function of wind speed. Sunglint is an additional contributor to the TOA radiance and is calculated using the Cox and Munk (1954) model. In areas of significant sunglint, the optical thickness is not calculated since the sunglint depends on wind speed and direction which are not precisely known.

Over the land, the surface albedo varies with wavelength. Areas of dark, dense vegetation have a very low reflectance in the red and blue bands. Aerosols will make these regions appear brighter as they scatter the light as it travels back to the sensor from the surface. In the middle IR, the wavelength of the radiation is too long to be affected by this scattering and thus provides a more accurate representation of the surface. Previous work by Kaufman *et al*. (1997) for MODIS has established a relationship between the reflectances

in the middle IR and in the red and blue regions. This statistical relationship is used to calculate surface reflectance in the visible range from the measured reflectance in the middle IR. A process of elimination finds regions dark enough for this relationship to hold. A pixel must meet a series of criteria in order to be considered dark, thus preventing bright pixel (e.g., snow and sand) selection.

The aerosol module uses data from VIIRS and from outside sources. The Read Input Module reads in the ancillary/auxiliary data that have been pre-processed by the Gridding module and readies it for use by the aerosol module. The data not directly used by the module for optical depth, size parameter or suspended matter calculation are used for quality checks of the products, such as identification of cloud or sunglint contamination. The aerosol retrievals are only required for non-cloudy daytime conditions. Therefore, any data contaminated by cloud cover not within the daytime definition will be flagged.

The definition of “daytime” for the aerosol EDRs has been established to be solar zenith angles less than 70°, and “cloudy” has been defined as any cloud cover within a pixel. “Extended daytime” (solar zenith angles between 70° and 80°) pixels are processed identical to “daytime” but are flagged to indicate their illumination state and suspect quality. “Twilight” (solar zenith angles between 80° and 85°) pixels are either assigned climatology or use interpolation from surrounding regions. During “night” (solar zenith angles greater than 85°), no processing occurs.

The VIIRS Cloud Mask SDR will provide information on cloud cover, land type, snow/ice contamination and sunglint contamination. The algorithm will use this information to determine which optical thickness retrieval method to employ since land and oceans each have different methods of retrieval. The cloud mask information for each pixel is read. The algorithm will use the cloud confidence, cloud mask quality, land/water, adjacent pixel cloud confidence and cirrus detected bits. For further details on the cloud mask format please refer to the Cloud Mask Version 5 ATBD *[Y2412]*.

If all other geophysical and viewing factors are the same, reflectance increases as AOT increases. The aerosol LUT contains pre-computed values of the atmospheric components of TOA reflectance vs. AOT and aerosol model spanning the envelope of viewing and illumination geometries. The algorithm simply brackets the observed TOA reflectance with the TOA reflectance calculated from the viewing geometry interpolated LUT parameters (i.e., searches for the closest values, both larger and smaller than observed, within the LUT) and interpolates on the corresponding AOT values. AOT retrievals are performed for each aerosol model (i.e., 5 for land and 2020 for ocean). The optimal model is the one for which the residual is minimized. The residual is defined as the sum of the squares of the differences between observed and calculated reflectances for all VIIRS bands used in the model determination. Over-Land and Over-Ocean processing differs with respect to the aerosol models used and the surface reflectance calculation.

3.2.1 Theoretical Description of Aerosol Optical Thickness Retrievals over Ocean

The retrieval of the aerosol properties over ocean is a direct adaptation of the algorithm developed by Kaufman and Tanré (1998) over ocean. Aerosol Optical Thickness (AOT)

and Aerosol Model are retrieved based on VIIRS reflectances in the following bands: M5 (0.672μm), M6 (0.746μm), M7 (0.865μm), M8 (1.24μm), M10 (1.61μm) and M11 (2.25μm). There are 4 small-mode models, 5 large-mode models and 101 different fractional amounts to be considered (i.e., 0% Small-Mode Model/100% Large-Mode Model, 1% Small-Mode Model/99% Large-Mode Model, …, 100% Small-Mode Model/0% Large-Mode Model). The algorithm appraises all 2020 possible Over-Ocean Aerosol Models.

3.2.1.1 Modeling of multiple mode aerosols

For inversion of mixing of two aerosol modes, we re-use the equation given by Kaufman and Tanré (1998), based on the Wang and Gordon suggestion (Applied Optics, 1994), which approximates the top of the atmosphere reflectance for the combination of the small and large mode, $\rho_{toa}^{c}(\tau_a)$ at a given aerosol optical thickness, τ_a as a linear combination of the small mode, ρ_{toa}^{s} and the large mode, ρ_{toa}^{l}:

$$\rho_{toa}^{c}(\tau_a) = \eta\rho_{toa}^{s}(\tau_a) + (1-\eta)\rho_{toa}^{l}(\tau_a) \quad (3)$$

For each value of τ_a in the LUT (in the geometry of the observations), the algorithm computes 4 (small mode) x 5 (large mode) x 101 (percentage varying from 0 to 100) possible combinations for each spectral band, $\rho_{toa}^{c}(\tau_a)^{i}$.

3.2.1.2 Optical Depth Retrieval

For each possible combination, the optical thickness is inverted for the M7 reference band τ_a^{inv} such that,

$$\rho_{toa}^{c}(\tau_a^{inv})^{k} = \rho_{obs}^{k} \quad (4)$$

Where ρ_{obs}^{k} is the reflectance observed in band, k (for VIIRS, k is the M7 band).

In other words, τ_a^{inv} is the optical depth that allows the calculated reflectance to match the observed reflectance.

Equation (7) is computed for the values of AOT in the LUT to find the two AOT values that bracket ρ_{obs}^{k} (e.g., τ_a^{lut1} and τ_a^{lut2}) so that

$$\rho_{toa}^{c}(\tau_a^{lut1})^{k} \le \rho_{obs}^{k} < \rho_{toa}^{c}(\tau_a^{lut2})^{k}$$

A simple linear interpolation is used to compute τ_a^{inv} as:

$$\tau_a^{inv} = \tau_a^{lut1} + \frac{\tau_a^{lut2} - \tau_a^{lut1}}{\rho_{toa}^c(\tau_a^{lut2}) - \rho_{toa}^c(\tau_a^{lut1})}\left(\rho_{obs} - \rho_{toa}^c(\tau_a^{lut1})\right) \quad (5)$$

This value is computed for each aerosol model.

3.2.1.3 Residual Calculation

This retrieved AOT is then used to compute TOA reflectances in the other 5 bands (M5, M6, M8, M10 and M11). These calculated TOA reflectances are differenced with the actual observations to produce a residual as follows:

$$\mathrm{Re}\,sidual^c = \frac{1}{n}\sum_{i=1}^{n}\left(\rho_{toa}^c(\tau_a^{inv})^i - \rho_{obs}^i\right)^2 \quad (6)$$

Where n is 5, the number of bands used for residual calculation,

ρ_{obs}^i is the reflectance observed in band i.

The lowest residual from among the 2020 aerosol models is the retrieved model along with its corresponding AOT.

After the inversion is performed for each pixel, and the lowest residual is determined, the lowest residual is compared to a predefined threshold (implemented as a configurable parameter). If the lowest residual exceeds the predefined threshold, the quality of that retrieval is downgraded to “excluded”. This residual threshold test will exclude retrievals with a variety of contamination conditions missed by the pre-inversion data screening including, sub-pixel clouds, cloud shadows and turbid water.

3.2.1.4 Modeling of the Signal over Ocean

Following the 6S code (Vermote et. al. IEEE, 2007), the reflectance at the top of the atmosphere, ρ_{toa}, over ocean is modeled as follows:

$$\rho_{toa} = Tg^{og}Tg^{O_3}\left[\begin{array}{l}(\rho_{R+A} - \rho_R(P_0))Tg_{H_2O}(U_{H_2O}/2) + \rho_R(P) \\ + Tg_{H_2O}(U_{H_2O})\left[\begin{array}{l}T_{R+A}(\theta_s)T_{R+A}(\theta_v)\dfrac{\rho_{w+wc}}{1 - S_{R+A}\rho_{w+wc}} + e^{-\tau_{R+A}m}\rho_G \\ + t_{R+A}^d(\theta_s)e^{-\tau_{R+A}/\cos(\theta_v)}\overline{\rho_G} + t_{R+A}^d(\theta_v)e^{-\tau_{R+A}/\cos(\theta_s)}\overline{\rho_G}' \\ + t_{R+A}^d(\theta_s)t_{R+A}^d(\theta_v)\overline{\overline{\rho_G}} + \dfrac{T_{R+A}(\theta_s)T_{R+A}(\theta_v)S_{R+A}\overline{\overline{\rho_G}}^2}{1 - S_{R+A}\overline{\overline{\rho_G}}}\end{array}\right]\end{array}\right] \quad (7)$$

Where,

Tg^{og} is the gaseous transmission of the gases other than ozone or water vapor,

Tg^{o_3} is the ozone gaseous transmission,

$Tg_{H_2O}(U_{H_2O})$ is the water vapor gaseous transmission for the vertical total column water vapor (U_{H_2O}),

$Tg_{H_2O}(U_{H_2O}/2)$ is the water vapor gaseous transmission for half the vertical total column water vapor (U_{H_2O}/2), which accounts for the assumption that aerosol and water vapor are probably well mixed,

ρ_{R+A} is the atmospheric intrinsic reflectance (molecules and aerosols) (from LUT),

P is the actual surface pressure [atm],

P_0 is the standard surface pressure = 1 atm,

$\rho_R(P)$ is the Rayleigh intrinsic reflectance (molecules only) at pressure P,

$\rho_R(P_0)$ is the Rayleigh intrinsic reflectance (molecules only) at standard pressure = 1 atm,

θ_s is the solar zenith angle,

θ_v is the view zenith angle,

$T_{R+A}(\theta_s)$ is the total (direct and diffuse) downward atmospheric transmission (from LUT, requires adjustment for actual surface pressure (see Equation (9))),

$T_{R+A}(\theta_v)$ is the total (direct and diffuse) upward atmospheric transmission (from LUT, requires adjustment for actual surface pressure (see Equation (9))),

$t^d_{R+A}(\theta_s)$ is the diffuse downward atmospheric transmission,
$t^d_{R+A}(\theta_s) = T_{R+A}(\theta_s) - e^{-(\tau_R+\tau_A)/\cos(\theta_s)}$

$t^d_{R+A}(\theta_v)$ is the diffuse upward atmospheric transmission,

τ_{R+A} is the total optical thickness (molecules and aerosols),

m is the air mass ($1/\cos(\theta_s)+1/\cos(\theta_v)$)

S_{R+A} is the atmospheric spherical albedo (from LUT, requires adjustment for actual surface pressure (see Equation (16))),

ρ_{w+wc} is the contribution of the water and whitecaps (assumed Lambertian),

ρ_G is the sunglint directional reflectance,

$\overline{\rho_G}$ is the normalized integral of the downward irradiance by the sunglint directional reflectance,

$\overline{\rho_G}'$ is the reciprocal quantity of $\overline{\rho_G}$ for the upward coupling,

$\overline{\overline{\rho_G}}$ is approximated as the sunglint spherical albedo.

3.2.1.5 Computation of Calculated TOA Reflectance Quantities

Two other approximations are done to assist the computation of TOA reflectance. Equation (8) adjusts the LUT atmospheric intrinsic reflectance from standard to actual surface pressure. This is done explicitly in Equation (7) but shown again here for completeness:

$$\rho^i_{atm}(\theta_s,\theta_v,\phi,P,Aer^i,U_{H_2O}) = \rho^i_R(\theta_s,\theta_v,\phi,P) + \left(\rho^i_{R+Aer}(\theta_s,\theta_v,\phi,P_0,Aer^i) - \rho^i_R(\theta_s,\theta_v,\phi,P_0)\right)Tg^i_{H_2O}(m,\frac{U_{U_{H_2O}}}{2}) \quad (8)$$

The same approach is applied to the transmission term as follows:

$$T^i_{atm}(\theta,P,Aer^i) = T^i_{atm}(\theta,P_0,Aer^i)\frac{T^i_R(\theta,P)}{T^i_R(\theta,P_0)} \quad (9)$$

Then terms in Equations (7, 8 and 9) for a particular aerosol model, optical thickness and band are done by combining analytical expression or pre-computed LUTs as follows:

$Tg^i_{OG}(m,P)$ **- Gaseous Transmission by other Gases**

The gaseous transmission by gases other than water or ozone in the VIIRS bands can be written as a function of the air mass, m, and pressure P (in atm), as :

$$Tg^i_{OG}(m,P) = \exp\left[m\left(a^i_0P + a^i_1Log(P)\right) + Log(m)\left(b^i_0P + b^i_1Log(P)\right) + mLog(m)\left(c^i_0P + c^i_1Log(P)\right)\right] \quad (10)$$

$Tg^i_{O_3}(m,U_{O_3})$ **- Ozone Gaseous Transmission**

The ozone gaseous transmission in the narrow VIIRS bands (in the Chappuis band) is modeled as :

$$Tg^i_{O_3}(m,U_{O_3}) = e^{-ma^i_{o3}U_{O3}} \quad (11)$$

$\rho^i_R(\theta_s,\theta_v,\phi,P_0)$**, Molecular Atmospheric Reflectance at Standard Pressure**

This quantity is computed by the subroutine CHAND.f that accepts as direct input the geometrical conditions ($\square_s$,$\square_v$,$\square$) (where $\square_s$ (resp. $\square_v$) is the cosine of the solar (resp. view) zenith angle, and $\square$ the relative azimuth) and the molecular optical thickness in that case at standard pressure, which is pre-computed (by 6S), $\square_R$.

$\rho^i_R(\theta_S,\theta_v,\phi,P)$**, Molecular Atmospheric Reflectance at Actual Pressure**

The adjustment is done simply by adjusting the molecular optical thickness, according to:

$\square_R(P)$= P $\square_R$ (12)

With P, the pressure, expressed in atmospheres.

$\rho^i_{R+A}(\theta_s, \theta_v, \phi, P_0, Aer^i)$ **Intrinsic Reflectance at Standard Pressure**

The quantity is pre-computed by 6S in a LUT for each band and aerosol model (P_A,□□□□The step in solar zenith angle is 4° and in view angle 4° corresponding to the Gauss quadrature of 24 angles (with the nadir added). The step is kept constant in scattering angle (4°), □□□defined as:

$$\cos(\Theta) = -\cos(\theta_s)\cos(\theta_v) - \cos(\phi)\sin(\theta_s)\sin(\theta_v) \quad (13)$$

Resulting in a variable number of steps for each □s, □v configuration. The indexing to the correct values in the LUT is achieved through the use of the ANGLE lookup table, which tracks the geometry computed for each □s, □v configuration. Though more expensive and more complicated to interpolate, this structure achieves a higher precision with a reduced size LUT, for a term for which accuracy is critical.

The step in AOT is variable to optimize the performance of the correction with the error induced by the interpolation (i.e., finer at lower AOT values). The AOT values used are as follows: 0.01, 0.05, 0.10, 0.2, 0.3, 0.4, 0.6, 0.8, 1.0, 1.2, 1.4, 1.6, 1.8 and 2.0.

$T^i_{R+A}(\theta, P_0, Aer^i)$ **Atmospheric Transmission at Standard Pressure**

This quantity is pre-computed by 6S using the successive order of scattering method, and illuminating the bottom of the layer with isotropic light. 6S accounts for the aerosol-molecule mixing within the atmosphere. The values are computed with a step of 4° in □S and for each aerosol model and each band for the predefined values of □A. The interpolation for any □S□and □□□is relatively straightforward since this table has only 2 dimensions. The table volume is also very modest.

$T^i_R(\theta, P_0)$ **Molecular (Rayleigh) Transmission at Standard Pressure.**

The molecular transmission at standard pressure is computed using the value of molecular optical depth at standard pressure, □R. Using the two-stream method, the molecular transmission is approximated by:

$$T^i_R(\theta, P_0) = \frac{\left[\frac{2}{3} + \cos(\theta)\right] + \left[\frac{2}{3} - \cos(\theta)\right] e^{-\tau_R/\cos(\theta)}}{\frac{4}{3} + \tau_R} \quad (14)$$

$T^i_R(\theta, P)$ **Molecular (Rayleigh) Transmission at Actual Pressure**

Replace □R in Equation (14) with □R(P) (Equation 12) .

$S^i_{R+A}(P, Aer^i)$ A**tmospheric Spherical Albedo at Actual Pressure**

Since $S^i_{atm}(P, Aer^i) = 1 - \int_0^1 \mu T(\mu) d\mu$ (15)

Where T(□□□is the transmission for □ where □=cos(□)

By ignoring the water vapor dependence on the atmospheric intrinsic reflectance (S acting as a second order effect), we can write the same relation as that for the atmospheric intrinsic reflectance:

$$S^i_{atm}(P, Aer^i) = (S^i_{atm}(P_0, Aer^i) - S^i_R(P_0)) + S^i_R(P) \quad (16)$$

So the $S^i_{atm}(P_0, Aer^i)$ is stored in a pre-calculated LUT depending only on aerosol optical depth and model. The $S^i_R(P)$ term is computed by an analytic expression based on the integral of Equation (17) that is:

$$S^i_R(P) = \frac{1}{4+3\tau_R}\left[3\tau_R - 4E_3(\tau_R) + 6E_4(\tau_R)\right] \quad (17)$$

Where E_3 and E_4 are exponential integral functions.

The exponential integrals of order n (n>0) are defined as:

$$E_n(x) = \int_1^\infty \frac{e^{-xt}}{t^n} dt \quad (18)$$

They satisfy the recurrence relation:

$$nE_{n+1}(x) = e^{-x} - xE_n(x) \quad (19)$$

that is used to compute $E_4(x)$ and $E_3(x)$ from $E_1(x)$.

With $E_1(x)$ approximated by:

$$E_1(x) = \sum_{i=0}^{5} a_i x^i \text{ -log(x)} \quad (20)$$

where

a_0= -0.57721566

a_1= 0.99999193

a_2= -0.24991055

a_3= 0.05519968

a_4= -0.00976004

a_5= 0.00107857

The approximation for $E_1(x)$ is accurate to within 2e-07 for 0<x<1

ρ_{w+wc} Water and Whitecaps Reflectance

The reflectance of both dark water and whitecaps is assumed Lambertian. Chlorophyll concentration varies throughout the global surface waters and must be known to determine water reflectance. To avoid additional ancillary data requirements that would be rather cumbersome for an operational system, a constant chlorophyll concentration is assumed equal to 0.4 mg m^{-3}. This assumption is reasonable for most oceanic conditions and

simplifies the water reflectance to a band-specific constant value. For M6, M7, M8, M10 and M11, resultant water reflectance is zero. Only M5 exhibits a non-zero water reflectance of 0.001.

Whitecap reflectance is a product of their effective reflectance (0.22) and their coverage, which is dependent upon wind speed as follows:

$$\text{Whitecap Coverage} = 2.95\text{E-}06\ [\text{Wind Speed (m s}^{-1})]^{3.52} \quad (21)$$

The individual water and whitecap reflectances are simply summed to yield a single term.

ρ_G Sunglint Directional Reflectance

ρ_G is computed from the subroutine GLINT.f in 6S. The GLINT.f subroutine requires the following inputs: wind speed (m s^{-1}), seawater index of refraction (nd), seawater extinction coefficient (nd), relative wind azimuth (degrees), solar zenith angle (degrees), satellite zenith angle (degrees) and relative satellite azimuth angle (degrees). The relative satellite azimuth must be solar azimuth minus satellite azimuth. Likewise, the relative wind azimuth must be solar azimuth minus wind azimuth. In addition, the relative wind azimuth must be adjusted to ensure it is within the range 0°-360°. The index of refraction and extinction coefficient are both band-specific constants set according to Table 5.

TABLE 5. SEAWATER INDEX OF REFRACTION AND EXTINCTION COEFFICIENT VALUES FOR VIIRS BANDS

VIIRS Band	Seawater Index of Refraction	Seawater Extinction Coefficient
M5	1.33700	0.0
M6	1.33600	0.0
M7	1.33432	0.0
M8	1.32936	0.00004
M10	1.32270	0.00009
M11	1.29793	0.00045

The required Fresnel coefficient of reflection is computed within GLINT.f as explained in Born and Wolf (1975).

$\overline{\rho_G}$ Normalized Integral of Downward Irradiance by Sunglint Directional Reflectance.

$\overline{\rho_G}$ is pre-computed in a LUT depending on the geometry and the optical thickness for a particular aerosol model.

$\overline{\rho_G'}$ is the "reciprocal" of $\overline{\rho_G}$ and is also extracted from the LUT used for $\overline{\rho_G}$. Each Sunglint LUT file contains a single dataset, $\overline{\rho_G}$, and is specific for a given band and aerosol model. The reciprocal parameter $\overline{\rho_G'}$ is extracted from the same dataset by swapping solar zenith and satellite zenith angles. Unlike the Atmospheric LUT, the Sunglint LUT stores $\overline{\rho_G}$ as a function of 3 angular variables: solar zenith, satellite zenith and relative azimuth. Table 6 provides bins at which $\overline{\rho_G}$ is sampled. For intermediate values of the arguments, $\overline{\rho_G}$ and $\overline{\rho_G'}$ should be obtained with linear interpolation.

TABLE 6. SUNGLINT LUT ARGUMENTS

Argument	Dimension	Bins
550nm AOT	15	0.01, 0.05, 0.10, 0.15, 0.20, 0.30, 0.40, 0.60, 0.80, 1.00, 1.20, 1.40, 1.60, 1.80, 2.00
Solar Zenith Angle	21	0°, 4°, 8°, 12°, 16°, 20°, 24°, 28°, 32°, 36°, 40°, 44°, 48°, 52°, 56°, 60°, 64°, 68°, 72°, 76°, 80°
Satellite Zenith Angle	21	0°, 4°, 8°, 12°, 16°, 20°, 24°, 28°, 32°, 36°, 40°, 44°, 48°, 52°, 56°, 60°, 64°, 68°, 72°, 76°, 80°
Relative Azimuth	21	0°, 9°, 18°, 27°, 36°, 45°, 54°, 63°, 72°, 81°, 90°, 99°, 108°, 117°, 126°, 135°, 144°, 153°, 162°, 171°, 180°

$\overline{\overline{\rho_G}}$ Sunglint Spherical Albedo

This term is approximated as the sunglint spherical albedo, which is a band-dependent constant set according to Table 7.

TABLE 7. SUNGLINT SPHERICAL ALBEDO VALUES FOR VIIRS BANDS

VIIRS Band	Sunglint Spherical Albedo
M5	0.0661
M6	0.0651
M7	0.0648
M8	0.0640
M10	0.0629
M11	0.0590

3.2.2 Theoretical Description of Aerosol Optical Thickness Retrievals over Land

Aerosol retrieval over land surfaces follows the basic methodology as the over ocean case. The important differences include utilized aerosol models and surface reflectance assumptions.

The aerosol models considered and characterization of the surface must necessarily change however. AOT and Aerosol Model are retrieved based on VIIRS reflectances in the following bands: M1 (0.412 □m), M2 (0.445 □m), M3 (0.488μm), M5 (0.672μm) and M11 (2.25 □m). There are 5 Aerosol Models to be considered.

Land pixels must be evaluated to avoid processing “bright” pixels, which are pixels for which the following tests are both true:

$$(\rho_{M8} - \rho_{M11}) / (\rho_{M8} + \rho_{M11}) < 0.05 \quad (22)$$

$$\rho_{M11} > 0.3 \quad (23)$$

For those pixels not discarded as bright, an additional test is applied to discern soil-dominated scenes from those primarily composed of surface vegetation. The following test must be true for pixels to be labeled as “vegetation-dominated”:

$$(\rho_{M8} - \rho_{M11}) / (\rho_{M8} + \rho_{M11}) > 0.2 \quad (24)$$

This surface type discrimination allows quality flags to differentiate between more accurate and less accurate retrievals due to estimation of the surface reflectance in the visible. Figure 8 illustrates land pixel classification for the entire envelope of possible M8 and M11 reflectances.

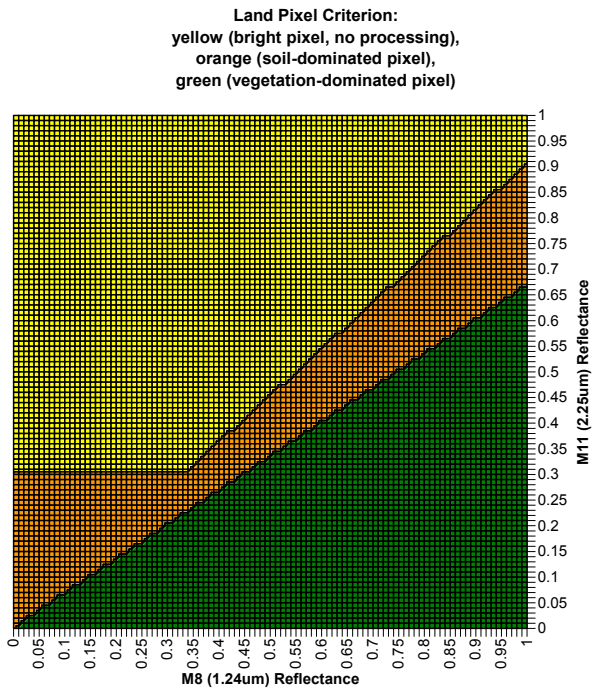

FIGURE 8. CLASSIFICATION OF LAND PIXELS BASED ON M8 AND M11 REFLECTANCES: BRIGHT PIXELS IN YELLOW, SOIL-DOMINATED PIXELS IN ORANGE AND VEGETATION-DOMINATED PIXELS IN GREEN.

3.2.2.1 Over-Land Aerosol Models

The aerosol models used in the inversion stem from Dubovik *et al.* (2001). Twelve locations worldwide, where significant statistics of size distributions were available (from 300 to 2400 measurements), were analyzed to derive both size parameters and optical properties of the aerosols following an approach similar to the one presented in (Remer and Kaufman, 1998). From these studies, we extracted 5 basics aerosols types: Dust, Oceanic, Smoke-High absorption, Smoke-Low absorption, Urban-High absorption and Urban-Low absorption. The Oceanic model is not included due to exclusion of coastal pixels in the land retrieval and the infrequency of oceanic aerosols inland.

Dust corresponds to desert dust, Oceanic to marine aerosol. Biomass burning produces smoke with low absorption (high single scatter albedo), while High absorption corresponds typically to Savanna burning in South Africa. Urban-Low absorption corresponds to relatively clean urban, industrial aerosol (e.g., GSFC site) and High absorption corresponds to more polluted urban environments (e.g., Mexico City). As in Remer and Kaufman (1998), the characteristics of the aerosol model vary as a function of the aerosol loading or optical thickness. The size distribution is very well represented by a bi-lognormal distribution. The complex index of refraction for dust is defined at the following wavelengths: 0.350, 0.400, 0.412, 0.443, 0.470, 0.488, 0.515, 0.550, 0.590, 0.633, 0.670, 0.694, 0.760, 0.860, 1.240, 1.536, 1.650, 1.950, 2.250 an 3.750 microns. Parameters used for each model are as follows:

Dust

Refractive indices
Refractive index real = 1.48
Refractive index imaginary = 0.0025, 0.0025, 0.0025, 0.0025, 0.0023, 0.0021, 0.0019, 0.0016, 0.0013, 0.0010, 0.0007, 0.0007, 0.0007, 0.0006, 0.0006, 0.0006, 0.0006, 0.0006, 0.0006
Size parameter (small particle mode)
Volume mean radius = 0.12 (□m)
Standard deviation = 0.49 + 0.10□$_{1020nm}$
Volume concentration = 0.02 + 0.02□$_{1020nm}$
Size parameter (coarse particle mode)
Volume mean radius = 1.90 (□m)
Standard deviation = 0.63 - 0.10□$_{1020nm}$
Volume concentration = 0.9□$_{1020nm}$ (□m^3/□m^2)

Smoke, High Absorption

Refractive indices
Refractive index real = 1.51
Refractive index imaginary = 0.021
Size parameter (small particle mode)
Volume mean radius = 0.12+0.025□$_{440nm}$ (□m)
Standard deviation = 0.40
Volume concentration = 0.12□$_{440nm}$ (□m^3/□m^2)
Size parameter (coarse particle mode)
Volume mean radius = 3.22+0.71□$_{440nm}$ (□m)
Standard deviation = 0.73
Volume concentration = 0.09□$_{440nm}$ (□m^3/□m^2)

Smoke, Low Absorption

Refractive indices
Refractive index real = 1.47
Refractive index imaginary = 0.0093
Size parameter (small particle mode)
Volume mean radius = 0.13+0.04□$_{440nm}$ (□m)
Standard deviation = 0.40
Volume concentration = 0.12□$_{440nm}$ (□m^3/□m^2)
Size parameter (coarse particle mode)
Volume mean radius = 3.27+0.58□$_{440nm}$ (□m)
Standard deviation = 0.79
Volume concentration = 0.05□$_{440nm}$ (□m^3/□m^2)

Urban, Low absorption

Refractive indices
Refractive index real = 1.41-0.03□$_{440nm}$
Refractive index imaginary = 0.003
Size parameter (small particle mode)
Volume mean radius = 0.12+0.11□$_{440nm}$ (□m)
Standard deviation = 0.38
Volume concentration = 0.15□$_{440nm}$ (□m^3/□m^2)
Size parameter (coarse particle mode)
Volume mean radius = 3.03+0.49□$_{440nm}$ (□m)
Standard deviation = 0.75
Volume concentration = 0.01+0.04□$_{440nm}$ (□m^3/□m^2)

Urban, High absorption

Refractive indices
Refractive index real = 1.47
Refractive index imaginary = 0.014
Size parameter (small particle mode)
Volume mean radius = 0.12+0.04□$_{440nm}$ (□m)
Standard deviation = 0.43
Volume concentration = 0.12□$_{440nm}$ (□m^3/□m^2)
Size parameter (coarse particle mode)
Volume mean radius = 2.72+0.60□$_{440nm}$ (□m)
Standard deviation = 0.63
Volume concentration = 0.11□$_{440nm}$ (□m^3/□m^2)

The land aerosol retrieval uses the blue band (M3) to compute an AOT (at 550 nm) value for each model. Then, the expected TOA reflectance is computed in the red band (M5) for each model using the value of AOT (at 550 nm) computed using the blue band. The land aerosol model with the smallest difference between the modeled and observed TOA reflectance in the red band (the lowest residual) is selected. After the inversion is performed for each pixel, and the lowest residual is determined, the lowest residual is compared to a predefined threshold (implemented as a configurable parameter). If the lowest residual exceeds the predefined threshold, the quality of that retrieval is downgraded to “excluded”. This residual threshold test will exclude retrievals with a variety of contamination conditions missed by the pre-inversion data screening including, sub-pixel clouds, cloud shadows and surface types with very different spectral reflectance relationships than most vegetated surface types.

3.2.2.2 Spectral Albedo Shape used for Aerosol Retrieval over Land

3.2.2.2.1 Introduction

Aerosol retrieval over land uses the visible wavelengths where the aerosol effects are usually strongest for retrieving the optical thickness. The wavelengths used are located in the blue (0.412μm-0.480μm) and the red (0.645μm-0.670μm) portion of the spectrum. In order to retrieve aerosol, the spectral shape of the surface reflectance needs to be assumed at those wavelengths, so the only unknowns (given that all the other ancillary data such as pressure and absorbing gas concentrations are known) are the aerosol optical thickness, aerosol model and the surface reflectance at a single wavelength. In previous version of the code, constant relationships between the surface reflectance in the SWIR (2.13μm) and the surface reflectances in blue and red have been used. This technique was taken from the aerosol retrieval group for MODIS (Kaufman and Tanre, 1996; Kaufman *et al.*, 1997). For this method, the reflectance in the blue is assumed to be ¼ of the SWIR and the reflectance in the red is assumed to be ½ of the SWIR. That relationship has been demonstrated by comparing to ground data pre-launch and on a variety of vegetated targets post-launch and also by theoretical simulation of a vegetation radiative transfer model (Kaufman *et al.*, 1997).

However, this relationship was only validated for vegetated targets and it has been shown that larger deviations could be observed as the reflectance of the target increases with a decrease in the vegetation cover. The land cover is not the only factor responsible for an increase in the reflectance as all natural targets deviate from the Lambertian assumption. Increases in the reflectance could be observed with variations in the geometry.

Recent advances to the MODIS Surface Reflectance (MOD09) algorithm for the collection 5 reprocessing provide improved performance over an increased range of surface conditions. By retrieving surface reflectances near AERONET sites using the measured aerosol properties and the 6SV radiative transfer model (RTM), a more robust relationship between the surface reflectances in the MODIS bands for vegetated and semi-vegetated backgrounds has been established. This analysis is detailed in section 3.2.2.2.2 below. The MODIS bands used are 1, 3, 7, 8, 9 and 10 which correspond to VIIRS bands M5, M3, M11, M1, M2 and M3 respectively. The expected ratio between each band and MODIS band 1 has been derived from the atmospherically corrected surface reflectance data surrounding the AERONET sites. Because MODIS band 10 is closer in band center to VIIRS band M3, the ratio derived for this band will be used as the initial value.

3.2.2.2.2 Data set description

This section reflects the previous version of the algorithm and will be updated with the next revision of the ATBD.

We selected 41 cases based on Landsat TM geocover data set (http: //geocover.glfc.umd.edu) near coincident with MODIS-Terra and sun photometer data from AeroNet to perform accurate atmospheric correction. The list of cases is given in Table 8, which lists the country, geographic location, date, latitude and longitude of the sun photometer, type of land cover, altitude and the measured aerosol optical thickness at 550nm.

TABLE 8. SURFACE TYPE CORRECTION TEST DATASET.

Country	SWIR Reflectance	date	Land Cover	Name of the photometer	lat	long	alt (m)	AOT 550nm
Brazil	0.150	8/11/2001	Vegetation	Abracos_Hill	-10.76	-62.36	200	0.15
South Korea	0.096	9/23/2001	Vegetation	Anmyon	36.32	126.19	47	0.10
USA	0.075	5/27/2002	Forest	Bonanza_Creek	64.74	-148.32	150	0.10
USA	0.185	9/17/2000	Rural	BONDVILLE	40.05	-88.37	212	0.10
Canada	0.117	7/26/2000	Rural	Bratts_Lake	50.28	-104.70	587	0.20
Canada	0.085	8/5/2001	Rural	Bratts_Lake	50.28	-104.70	587	0.10
USA	0.120	9/20/2002	Mountains	BSRN_BAO_Boulder	40.03	-105.00	1604	0.05
USA	0.142	9/24/2001	Mountains	BSRN_BAO_Boulder	40.03	-105.00	1604	0.10
Argentina	0.116	12/20/2000	Rural - Urban	CEILAP_BA	-34.57	-58.50	10	0.05
Australia	0.359	8/16/2002	Desert	Coleambally	-34.81	146.06	127	0.05
Bolivia	0.327	8/1/2000	Rural	Concepcion	-16.14	-62.03	500	0.20
Argentina	0.114	1/1/2001	Rural	Cordoba-CETT	-31.52	-64.46	730	0.20
France	0.078	8/24/2000	Rural - Urban	Creteil	48.79	2.44	57	0.15
Canada	0.094	8/10/2002	Rural - Forest - Lakes	Egbert	44.23	-79.75	264	0.10
USA	0.256	10/5/2001	Urban - Rural - Lake	GSFC	39.03	-76.88	50	0.20
France	0.255	8/24/2000	Rural - Urban	Lille	50.61	3.14	60	0.35
France	0.291	5/23/2001	Rural - Urban	Lille	50.61	3.14	61	0.30
USA	0.240	6/15/2000	Rural-Desert	Maricopa	33.07	-111.97	360	0.07
USA	0.114	4/19/2000	Rural-Desert	Maricopa	33.07	-111.97	360	0.06
USA	0.118	10/5/2001	Urban - Rural - Lake	MD_Science_Center	39.28	-76.62	15	0.20
Moldova	0.137	5/25/2001	Rural	Moldova	47.00	28.82	205	0.10
Russia	0.155	5/30/2002	Rural - Urban	Moscow_MSU_MO	55.70	37.51	192	0.10
Burkina	0.252	11/3/2001	Semi-arid	Ouagadougou	12.20	-1.40	290	0.25

Country	SWIR Reflectance	date	Land Cover	Name of the photometer	lat	long	alt (m)	AOT 550nm
France	0.123	8/24/2000	Rural - Urban	Palaiseau	48.70	2.21	156	0.15
USA	0.160	8/6/2001	Rural - Mountains	Rimrock	46.49	-116.99	824	0.05
USA	0.414	5/1/2000	Desert	Rogers_Dry_Lake	34.93	-117.89	680	0.10
Italy	0.163	6/9/2001	Urban	Rome_tor_vergata	41.84	12.65	130	0.15
Italy	0.147	8/3/2001	Urban	Rome_tor_vergata	41.84	12.65	131	0.45
Israel	0.456	3/8/2002	Desert	Sede_Boker	30.86	34.78	480	0.10
USA	0.303	5/9/2000	Desert	Sevilleta	34.35	-106.89	1477	0.06
USA	0.289	6/4/2001	Desert	Sevilleta	34.35	-106.89	1477	0.10
Japan	0.063	4/15/2001	Forest	Shirahama	33.69	135.36	10	0.25
Japan	0.083	4/22/2001	Forest	Shirahama	33.69	135.36	10	0.25
USA	0.203	6/29/2002	Rural	Sioux_Falls	43.74	-96.63	500	0.15
USA	0.141	7/15/2002	Rural	Sioux_Falls	43.74	-96.63	500	0.20
USA	0.094	8/4/2001	Rural	Sioux_Falls	43.74	-96.63	500	0.15
Canada	0.051	9/17/2001	Forest	Thompson	55.78	-97.83	218	0.04
Australia	0.380	5/17/2000	Desert	Tinga-Tingana	-28.98	139.99	38	0.02
USA	0.119	5/1/2000	Urban	UCLA	34.07	-118.45	131	0.15
Canada	0.042	8/12/2001	Forest-Lakes	Waskesiu	53.92	-106.07	550	0.03
China	0.339	5/31/2001	Desert - Mountain	Yulin	38.28	109.72	1080	0.10

3.2.2.2.3 Data analysis

This section reflects the previous version of the algorithm and will be updated with the next revision of the ATBD.

The data are statistically analyzed to generate a relationship between SWIR reflectance and visible reflectances (surface only). Figure 9 shows the relationship between the red, blue and SWIR surface reflectances obtained by accurate atmospheric correction of the MODIS top of atmosphere reflectances (using the aerosol optical thickness and size distribution). As shown in Figure 9 and as already pointed out by Kaufman *et al.* (1997), the simple relationship holds until the value of the SWIR nadir reflectance reaches 0.15, which covers most of the vegetated areas. Based on this dataset, we have developed a variable relationship between the SWIR and the visible. Instead of using an arbitrary threshold in the reflectance in the SWIR that may vary as the function of the observation conditions, we use a normalized index using MODIS Bands 5 (1.24μm) and 7 (2.13μm), which are less sensitive to the BRDF and atmospheric effect. The reflectances in MODIS Band 3 (0.47μm) and Band 1 (0.67μm) are estimated from Band 7 (2.13μm) as follows:

If the normalized index $(\rho_5-\rho_7)/(\rho_5+\rho_7)$ is higher than 0.20 (vegetated area), a relationship close to the one used by Kaufman *et al.* (1997) is used:

$$\rho_1 = 0.55\ \rho_7 \quad (25)$$

$$\rho_3 = 0.32\ \rho_7 \quad (26)$$

If the normalized index $(\rho_5-\rho_7)/(\ \rho_5+\rho_7)$ is lower than 0.20 (soil dominated), an updated relationship is used:

$$\rho_1 = -0.113 + 1.03\ \rho_7 \quad (27)$$

$$\rho_3 = -0.061 + 0.54\ \rho_7 \quad (28)$$

Figures 10 and 11 show the comparison between the "estimated" reflectance and the "measured" ones in Bands 1 and 3 using this updated approach.

The above equations extend the range of surface reflectances over which the AOT retrieval is possible. With these equations, the new criterion for stopping retrieval due to pixel brightness is formulated as follows:

$(\rho_5 - \rho_7)/(\ \rho_5 + \rho_7) < 0.05$ and $\rho_7 > 0.300$

The coefficients were generated for MODIS Bands 1 (0.67μm), 3 (0.47μm) and 7 (2.13μm), which are similar to VIIRS bands M5 (0.672μm), M3 (0.488μm) and M11 (2.25μm) respectively. The SWIR channels are less sensitive to band location, while the red bands are almost identical. The blue band centers are distant enough to warrant slight modification via linear interpolation. After adjustment, the relationships for VIIRS are as follows:

Vegetation-dominated pixels:

$$\rho_{M5} = 0.55\ \rho_{M11} \quad (29)$$

$$\rho_{M3} = 0.3407\ \rho_{M11} \quad (30)$$

Soil-dominated pixels:

$$\rho_{M5} = -0.113 + 1.03\ \rho_{M11} \quad (31)$$

$$\rho_{M3} = -0.06568 + 0.5841\ \rho_{M11} \quad (32)$$

The M11 reflectances must be corrected for gas absorption prior to use in the above relationships. Correction is applied by dividing the TOA M11 reflectances by the gas transmissions for water vapor, ozone and other gases.

Experience on MODIS has shown that these empirical relationships do not hold when sub-pixel water is present. Therefore, an additional test to screen for sub-pixel water has been implemented. The moderate resolution NDVI is computed using bands M5 and M7. If the NDVI of an otherwise valid pixel does not exceed a predefined threshold (implemented as a configurable parameter, nominal value of 0.1 based on MODIS heritage), then the pixel is flagged as being water contaminated and no inversion is performed.

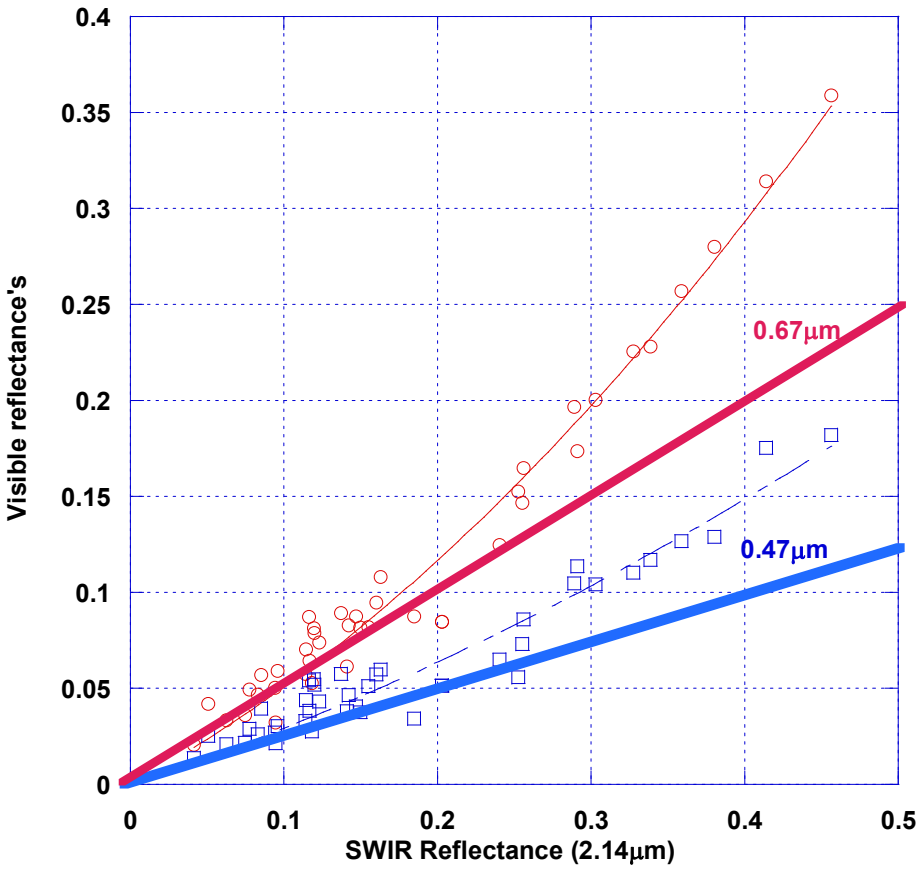

FIGURE 9. SURFACE REFLECTANCES OBSERVED IN THE BLUE AND RED MODIS CHANNELS AS A FUNCTION OF THE SWIR SHOWING THE DEVIATION FROM THE SIMPLE RELATION DEFINED BY KAUFMAN ET AL. (1997) AS THE COVER TYPE RANGES FROM VEGETATION TO SEMI-ARID AND DESERT.

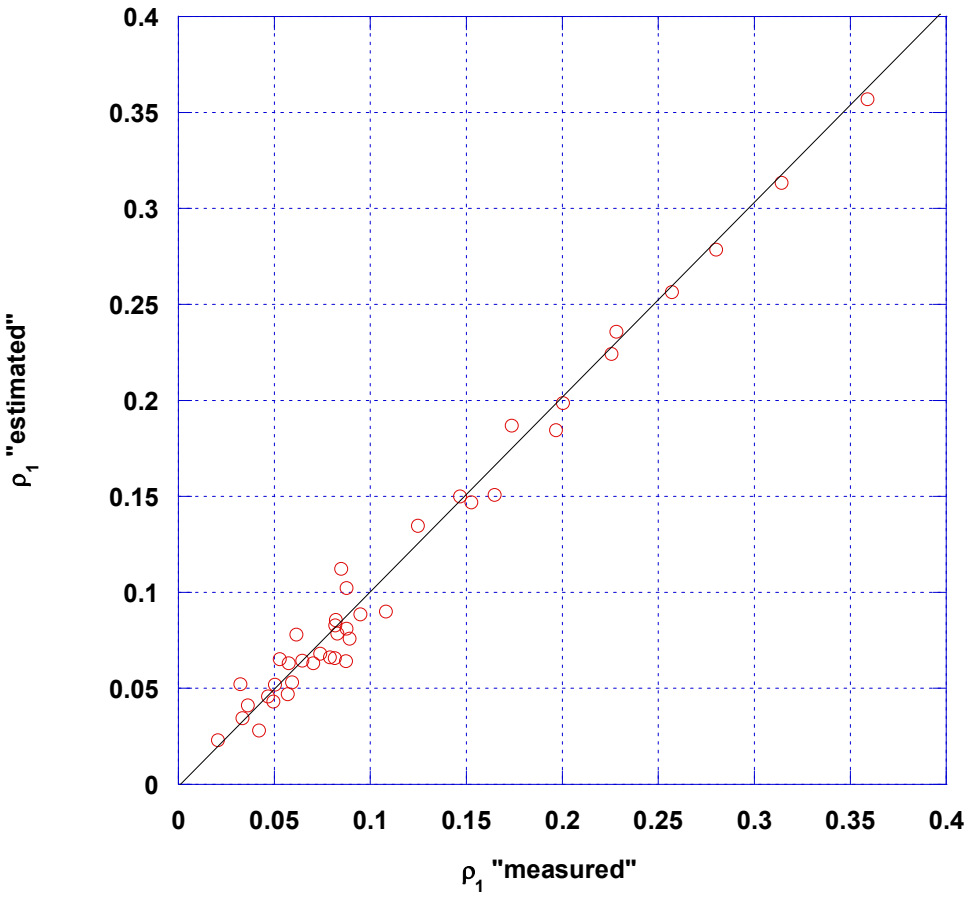

FIGURE 10. COMPARISON OF THE "ESTIMATED" (USING THE UPDATED APPROACH) AND "MEASURED" REFLECTANCES IN MODIS BAND 1.

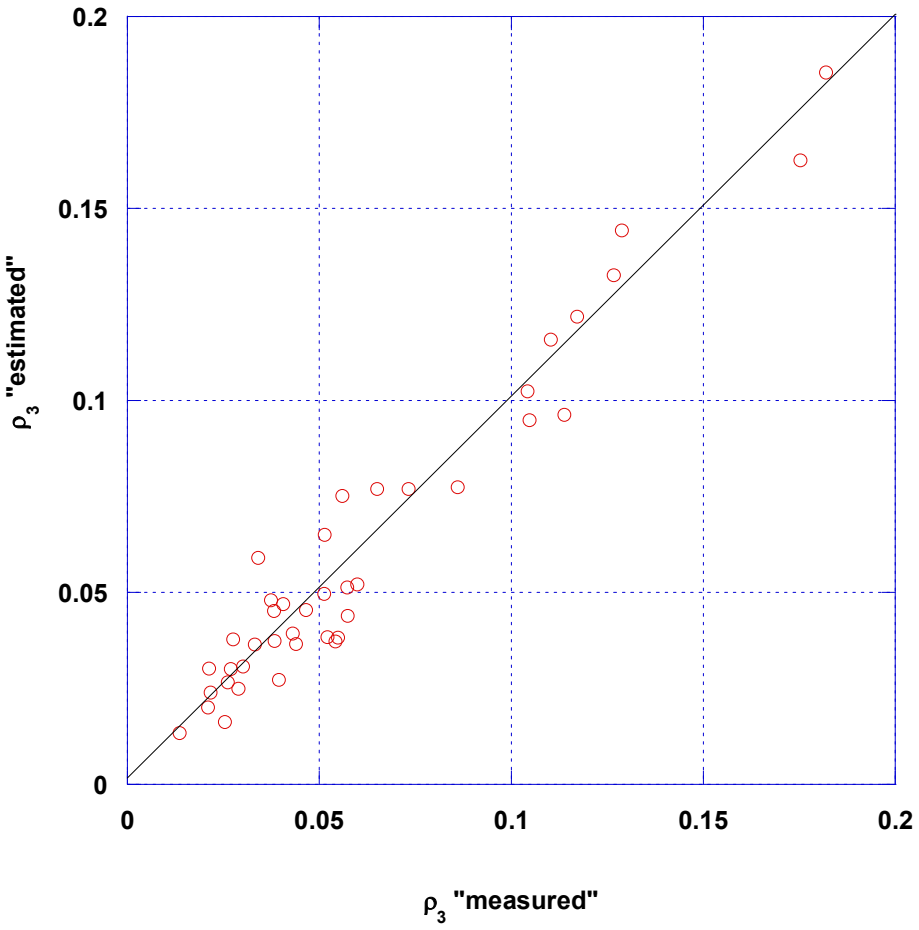

FIGURE 11. COMPARISON OF THE "ESTIMATED" (USING THE UPDATED APPROACH) AND "MEASURED" REFLECTANCES IN MODIS BAND 3.

3.2.2.2.4 Conclusion

This section reflects the previous version of the algorithm and will be updated with the next revision of the ATBD.

The developed relationships are expected to be insensitive to the BRDF effect, which will affect SWIR and visible similarly (Kaufman *et al.*, 1997). However, accurate atmospheric correction, taking into account the coupling before BRDF and atmosphere, is needed to verify that assumption.

The statistical relationships developed herein are effective, but they could be refined further, especially the relationship in the lower reflectance range, given the soil and vegetation fraction could be assessed. That may be difficult or not necessary if shorter wavelength are to be used (0.412μm), or other sources of error are dominating the accuracy of the retrieval.

3.2.2.3 Accounting for Atmosphere-Surface BRDF Coupling in the Aerosol Retrieval Algorithm

The algorithm theoretical basis for proper surface BRDF accounting is presented herein. However this surface characterization has not been implemented in the corresponding retrieval code, which assumes Lambertian surface behavior.

3.2.2.3.1 Introduction

The coupling between the atmosphere and the surface BRDF can introduce substantial biases in the aerosol retrieval over vegetated area of the order the accuracy of the product *[AL60822-VIR-005]* and should be taken into account. At first glance, that process seems complicated since it involves knowledge of the BRDF of the surface. However, since it is a second order effect, the error could be reduced significantly by using a simple BRDF shape based on the NDVI as it is done for the operational atmospheric correction over land. This document present the step by step algorithm we are recommending, it involves in the first part, the derivation of the optical depth using the Lambertian approximation (accounting for surface type correction in the SWIR-VIS relationship), then a derivation of the NDVI, and finally the “refined” optical depth retrieval accounting for BRDF atmosphere coupling. For simplicity, the process describes the retrieval of the optical thickness in one band assuming that the aerosol model is known.

3.2.2.3.2 Retrieval in the Lambertian Case

For the Lambertian case, the retrieval of the optical thickness consists in matching the reflectance at the top of the atmosphere observed in the visible band, ρ_{obs} with the estimation based on the solution of the radiative transfer equation in the Lambertian infinite target case. Knowing that the top of the atmosphere reflectance is written as:

$$\rho_{toa}(\tau_A) = Tg^{og} Tg^{O_3} \left[\begin{array}{l} (\rho_{R+A}(\tau_A) - \rho_R(P_0)) Tg_{H_2O}(U_{H_2O}/2) + \rho_R(P) \\ + Tg_{H_2O}(U_{H_2O}) T_{R+A}(\tau_A, \theta_s) T_{R+A}(\tau_A, \theta_v) \dfrac{\rho_{surf}}{1 - S_{R+A}\rho_{surf}} \end{array} \right] \quad (33)$$

Where,

Tg^{og} is the gaseous transmission of the gases other than ozone or water vapor,

Tg^{O_3} is the ozone gaseous transmission,

$Tg_{H_2O}(U_{H_2O})$ is the water vapor gaseous transmission for the total integrated amount of water vapor (U_{H_2O}),

$Tg_{H_2O}(U_{H_2O}/2)$ is the water vapor gaseous transmission for half of total integrated amound of water vapor (U_{H_2O}), trying to account for the fact the aerosol and vapor are probably well mixed,

ρ_{R+A} is the atmospheric intrinsic reflectance (molecules and aerosols),

P is the actual pressure [atm],

P_0 is the standard pressure = 1 atm,

$\rho_R(P)$ is the Rayleigh intrinsic reflectance (molecules only) at pressure P,

θ_s is the solar zenith angle,

θ_v is the view zenith angle,

$T_{R+A}(\theta_s)$ is the total (direct and diffuse) downward atmospheric transmission,

$T_{R+A}(\theta_v)$ is the total (direct and diffuse) upward atmospheric transmission,

$t^d_{R+A}(\theta_s)$ is the diffuse downward atmospheric transmission,

$t^d_{R+A}(\theta_v)$ is the diffuse upward atmospheric transmission,

We matched the observed reflectance ρ_{obs}, with an estimate of ρ_{toa} for the retrieved optical depth, τ_A^{ret},

$$\frac{\rho_{obs}}{Tg^{og}Tg^{O_3}} - \rho_R(P) = (\rho_{R+A}(\tau_A^{ret}) - \rho_R(P_0))Tg_{H_2O}(U_{H_2O}/2)$$
$$+ Tg_{H_2O}(U_{H_2O})T_{R+A}(\tau_A^{ret},\theta_s)T_{R+A}(\tau_A^{ret},\theta_v)\frac{\rho_{surf}^{est}}{1 - S_{R+A}(\tau_A^{ret})\rho_{surf}^{est}} \quad (34)$$

3.2.2.3.3 Estimating Surface BRDF Parameters

Using the retrieved optical depth from Equation (34), atmospheric correction is performed using the Lambertian assumption in the red (M5 at 0.672□m) and in the Near Infrared (M7 at 0.865□m), and the Normalized Difference Vegetation Index is computed as:

$$NDVI = \frac{\rho_{surf}^{M7} - \rho_{surf}^{M5}}{\rho_{surf}^{M7} + \rho_{surf}^{M5}} \quad (35)$$

The NDVI is an input to determine the BRDF shape coefficient P_2' for Li Sparse reciprocal and P_3'for Ross Thick which are given in Figure 12 as a function of vegetation cover. A simple linear relationship between NDVI and P_2', P_3' is used.

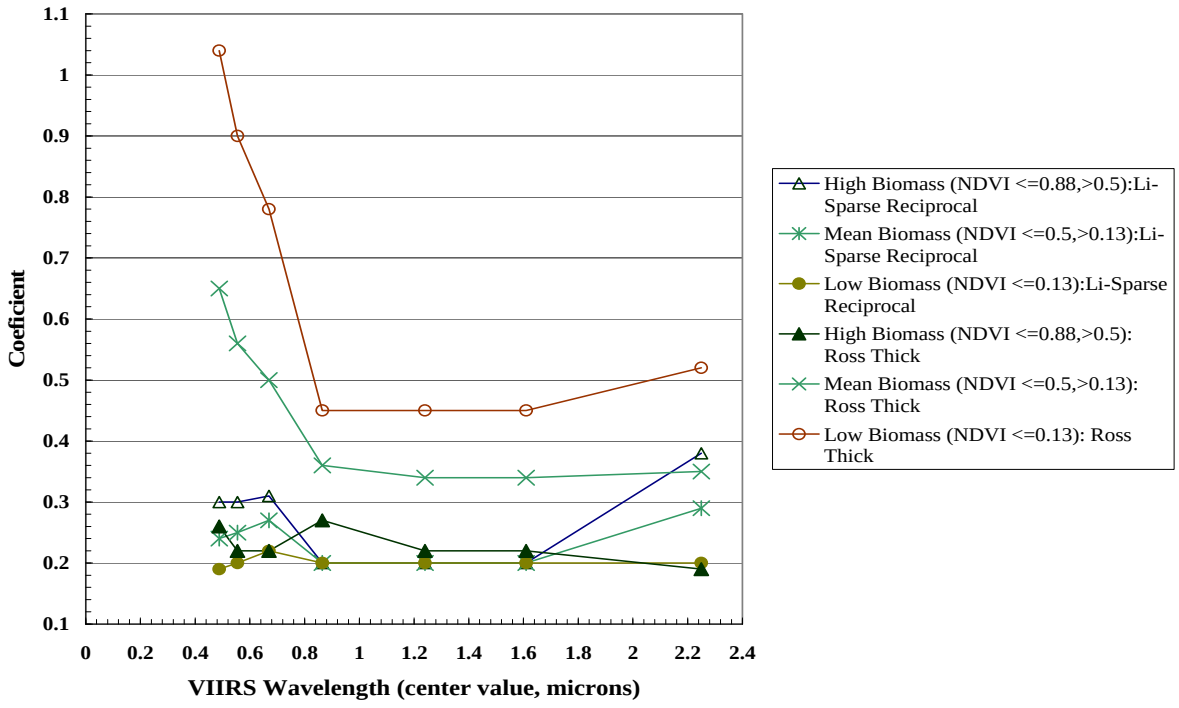

FIGURE 12. RELATIONSHIP BETWEEN BRDF SHAPE AND NDVI

3.2.2.3.4 Accounting Surface BRDF Parameters in the Solution of the Radiative Transfer Equation

Using the BRDF shape coefficients, the solution of the equation of transfer is updated to account for BRDF atmosphere coupling and Equation (34) is now written as:

$$\frac{\rho_{obs}}{Tg^{og}Tg^{O_3}} - \rho_R(P) = (\rho_{R+A}(\tau_A^{ret}) - \rho_R(P_0))Tg_{H_2O}(U_{H_2O}/2)$$
$$+ Tg_{H_2O}(U_{H_2O}) \begin{bmatrix} e^{-(\tau_R+\tau_A^{ret})/\mu_s} e^{-(\tau_R+\tau_A^{ret})/\mu_v} \rho_{surf}^{est} \\ + e^{-(\tau_R+\tau_A^{ret})/\mu_v} t_d(\tau_A^{ret},\mu_s)\overline{\rho}_{surf}^{est}(\tau_A^{ret}) + e^{-(\tau_R+\tau_A^{ret})/\mu_s} t_d(\tau_A^{ret},\mu_v)\overline{\rho}'^{est}_{surf}(\tau_A^{ret}) \\ + t_d(\tau_A^{ret},\mu_v)t_d(\tau_A^{ret},\mu_s)\overline{\overline{\rho}}_{surf}^{est} \\ + \frac{T_{R+A}(\tau_A^{ret},\mu_s)T_{R+A}(\tau_A^{ret},\mu_v)S_{R+A}(\tau_A^{ret}))\left(\overline{\overline{\rho}}_{surf}^{est}\right)^2}{1 - S_{R+A}(\tau_A^{ret})\overline{\overline{\rho}}_{surf}^{est}} \end{bmatrix} \quad (36)$$

Where the three quantities $\overline{\rho}_{surf}^{est}(\tau_A^{ret})$, $\overline{\rho}'^{est}_{surf}$ and $\overline{\overline{\rho}}_{surf}^{est}$ are computed using the shape coefficients,P_2' and P_3', the estimated reflectance, ρ_{surf}^{est}, and lookup table of coupling kernel. The BRDF of the surface, $\rho_{surf}^{brdf}(\theta,\theta',\phi)$ is described by:

$$\rho_{surf}^{brdf}(\theta,\theta',\phi) = \alpha\left[1 + P'_2 K_{LSR}(\theta,\theta',\phi) + P'_3 K_{RT}(\theta,\theta',\phi)\right] \quad (37)$$

Where,

$$\alpha = \frac{\rho_{surf}^{est}}{1 + P'_2 K_{LSR}(\theta_s,\theta_v,\phi_s - \phi_v) + P'_3 K_{RT}(\theta_s,\theta_v,\phi_s - \phi_v)} \quad (38)$$

So that for the observation geometry, $\rho_{surf}^{brdf}(\theta_s,\theta_v,\phi_s - \phi_v) = \rho_{surf}^{est}$,

From Equation (37), we can see that the coupling quantities are computed according to:

$$\overline{\rho}_{surf}^{est}(\tau_A^{ret}) = \alpha\left[1 + P'_2 \overline{K}_{LSR}(\tau_A^{ret},\theta_s,\theta_v,\phi_s - \phi_v) + P'_3 \overline{K}_{RT}(\tau_A^{ret},\theta_s,\theta_v,\phi_s - \phi_v)\right] \quad (39)$$

$$\overline{\rho}'^{est}_{surf}(\tau_A^{ret}) = \alpha\left[1 + P'_2 \overline{K}_{LSR}(\tau_A^{ret},\theta_v,\theta_s,\phi_s - \phi_v) + P'_3 \overline{K}_{RT}(\tau_A^{ret},\theta_v,\theta_s,\phi_s - \phi_v)\right] \quad (40)$$

$$\overline{\overline{\rho}}_{surf}^{est} = \alpha\left[1 + P'_2 \overline{\overline{K}}_{LSR} + P'_3 \overline{\overline{K}}_{RT}\right] \quad (41)$$

The quantities $\overline{K}_{LSR}(\tau_A,\theta,\theta',\phi)$ and $\overline{K}_{RT}(\tau_A,\theta,\theta',\phi)$ are stored in a 4 dimensional lookup table as a function of the aerosol optical depth, τ_A, the incidence angle θ, the observation angle θ' and the azimuth ϕ (for a standard aerosol model). The quantities $\overline{\overline{K}}_{LSR}$ and $\overline{\overline{K}}_{RT}$ are constants (the white sky albedo for the kernels).

3.2.2.4 Accounting for Adjacency Effects in the Aerosol Retrieval Algorithm

The algorithm theoretical basis for adjacency effects accounting is presented herein. However this correction has not been implemented in the corresponding retrieval code at this time.

3.2.2.4.1 Introduction

The adjacency effects which are related to the contribution of the pixel around the viewed pixels can have substantial impact on the aerosol retrieval *[AL60822-VIR-005]* and should be taken into account. At first glance, that process seems complicated since it involves knowledge of the surface reflectance which can only be obtained after atmospheric correction and therefore derivation of the optical thickness. One can think of the iterative process by which the reflectance is corrected using the infinite target assumption for aerosol retrieval and then subsequently refined by iteration, however this process can be costly in CPU and the convergence may not be assured. Since we are already using some estimate of the reflectance for the pixel where we retrieve the optical thickness (based on the SWIR-VIS relationship) one can think of using the same relationship to estimate the contribution of the pixel background. This approach although not exact, since based on an empirical relationship will substantially reduced the biases introduced by the adjacency effects.

3.2.2.4.2 Modifying the Lambertian Case to Account for Target Heterogeneity

If the target is of infinite dimension, the equation of transfer (here rewritten without absorption to simplify the writing, is

$$\rho_{toa} = \rho_{R+A} + \frac{T_{R+A}\rho_s}{1 - S_{R+A}\rho_s} \tag{42}$$

In the case where we cannot consider the target to be of infinite radius, the equation becomes:

$$\rho_{toa} = \rho_{R+A} + \frac{T_{R+A}(\theta_s)}{1 - S_{R+A}\rho_e}\left(e^{-\tau/\mu_v}\rho_s + t^d_{R+A}(\theta_v)\langle\rho_s\rangle_e\right) \tag{43}$$

$$\left\langle \rho_s \right\rangle_e = \frac{1}{2\pi} \int_0^{2\pi} \int_0^{\infty} \rho_s(r,\psi) \frac{dF(r)}{dr} dr d\psi \tag{44}$$

$$t_{R+A}^d(\theta) = T_{R+A}(\theta) - e^{-\tau_{R+A}/\mu} \tag{45}$$

Since we also have to take into account the directional effect, see previous report, we already using:

$$\rho_{toa} = \rho_{R+A} + \left[\begin{array}{l} e^{-\tau/\mu_s} e^{-\tau/\mu_v} \rho_{surf}^{est} + e^{-\tau/\mu_v} t_{R+A}^d(\theta_s) \overline{\rho}_{surf}^{est}(\tau_A^{ret}) + e^{-(\tau_R+\tau_A^{ret})/\mu_s} t_{R+A}^d(\theta_v) \overline{\rho}'^{est}_{surf}(\tau_A^{ret}) \\ + t_{R+A}^d(\theta_s) t_{R+A}^d(\theta_v) \overline{\overline{\rho}}_{surf}^{est} \\ + \dfrac{T_{R+A}(\theta_s) T_{R+A}(\theta_v) S_{R+A} \left(\overline{\overline{\rho}}_s\right)^2}{1 - S_{R+A}(\tau_A) \overline{\overline{\rho}}_{surf}^{est}} \end{array} \right] \tag{46}$$

We are proposing to update (46) by using:

$$\rho_{toa} = \rho_{R+A} + \left[\begin{array}{l} e^{-\tau/\mu_s} e^{-\tau/\mu_v} \rho_{surf}^{est} + e^{-\tau/\mu_v} t_{R+A}^d(\theta_s) \overline{\rho}_{surf}^{est}(\tau_A^{ret}) + e^{-(\tau_R+\tau_A^{ret})/\mu_s} t_{R+A}^d(\theta_v) < \overline{\rho}'^{est}_{surf}(\tau_A^{ret}) >_e \\ + t_{R+A}^d(\theta_s) t_{R+A}^d(\theta_v) < \overline{\overline{\rho}}_{surf}^{est} >_e \\ + \dfrac{T_{R+A}(\theta_s) T_{R+A}(\theta_v) S_{R+A} < \overline{\overline{\rho}}_{surf}^{est} >_e}{1 - S_{R+A}(\tau_A) < \overline{\overline{\rho}}_{surf}^{est} >_e} \end{array} \right] \tag{47}$$

Equation (47) is still an approximation of the signal, but will conserve the formalism previously defined, if the target is infinite (in that case (47) becomes (46)), Lambertian (in that case (47) becomes (34)) or both (in that case (47) becomes (33)).

The quantities $\overline{\rho}'^{est}_{surf}(\tau_A^{ret})$ and $\overline{\overline{\rho}}_{surf}^{est}$ could be estimated using the generalized SWIR-VIS relationship for each clear, land pixel of the image. For cloudy pixels it is necessary first to take into account the altitude of the cloud and have a knowledge of the aerosol profile, that means very near to cloud the correction will not be accurate. For water pixels, a method will have to be found to assess their reflectance's, the best method is probably to perform an atmospheric correction based on the "ocean" retrieval scheme results.

Using those quantities, we can compute, $< \overline{\rho}'^{est}_{surf}(\tau_A^{ret}) >_e$ and $< \overline{\overline{\rho}}_{surf}^{est} >_e$ using the operator:

$$\langle \rho \rangle_e = \frac{1}{2\pi} \int_0^{2\pi} \int_0^{\infty} \rho(r,\psi) \frac{dF(r)}{dr} dr d\psi \tag{48}$$

Which can be approximated for an “image” by:

$$\langle \rho \rangle_e = \sum_{j=-n}^{n} \sum_{i=-n}^{n} \frac{dF(r(i,j))}{dr} \rho(i,j) \tag{49}$$

So we will have,

$$< \overline{\rho}'^{est}_{surf}(\tau_A^{ret}) >_e = \sum_{j=-n}^{n} \sum_{i=-n}^{n} \frac{dF(r(i,j))}{dr} \overline{\rho}'^{est}_{surf}(\tau_A^{ret})(i,j) \tag{50}$$

And

$$< \overline{\overline{\rho}}^{est}_{surf} >_e = \sum_{j=-n}^{n} \sum_{i=-n}^{n} \frac{dF(r(i,j))}{dr} \overline{\overline{\rho}}^{est}_{surf}(i,j) \tag{51}$$

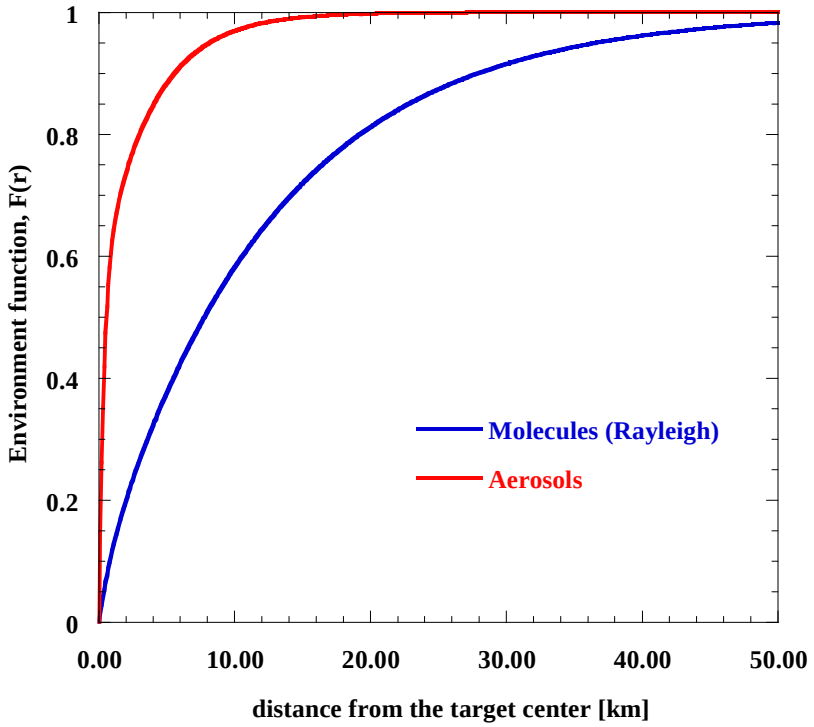

FIGURE 13. ATMOSPHERIC ENVIRONMENT FUNCTION AS A FUNCTION OF THE DISTANCE FROM THE TARGET CENTER, FOR MOLECULES AND AEROSOLS.

In practice, the atmosphere environment function, F(r) as shown in Figure 13, is computed by a weighting average of the individual molecules and aerosol environment functions using their respective upward diffuse transmissions,($\square_d^R(\theta_v)$ and $\square_d^A(\theta_v)$), that is:

$$F(r) = \frac{t_d^R(\theta_v)F^R(r) + t_d^A(\theta_v)F^A(r)}{t_d^{R+A}(\theta_v)} \tag{52}$$

3.2.3 Inversion using Look-Up Tables

Look-up Tables are used to find the aerosol optical properties (optical thickness, phase function, single-scattering albedo, etc.) corresponding to various aerosol models. The tables consist of pre-computed atmospheric parameters, which contribute to the TOA reflectance that would exist at the top of the atmosphere given specific aerosol conditions corresponding to the various aerosol models. The atmospheric parameters for 10 optical depths between the required measurement range of 0 to 2.0 are used. The best fit (least squares) between the observed TOA reflectance and a computed TOA reflectance determines the aerosol model and optical thickness.

The algorithm will use a variety of aerosol models to provide an accurate determination of the aerosol optical thickness. Over land, the tropospheric aerosol varies with latitude, longitude, and season. The geographic area also influences the type of aerosol present. Urban/industrial aerosols have different properties than rural aerosols. Over the ocean, additional LUTs are required to correctly compute the atmosphere-BRDF coupling from sunglint.

3.2.3.1 Mathematical Description of the Algorithm

All LUTs currently being used were generated using the 6S radiative transfer model. The aerosol LUT contains atmospheric parameters corresponding to 21 solar zenith angles, 20 viewing zenith angles, and a variable amount of azimuthal angles between sun and satellite (0 to 180 degrees) depending on the sun and view zenith angle so that the scattering angle step is effectively kept constant. The LUT is also computed for 15 optical thicknesses (0.05 – 2.0) and for 17 aerosol models. The LUT is also computed for each band used in the AOT retrieval. The observed TOA reflectance is compared to the TOA reflectance computed from the atmospheric parameters extracted from the LUT and the optical thickness for that pixel derived. The optical thickness values for all pixels are output to an IP for use with other VIIRS algorithms. The high quality IP pixels are aggregated to the appropriate horizontal cell size for EDR output.

3.2.3.2 General LUT Design

The purpose of using LUT in the AOT determination algorithm is to simplify inversion of the nonlinear RTM with selecting required RTM parameters from precalculated arrays [1]. (for references see Section 2.0). Main features of LUT design have been prescribed in [2]. Design of the current Aerosol LUT corresponds to the document [3].

The variables and other nomenclature presented within this LUT section differ from definitions used previously in this document. The AOT algorithm requires the following RTM parameters to be precalculated:

Downward transmittance, $t^D(m,b,\theta,\tau_{550})$,
Upward transmittance $t^U(m,b,\xi,\tau_{550})$,
Spherical albedo, $a(m,b,\tau_{550})$,
Aerosol optical thickness (AOT), $\tau(m,b,\tau_{550})$,
Atmospheric reflectance, $\rho(m,b,\theta,\xi,\alpha,\tau_{550})$,

where the arguments are:

τ_{550} is AOT at a reference wavelength 550 nm,
m is aerosol model index,
b is VIIRS spectral band index,
θ is solar zenith angle,
ξ is satellite zenith angle and
α is relative azimuth.

The following features of RTM parameters can be used to reduce the size of the aerosol LUT and to optimize its structure [2]:

1. $t^D(m,b,\theta,\tau_{550}) = t^U(m,b,\theta,\tau_{550})$,

2. $\rho(m,b,\theta,\xi,\alpha,\tau_{550}) = \rho(m,b,\xi,\theta,\alpha,\tau_{550})$.

4. ρ is best characterized as a function of θ, ξ and φ, where φ is the scattering angle.

5. For a given θ and ξ, only a limited range of φ exists.

The LUT design exploits some of these features. The LUT stores only one array of atmospheric transmission t^D instead of two separate arrays t^D and t^U. Also, LUT stores ρ as a function of θ, ξ and φ. The angle triplet is stored along a single dimension so only valid values of φ are actually populated in the LUT.

The LUT stores AOT ratios $r=\tau/\tau_{550}$ instead of τ. According to AOT algorithm requirements, parameters t^D, a and ρ are precalculated for both aerosol and Rayleigh scattering, while r accounts for aerosol scattering only.

The LUT is stored as HDF SDS file (HDF4.1r5) [3]. Section 3.2 describes the data structure, which stores LUT data when used by the AOT algorithm. Section 3.3 describes

the process of extracting from the LUT data structure information necessary for AOT determination.

3.2.3.3 LUT Data Structure

The *ReadLUT.c* function reads the file and stores LUT data in the computer memory as a data structure. The description of this data structure is in the include file *Determine_AOT.h*. Memory for most of the structure data members is allocated dynamically based on dimension parameters retrieved from the HDF file and from the include file *AerosolLUT.h*. Table 9 lists the dimension parameters and their sources. Table 10 lists values of arguments (bins), at which LUT dataset are sampled. Table 11 lists dimensions of the HDF file datasets. For clarity of the further discussion we need to discriminate the parameter name and the name of the LUT array containing its discrete values. Both those names where necessary are contained in Tables 7 and 8.

The upper 4 arguments in Table 10 define bin values for all the dimensions of datasets T, A, R and for the first 3 dimensions of P. The lower 4 lines in Table 10 are required to handle the 4th dimension of P. This dimension provides ρ for all possible combinations of θ, ξ and φ bins. The range of φ variations depends on θ and ξ as follows:

$$\varphi_{min} < \varphi < \varphi_{max}, \tag{53}$$

$$\varphi_{min}(\theta,\xi) = 180^{o} - |\theta + \xi| \tag{54}$$

$$\varphi_{max}(\theta,\xi) = 180^{o} - |\theta - \xi| \tag{55}$$

Due to a constant φ increment, $\Delta\varphi$, the number of stored P elements depends on θ and ξ. Array N_B contains these numbers for all pairs (Θ_i, Ξ_j), i=1,2,…,N_θ, j=1,2,…, N_ξ. For each pair (Θ_i, Ξ_j), P elements are arranged in the order of decreasing φ starting with $\varphi_{max}(\Theta_i, \Xi_j)$ as determined in (1b). The array S contains cumulative sums of N_B elements, which point directly at the value of 4th ρ index, which corresponds to φ_{max} for a given pair (Θ_i, Ξ_j). Since S contains essentially the same information as N_B, but is easier to use for data extraction, the AOT algorithm does not store N_B, in the data structure.

TABLE 9. ATMOSPHERIC LUT-ARRAY DIMENSION PARAMETERS

Parameter	Value	Source
Number of aerosol models, N_M	14	*AerosolLUT.h*
Number of VIIRS bands, N_B	10	*AerosolLUT.h*
Number of LUT attributes, N_A	9	*AerosolLUT.h*
Number of LUT datasets, N_D	4	*AerosolLUT.h*
Number of output arrays, N_O	5	*AerosolLUT.h*
Number of τ_{550} bins N_τ	15	HDF file
Number of θ^S bins, N_S	21	HDF file
Number of θ^V bins, N_V	20	HDF file
Total number of combinations of θ^S and θ^V bins, $N_{SV}=N_S*N_V$	420	HDF file
Total number of φ bins for all combinations of θ^S and θ^V bins, N_φ	5309	HDF file

TABLE 10. ATMOSPHERIC LUT-HDF FILE ATTRIBUTES.

Argument	LUT variable name	Dimension	Bin values
Aerosol model names		N_M	Dust, SmokeHigh, SmokeLow, UrbanClean, Urbanpolluted, OceanFine1, OceanFine2, OceanFine3, OceanFine4, OceanCoarse1, OceanCoarse2, OceanCoarse3, OceanCoarse4, OceanCoarse5
VIIRS band		N_λ	M1, M2, M3, M4, M5, M6, M7, M8, M10, M11
τ_{550}		N_τ	0.01, 0.05, 0.10, 0.15, 0.20, 0.30, 0.40, 0.60, 0.80, 1.00, 1.20, 1.40, 1.60, 1.80, 2.00
θ	Θ	N_θ	0^o, 4^o, 8^o, 12^o, 16^o, 20^o, 24^o, 28^o, 32^o, 36^o, 40^o, 44^o, 48^o, 52^o, 56^o, 60^o, 64^o, 68^o, 72^o, 76^o, 80^o
ξ	Ξ	N_ξ	0.0^o, 2.84090^o, 6.52107^o, 10.22295^o, 13.92975^o, 17.63841^o, 21.34798^o, 25.05805^o, 28.76843^o, 32.47901^o, 36.18973^o, 39.90054^o, 43.61144^o, 47.32240^o, 51.03339^o, 54.744420, 58.45547^o, 62.16656^o, 65.87766^o, 69.58876^o
Total number of φ bins for all combinations of θ^S and θ^V bins	N_φ	1	5309
φ increment	$\Delta\varphi$	1	4^o
Number of φ bins given θ and ξ bins	M	N_{SV}	Depending on Θ and Ξ bins.
Cumulative sums of $N_{\varphi SV}$ elements	S	N_{SV}	$S_0=0$, $S_i= S_{i-1}+ M_{i-1}$, $i>0$

TABLE 11. ATMOSPHERIC LUT-DATASET DIMENSIONS

Parameter	Dataset name	Number of dimensions	Dimensions
t^D	T	4	$N_M\times N_\tau\times N_B\times N_S$
a	A	3	$N_M\times N_\tau\times N_B$
r	R	3	$N_M\times N_\tau\times N_B$
ρ	P	4	$N_M\times N_\tau\times N_B\times N_\varphi$

3.2.3.4 Extracting data from the LUT structure

The inputs for the LUT data extraction function ExtractAerosolLUTData.c are solar zenith angle θ_0, satellite zenith angle ξ_0, relative azimuth α_0, aerosol model index m and band

index b. Based on these data, the function fills an output array $D_{n,p}$, $0 \le n \le N_\tau - 1$, $0 \le p \le 4$, where N_τ is a number of τ_{550} bins and p is a number of output RTM parameters t^D, t^U, a, r and ρ for given,

Parameters a and r are simply transferred into the 3rd and the 4th columns of the output array exactly as they appear in the LUT data structure:

$$D_{n3}=A_{m,n,b}, \quad (56)$$

$$D_{n4}=R_{m,n,b}, \quad (57)$$

The angular-dependent parameters t^D, t^U, ρ are given in the LUT for discrete bins of θ, ξ, φ while actual angles θ_0, ξ_0, φ_0 vary continuously. In order to preserve required retrieval accuracy, t^D, t^U, ρ are interpolated to θ_0, ξ_0, φ_0 before filling the output array.

Output t^D values go to the 1st column of the output array. These values are obtained with linear interpolation of T between the neighboring solar zenith angle bins Θ_i and Θ_{I+1}:

$$D_{n1}=T_{m,n,b,i}+(T_{m,n,b,i+1}-T_{m,n,b,i})*(\theta_0 - \Theta_i)/\Delta\theta, \qquad \Theta_i \le \theta_0 < \Theta_{i+1}. \quad (58)$$

Similarly, output t^U values fill the 2nd column of the output array. These values are obtained by linear interpolation of T between the neighboring bins satellite zenith angle Θ_j and Θ_{j+1}:

$$D_{n,2}=T_{m,n,b,j}+(T_{m,n,b,j+1}-T_{m,n,b,j})*(\xi_0 -\Theta_j)/\Delta\theta, \qquad \Theta_j \le \xi_0 < \Theta_{j+1}. \quad (59)$$

$\Delta\theta$ in (3) and (4) is a constant solar zenith angle increment.

The 5th column of the output array contains output ρ values. The interpolation of ρ is more complicated. This parameter is stored in the LUT dataset P as a function of 2 angular variables θ and φ. φ is a scattering angle, which is a function of θ, ξ, α:

$$\varphi(\theta,\xi,\alpha)=\mathrm{acos}(-\sin(\theta)\sin(\xi)\cos(\alpha) - \cos(\theta)\cos(\xi)). \quad (60)$$

The interpolation of ρ is carried out as follows.

1. For θ_0, ξ_0, lower and upper bins are found: $\Theta_i \le \theta_0 < \Theta_{i+1}$, $\Xi_j \le \xi_0 < \Xi_{j+1}$.
2. For each of 4 pairs of bins, (Θ_{i+u},Ξ_{j+v}), u=0,1, v=0,1, the scattering angle $\varphi(\Theta_{i+u},\Xi_{j+v})$ is found according to (6):

   $$\varphi(u,v) = \varphi(\Theta_{i+u}, \Xi_{j+v},\alpha_0). \quad (61)$$

3. For each of 4 pairs of bins, (Θ_{i+u},Ξ_{j+v}), u=0,1, v=0,1, the indices m(u,v) are found, which point at the P elements corresponding to upper scattering angle bin for $\varphi(u,v)$:

   $$m(u,v) = S_{x(u,v)}+k(u,v), \quad (62)$$

$x(u,v)=(i+u)*N_{\xi}+(j+v)$, (63)

$\varphi_{max}(u,v)-\Delta\varphi*k(u,v)\geq\varphi(u,v)>\varphi_{max}(u,v)-\Delta\varphi*(k(u,v)+1)$, (64)

where u=0,1, v=0,1, $\varphi_{max}(u,v)=\varphi_{max}(\Theta_{i+u},\Xi_{j+v})$ as determined by (1b), $\Delta\varphi$ is a constant scattering angle increment.

4. For each of 4 pairs of bins, (Θ_{i+u},Ξ_{j+v}), u=0,1, v=0,1, elements of P are interpolated to $\varphi(u,v)$:

$$\rho^*(u,v)=P_{m,n,b,m(u,v)}+(P_{m,n,b,m(u,v)}-P_{m,n,b,m(u,v)+1})*(\varphi(u,v)-\varphi_{max}(u,v)+\Delta\varphi*k(u,v))/\Delta\varphi. \quad (65)$$

5. The final interpolated estimate of atmospheric reflectance is found by 2D interpolation of $\rho^*(u,v)$, u=0,1, v=0,1, to the actual pair of solar and satellite zenith angles (θ_0,ξ_0):

$\rho^{**}(v)= \rho^*(0,v)+(\rho^*(1,v)-\rho^*(0,v))*(\theta_0-\Theta_i)/\Delta\theta$, v=0,1; (66)

$D[n][3]= \rho^{**}(0)+(\rho^{**}(1)-\rho^{**}(0))*(\xi_0 - \Xi_j)/(\Xi_{j+1} - \Xi_j)$. (67)

(9b) gives an output interpolated value of atmospheric reflectance for the input angles $(\theta_0,\xi_0, \alpha_0)$.

3.2.3.5 Conclusions

The Aerosol LUT has been designed and generated based on the requirements of the AOT Determination algorithm. The algorithm of extracting and angular interpolation of Aerosol LUT information has been developed and incorporated into the AOT Determination algorithm.

3.2.4 Calculation of Size Parameter

3.2.4.1 Physics of the Problem

The aerosol size parameter is defined as the Ångström wavelength exponent (α), where:

$$\alpha = -\frac{\ln\tau_1 - \ln\tau_2}{\ln\lambda_1 - \ln\lambda_2} \quad (68)$$

The SRD definition requires that bands 1 and 2 be narrow bands separated by at least 200 nm. If the aerosol particle size distribution is given by an inverse power law, such as a Junge distribution, then alpha can be related to the exponent in the power law.

The effective radius is defined as “the area weighted average radius of the aerosol particle size distribution, or equivalently, the ratio of the third to the second moments of the size distribution” *[Y-1].*

$$r_{eff} = \frac{\int r^3 \frac{dN(r)}{d\ln(r)} d\ln(r)}{\int r^2 \frac{dN(r)}{d\ln(r)} d\ln(r)} \quad (69)$$

3.2.4.2 Mathematical Description of the Algorithm

The Ångström exponent is calculated directly from the derived optical thicknesses of two bands using Equation (68). For effective radius, two approaches are available, in the first case and where we should expect the best is when the aerosol model has been identified using the multispectral approach, in the second when we have identified the model using angstrom exponent or suspended matter.

3.2.4.3 Direct approach

If an aerosol model has been successfully inverted using the multispectral approach, the effective radius can be directly computed using the size distribution of the dynamic model at the retrieved aerosol optical depth. In practice, the effective radius will be pre-computed as a function of optical depth and dynamic aerosol model.

3.2.5 Filling Bright Pixels with Interpolation or NAAPS / Climatology

This approach is used for the AOT IP only. The AOT EDR does not utilize NAAPS or climatology data.

3.2.5.1 The Interpolation Algorithm

The AOT retrieval algorithm fails to provide reliable retrieval of AOT if the underlying surface is excessively bright or when other exclusion conditions exist. The estimate of AOT over bright pixels can be obtained from the following sources. 1) If the bright area is small enough, one can expect that AOT over this area is almost the same as over surrounding dark pixels. In this case the AOT estimate can be obtained from interpolation. 2) If the bright area is too big to rely on spatial correlation between AOT at the edges of the bright

area and in the middle of it, an aerosol forecast model such as NAAPS or regional AOT climatology can be used if the forecast model data is not available. A special routine has been incorporated in the AOT module in order to provide AOT estimates over bright areas from these sources. After the AOT retrieval is done for all dark pixels in a whole granule of x×y pixels, the algorithm attempts to fill bright pixels by interpolation between the nearest dark pixels and/or by using NAAPS data (granulated to the VIIRS swath) or monthly climatology AOT value for a given region. The NAAPS / climatology is used only if the total weight of dark pixels within a certain neighborhood (searching window) of a current bright pixel is insufficient for interpolation. As a result, the algorithm fills small bright areas with interpolated AOTs, fills inner parts of extended bright areas (deserts, snow/ice) with NAAPS / climatology AOT and provides a smooth transition from interpolation to NAAPS / climatology at the edges of extended bright areas.

In general, AOT for the current bright pixel $\tau_{brt}(i_0,j_0)$ is calculated as a weighted sum of interpolated AOT, $\tau_{int}(i_0,j_0)$, and the NAAPS / climatology AOT, τ_{clim}:

$$\tau_{brt}(i_0,j_0)=p_{int}\tau_{int}(i_0,j_0)+p_{clim}\tau_{clim}, \quad (70)$$

$$p_{int}+p_{clim}=1$$

$\tau_{int}(i_0,j_0)$ is calculated as a weighted sum of retrieved AOT values $\tau_{ret}(i,j)$ for all pixels (i,j) within a searching window surrounding the current pixel. Accumulation of the weighted sum is performed sequentially over expanding squares, from the center of the searching window to its edges:

$$S_K=\sum_{i=i_0-K}^{i_0+K}\sum_{j=j_0-K}^{j_0+K} w(i-i_0,j-j_0), \quad (71)$$

$$\tau_{int\,K}(i_0,j_0)=\left[\sum_{i=i_0-K}^{i_0+K}\sum_{j=j_0-K}^{j_0+K}\tau_{ret}(i,j)w(i-i_0,j-j_0)\right]/S_K, \quad (72)$$

where K=1,2,…,DIST, i,j are coordinates of pixels, neighboring to the current bright one, DIST is a maximum distance (in pixels) from the current pixel within which pixels are participating in the interpolation. In fact, DIST determines the size of the searching window, which is 2DIST+1. The final AOT interpolated estimate, $\tau_{int}(i_0,j_0)$ is defined as

$$\tau_{int}(i_0,j_0)= \tau_{int\,K0.5}(i_0,j_0), \quad (73)$$

where $K_{0.5}$ is equal to the minimum K value at which, at which

$$S_{K0.5} \geq 0.5S_{DIST}, \quad (74)$$

S_{DIST} is the maximum possible value of the accumulated sum for the entire searching window:

$$S_{DIST}=\sum_{i=i_0-DIST}^{i_0+DIST}\sum_{j=j_0-DIST}^{j_0+DIST} w(i-i_0,j-j_0), \quad (75)$$

The weights w in (2,3,6) are determined as follows:

$w(i-i_0,j-j_0)=f(i-i_0,j-j_0)$ if the (i,j) pixel is “dark”

$w(i-i_0,j-j_0)=0$ if the (i,j) pixel is “bright”,

The function $f(i-i_0,j-j_0)$ decreases with the distance from the current pixel:

$$f(i-i_0,j-j_0)=\exp(-((i-i_0)^2+(j-j_0)^2)/(3\sigma)),\ \sigma=(DIST/2)^2. \quad (76)$$

This way of pixel accumulation, from the window center to its edges with stopping when the condition (5) is met, allows suppressing the influence of the far outliers within the searching window if there are enough dark pixels for interpolation in the close neighborhood of the bright pixel. On the other hand, if the amount of the dark pixel at the window center is insufficient, the interpolation accounts for distant dark at the edges of the searching window. Another advantage of this method of interpolation is that it requires the accumulation of fewer pixels than accumulation over the entire searching window. This reduces execution time required for interpolation.

The maximum value of S_{DIST}, S_{max}, takes place if all pixels within the entire searching window are dark:

$$S_{MAX}=\sum_{i=i_0-DIST}^{i_0+DIST}\sum_{j=j_0-DIST}^{j_0+DIST} f(i-i_0,j-j_0). \quad (77)$$

Intuitively, in this case the best interpolation accuracy is achieved. The interpolation accuracy deteriorates when the amount of dark pixels within the window is getting less or when they move farther from the window center. Since this corresponds to decreasing S_{DIST} from S_{MAX} to lesser values, the ratio S_{DIST}/S_{MAX} can be used as a measure of interpolation accuracy. When S_{DIST}/S_{MAX} becomes less than a certain threshold value Δ, the algorithm invokes NAAPS / climatology where possible to construct AOT estimate as a weighted sum of interpolation and NAAPS /climatology (1). According to that, relative contributions of interpolation and NAAPS / climatology into the final AOT estimate are:

$p_{int} = 1$, $p_{clim} = 0$ if the NAAPS / climatology AOT is unavailable or $S_{DIST}/S_{MAX}\geq\Delta$, (78)

$p_{int} = \Delta^* S_{MAX}/S_{DIST}$, $p_{clim}=1 - \Delta^* S_{MAX}/S_{DIST}$ if the NAAPS / climatology AOT is available and $S_{DIST}/S_{MAX}<\Delta$. (79)

As a result, the algorithm involves two user-defined parameters: the half-size of a searching window DIST and the interpolation threshold Δ. In our tests, we put DIST=20 and Δ=0.1 .

The interpolation algorithm marks pixels, filled with interpolation, NAAPS / climatology and with the mix of both with the special flag, qf_data.aotqf. This flag, which is initially set to 1 for all bright pixels, after the interpolation gets the following values:

qf_data.aotqf=2 for interpolation,

qf_data.aotqf=3 for interpolation + NAAPS / climatology,

qf_data.aotqf=4 for NAAPS / climatology.

The climatology AOT values are selected from the file aot_climatology.dat given the bright pixels’ latitudes and longitudes and the land/sea flag. The separate AOT models are used for such land regions as Far North, Far South, Sahara and Arabian deserts and for a

number of arid zones. If the pixel coordinates do not fall into the ranges for any specific region, the default and or sea aerosol models are used depending on the land/sea flag.

The parameters controlling the process of interpolation are set up in the Determine_AOT.f file. These parameters are:

DIST	searching window half-size (currently DIST=40)
DELTA	The threshold for using climatology (currently DELTA=0.1)
CLIMMODDIM	The number of climatic aerosol models used
DEFAULT_LAND	The number of default aerosol model for land
DEFAULT_OCEAN	The number of default aerosol model for ocean.

Currently DIST=40, DELTA=0.1, CLIMMODDIM=15, DEFAULT_LAND=13, DEFAULT_OCEAN=14, MONTH=6.

3.2.5.2 Constructing AOT Climatology

The most extended bright areas of the Earth's surface, over which climatology can be the only source of AOT estimates, typically correspond to snow and ice surfaces at high latitudes in the winter and to deserts covered with sand. We have made an attempt to construct AOT climatology for these regions from data of the AeroNet network. This network includes ground based photometric measurements of AOT at a large number of sites around the globe (see Figure 14). Cloud-free, quality assured sets of AOT measurements are available at the web site http://aeronet.gsfc.nasa.gov. In the ideal, AeroNet sites provide information about AOT throughout a year on the following wavelengths: 1020, 870, 670, 500, 440, 380, 340 nm. However, for some stations not all wavelengths are available and not for all months. In this study, we construct regionally averaged monthly mean AOT values for 6 regions from the monthly AOT for separate stations north of 40^{o}N and at the vicinity of the Sahara desert and the Arabian Peninsula[*)].

Besides AeroNet data for the regions, mentioned above, we have established AOT models for some arid zones of the Earth's surface, and the default models for land and ocean. The AOT models for arid zones are chosen given their coordinates and the land/sea flag. The default model for land is chosen if the coordinates of the bright pixel do not fall into any of other land regions and the land/sea flag points at "land". The ocean default model is chosen for all ocean pixels between 60^{o}N and 60^{o}S.

It is assumed that AOT values for all regions except the Far North region correspond to the land surface. According to that, the interpolation algorithm chooses an appropriate regional AOT climatology if the pixel coordinates fall into a proper latitudinal and longitudinal ranges and a sea/land flag corresponds to "land". For the Far North region only coordinate ranges are checked because we assume that the AOT climatology in this region is valid both over land and sea ice.

[*)] We thank the PI investigators of AERONET sites and their staff for establishing and maintaining the sites used in this investigation

Figure 15 shows locations of AeroNet sites north of 50°N. This area has been divided into 4 regions: Far North, America, Europe and Russia. Figures 16 to 19 show regionally averaged monthly mean AOT at the AeroNet wavelengths. Error bars on each plot show the standard deviation of regional AOTs. The error bars have zero extension when less than 2 sites within a given region provide measurements at a given wavelength.

Measurements in the Far North region are available only from March to October due to the polar night. One common feature of America, Europe and Russia regions is that both regional mean AOTs and their standard deviations are getting remar 0.5 ss in the winter season. The AOT standard deviations are also relatively small for the Far North region. This gives us a hope that the regional means of AOT for winter months in these regions are not too far from reality. Figure 20 shows spectral dependencies of regional mean AOT for each month and for 4 regions. The stars on those plots correspond to the VIIRS wavelengths, which are used in AOT retrieval. The AOT for wavelengths longer than 1020 μm, which are beyond the range of AeroNet wavelengths, should be found with extrapolation. On the Figures 16 to 19, mean AOT for those wavelengths are assumed to be equal to AOT at 1020 μm.

Figure 21 shows locations of AeroNet stations in the vicinity north of the Sahara desert and the Arabian Peninsula. For those regions, Figures 22 and 23 show monthly mean AOT at the AeroNet wavelengths. Unfortunately both regional mean AOT and their standard deviations are big enough for the desert regions throughout the year. This means that big spatial variability of AOT takes place over deserts, and the regional AOT means provide only rough estimate of the real AOT. Figure 24 shows spectral dependencies of regional mean AOT for each month and for 2 deserts separately and the average spectral dependency over both deserts.

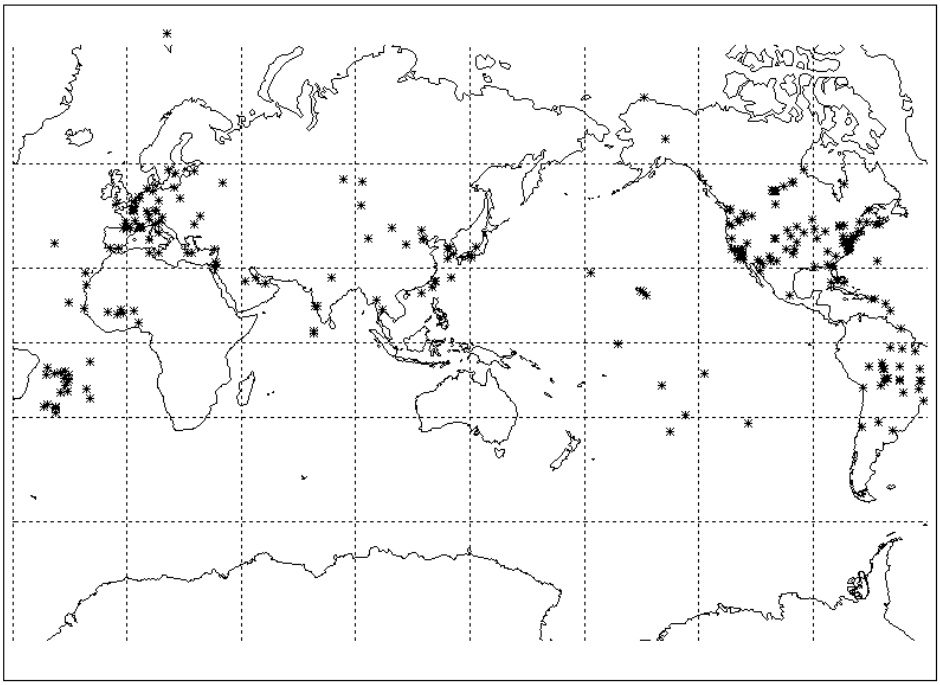

FIGURE 14. LOCATION OF GLOBAL AERONET SITES.

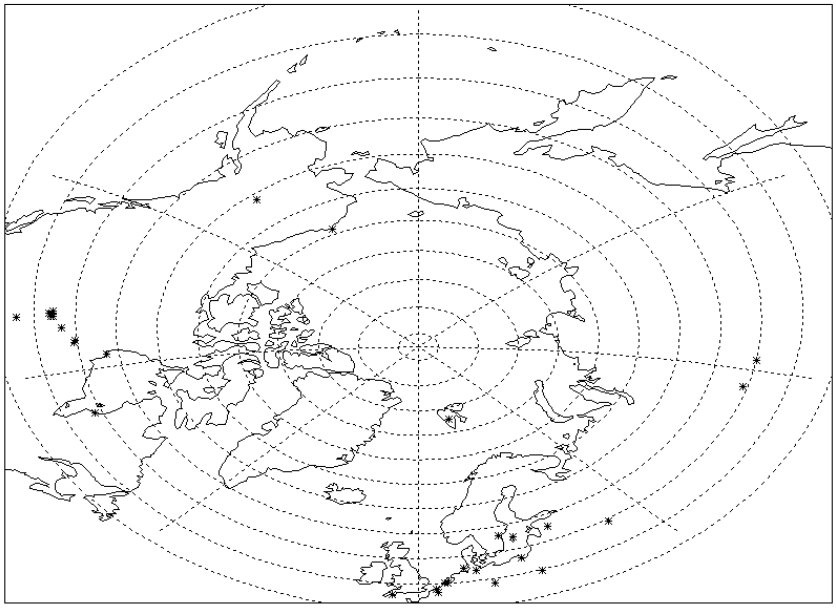

FIGURE 15. LOCATIONS OF AERONET SITES NORTH OF 50^{O}N.

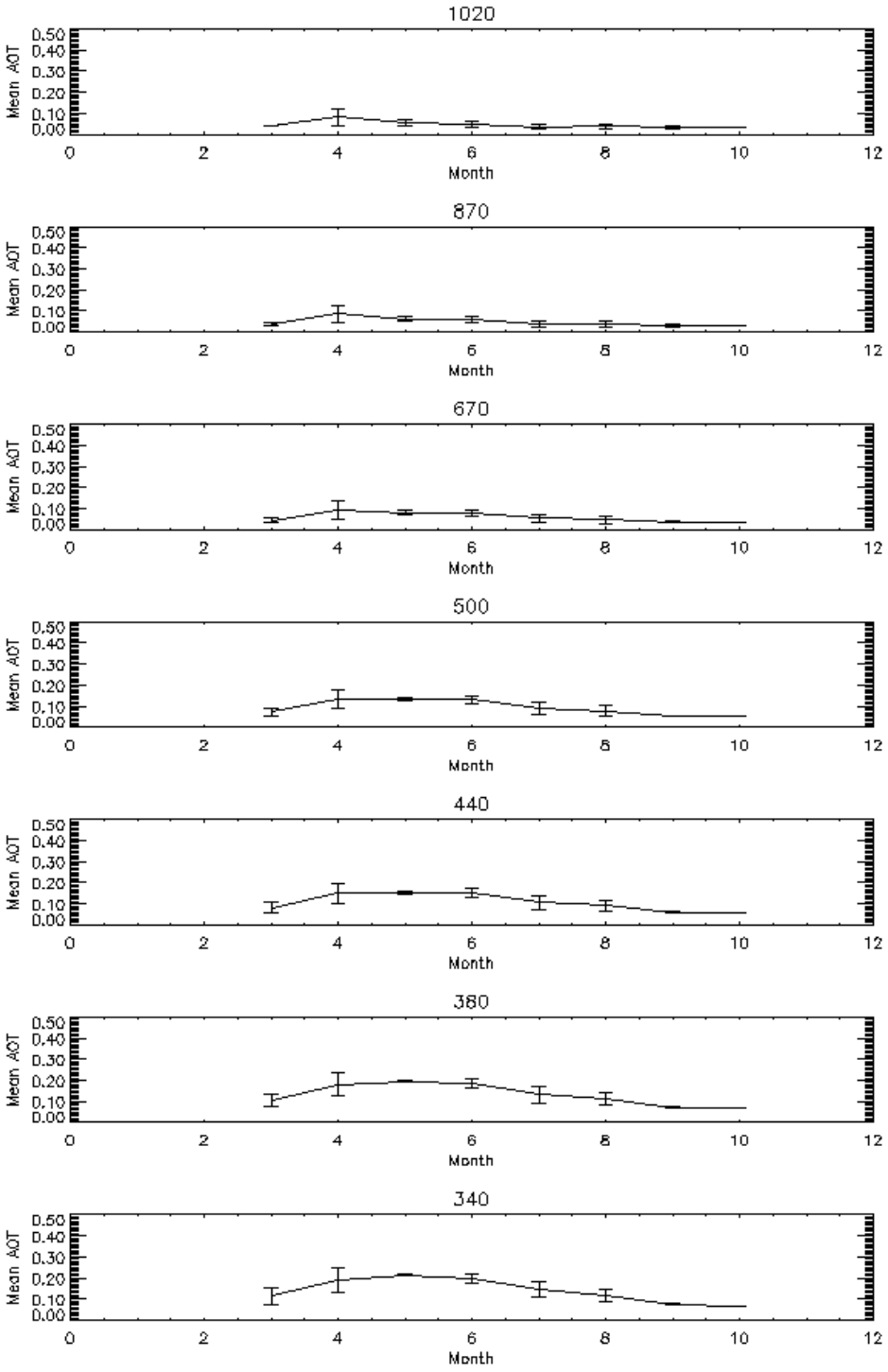

FIGURE 16. MEAN MONTHLY AOT FOR FAR NORTH REGION.

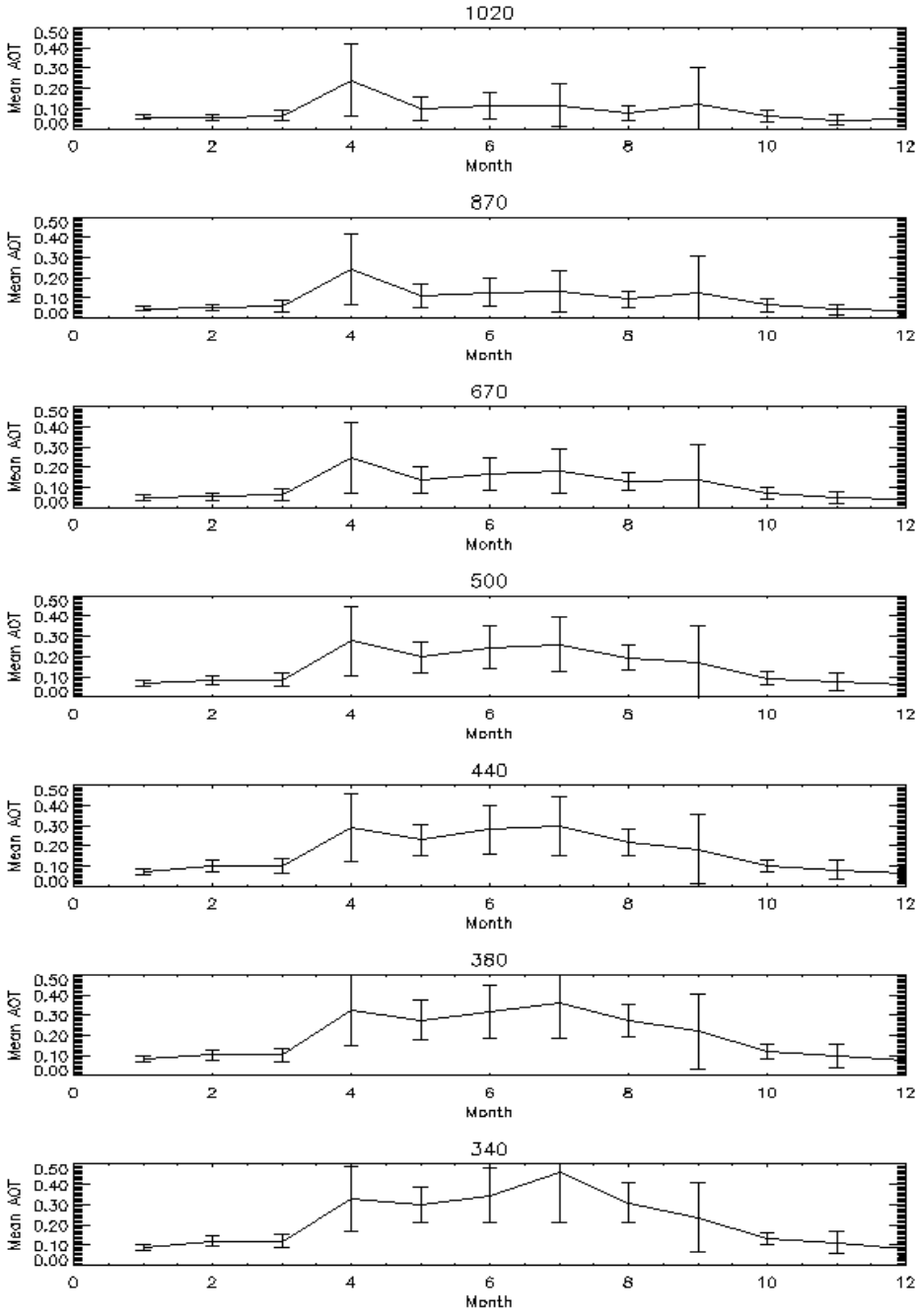

FIGURE 17. MEAN MONTHLY AOT FOR AMERICA.

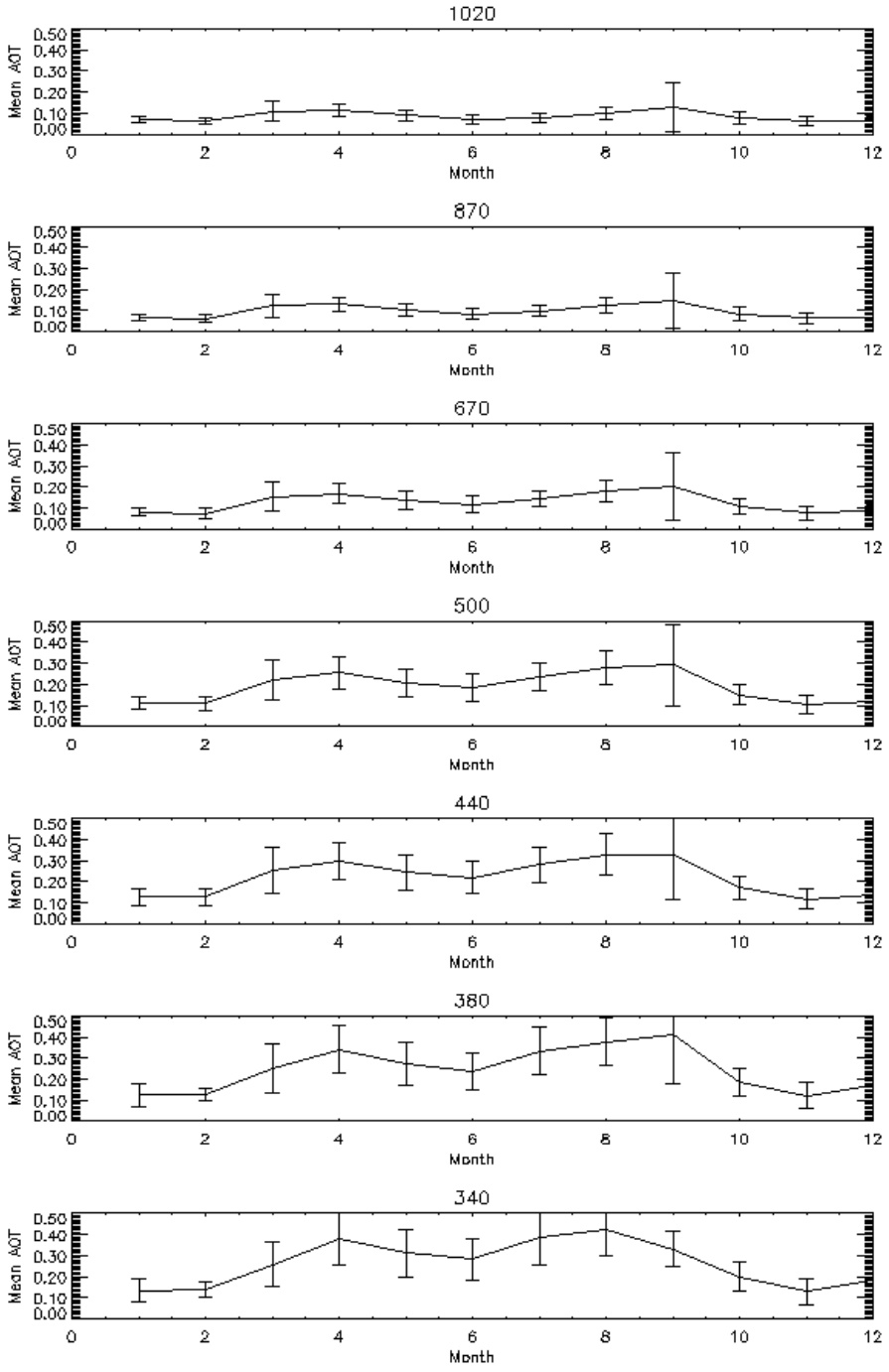

FIGURE 18. MEAN MONTHLY AOT FOR EUROPE.

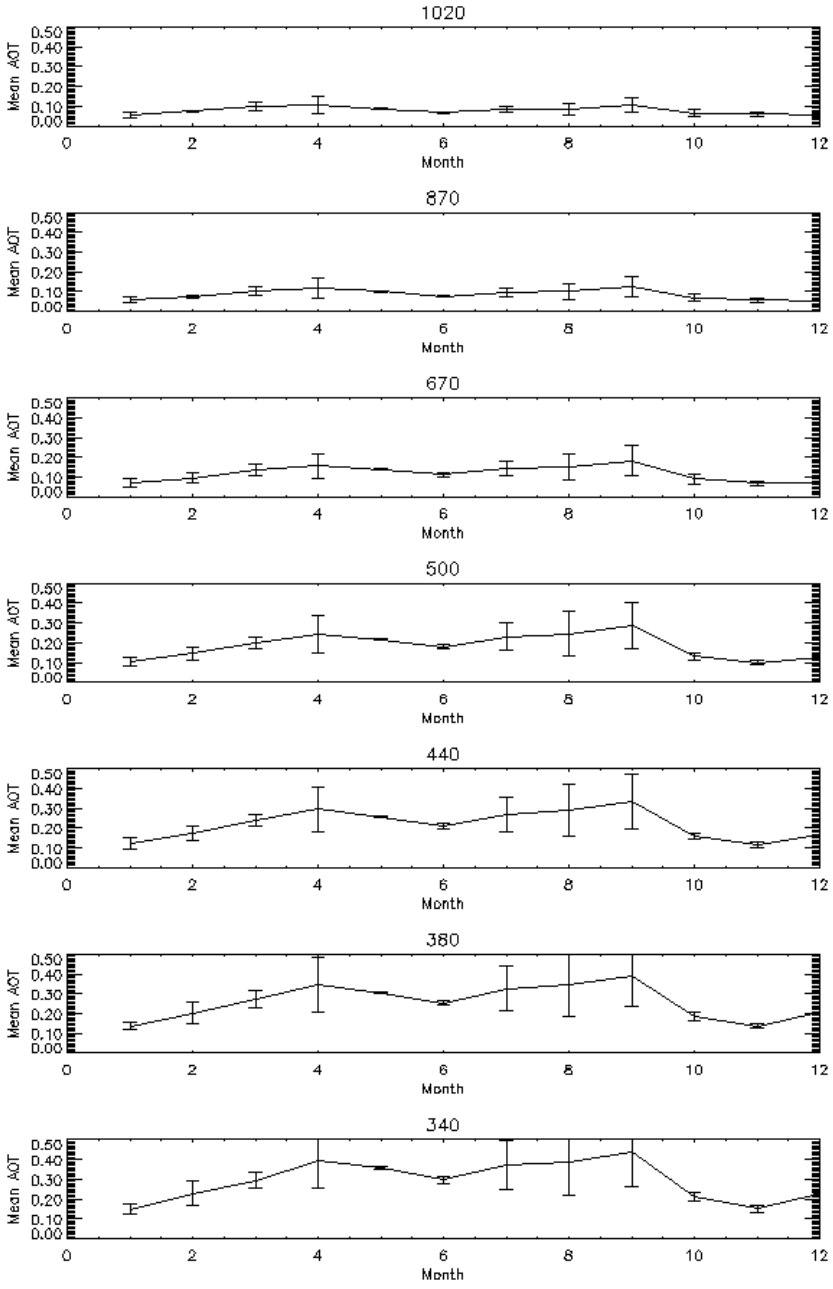

FIGURE 19. MEAN MONTHLY AOT FOR RUSSIA.

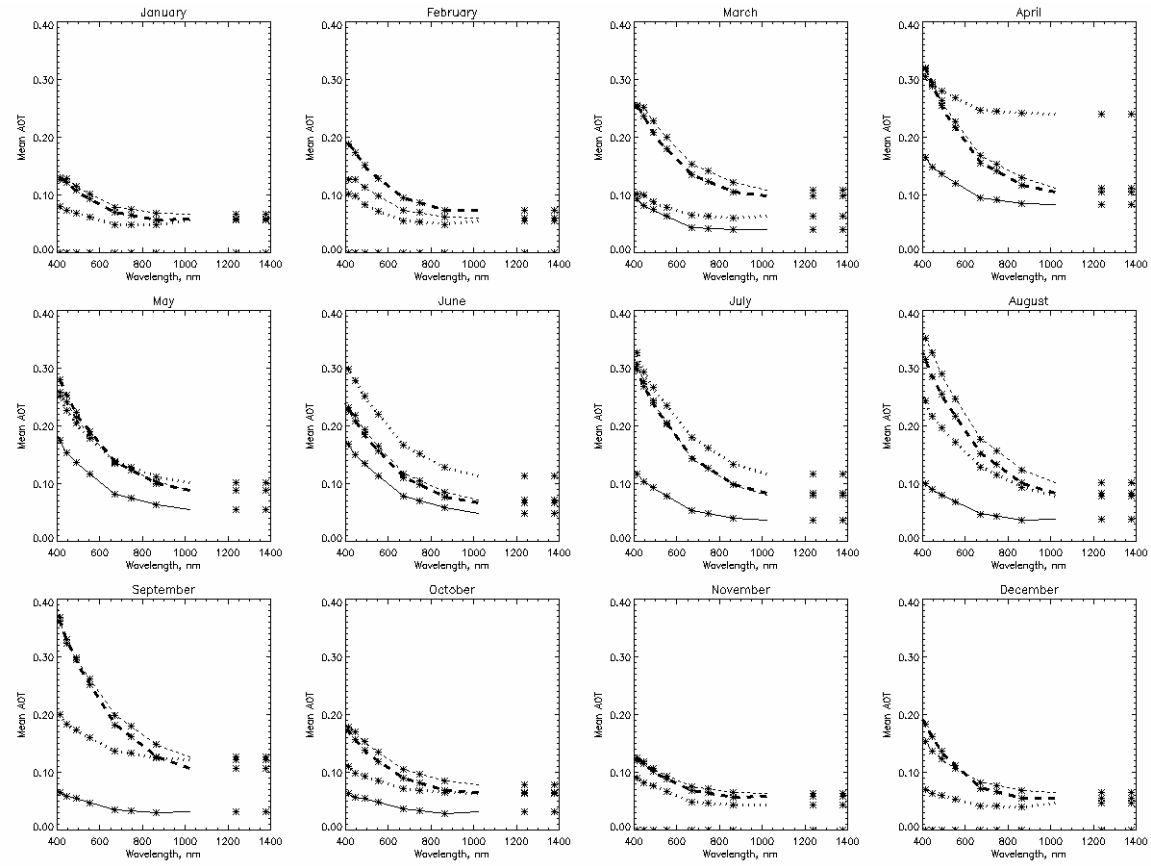

FIGURE 20. INTERPOLATED SPECTRAL DEPENDENCIES OF REGIONAL MONTHLY MEAN AOTS. STARS SHOW THE VIIRS WAVELENGTHS. CURVES FOR EUROPE, RUSSIA, AMERICA AND THE FAR NORTH ARE SHOWN FROM TOP TO BOTTOM ON EACH PLOT RESPECTIVELY.

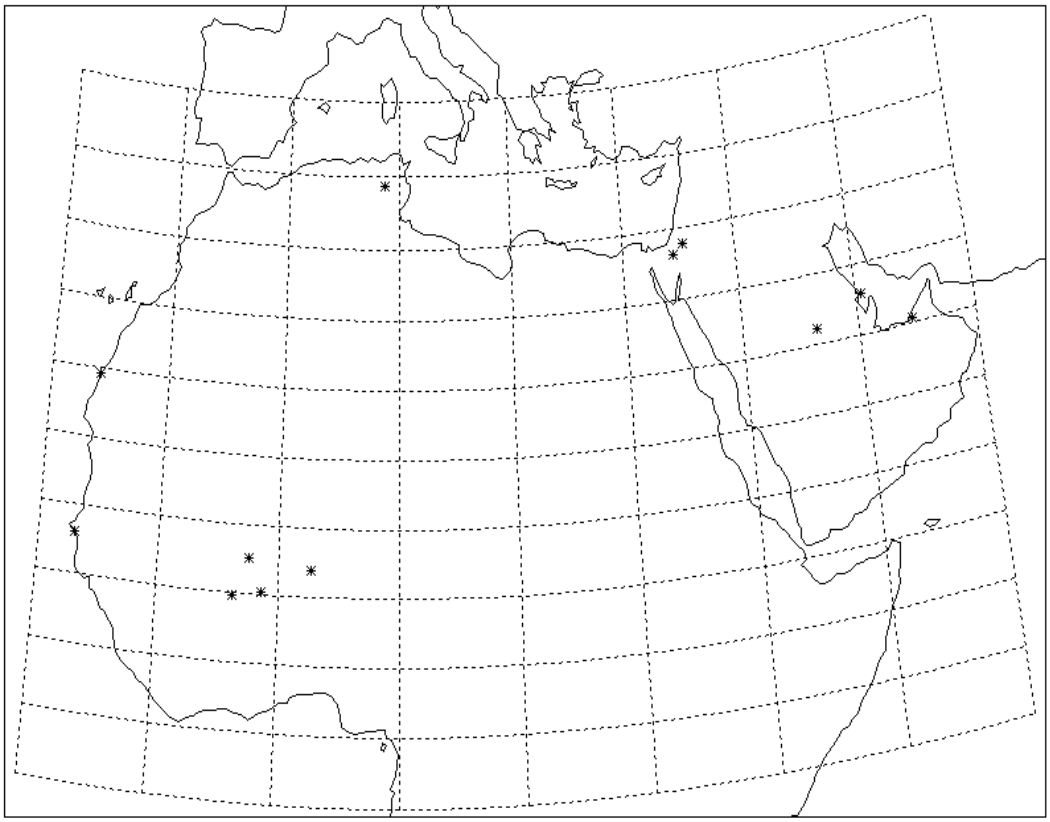

FIGURE 21. LOCATIONS OF AERONET SITES AROUND THE SAHARA DESERT AND ARABIAN PENINSULA.

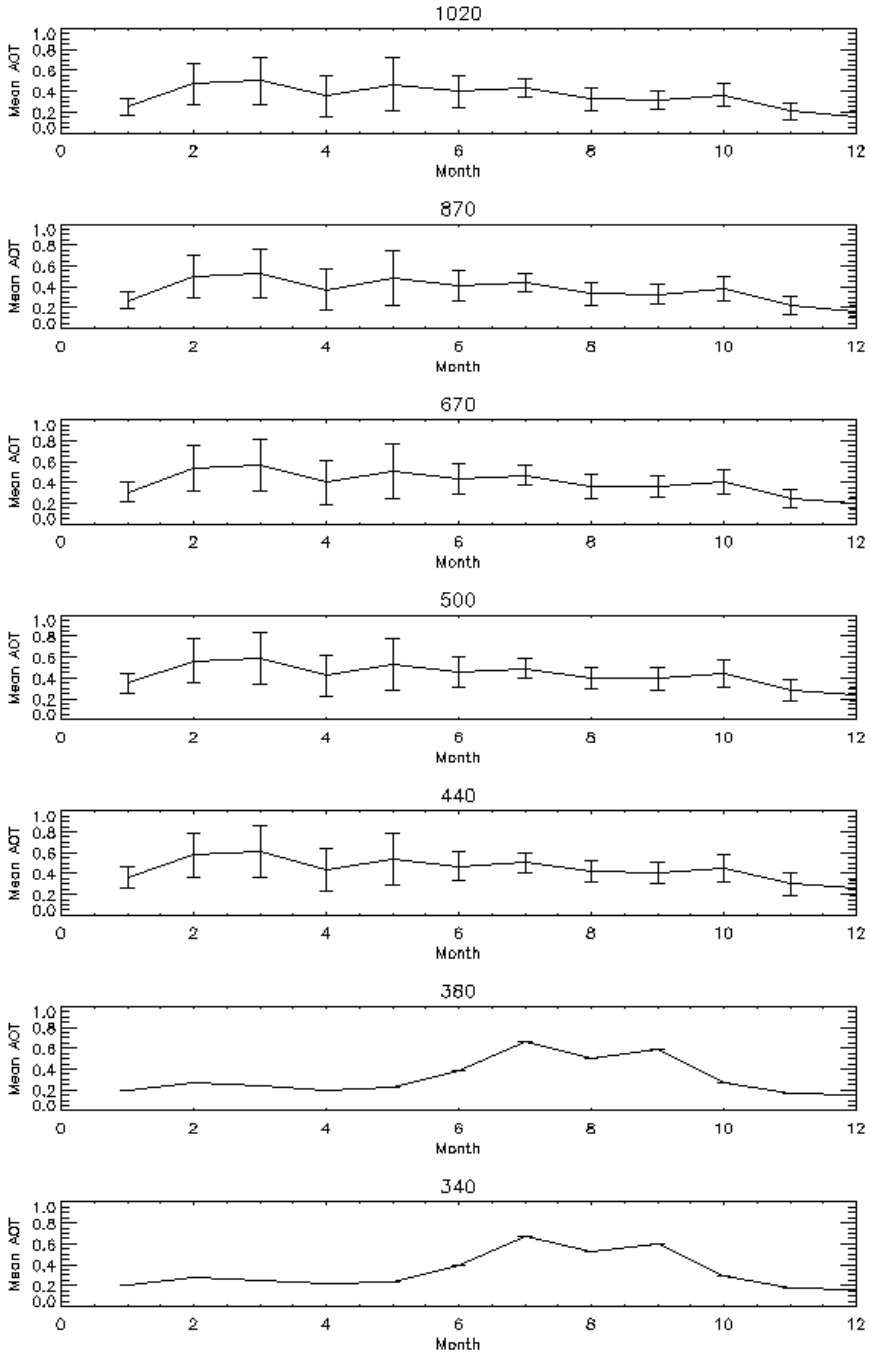

FIGURE 22. MEAN MONTHLY AOT FOR SAHARA DESERT.

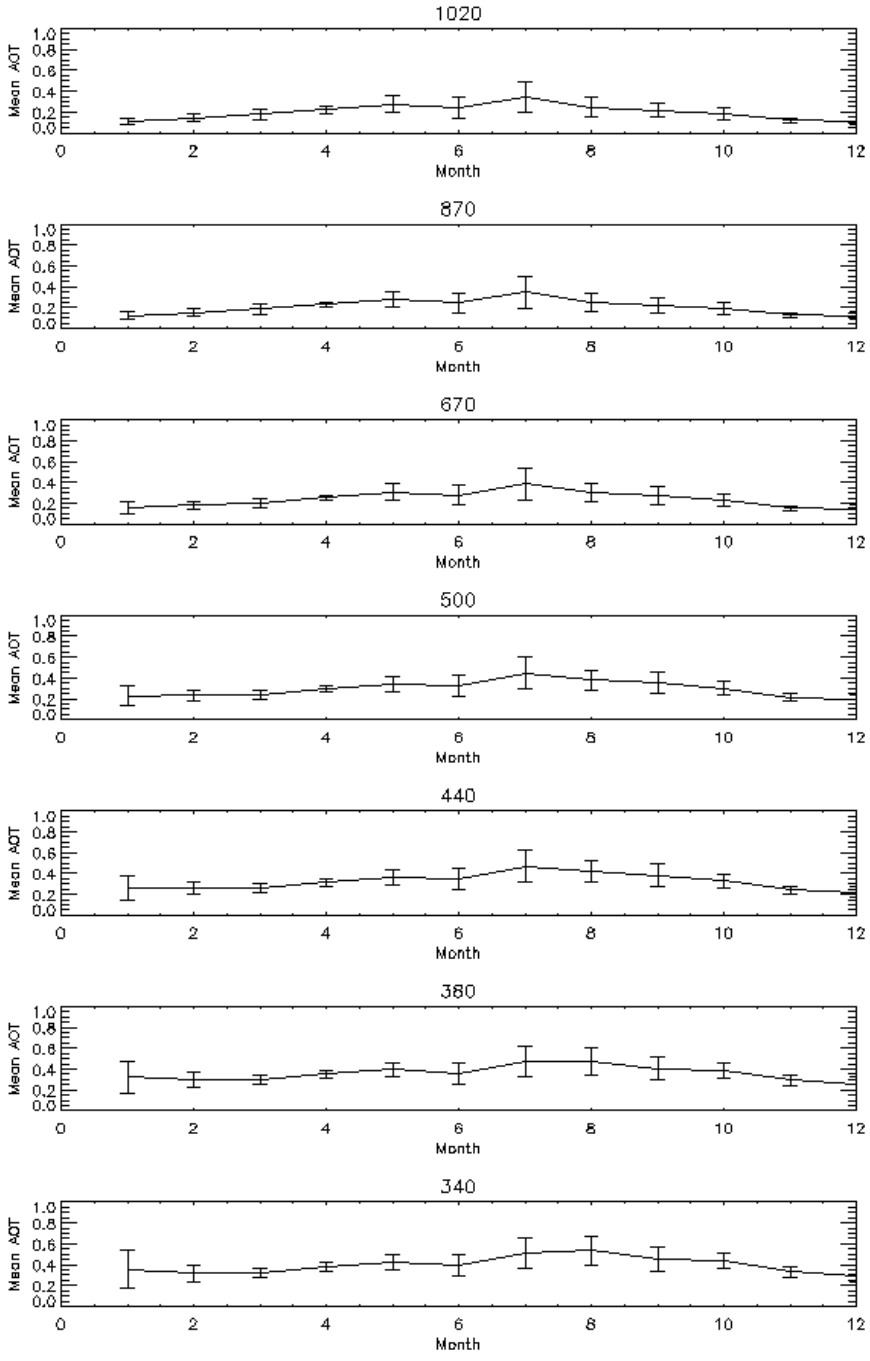

FIGURE 23. MEAN MONTHLY AOT FOR SAHARA DESERT.

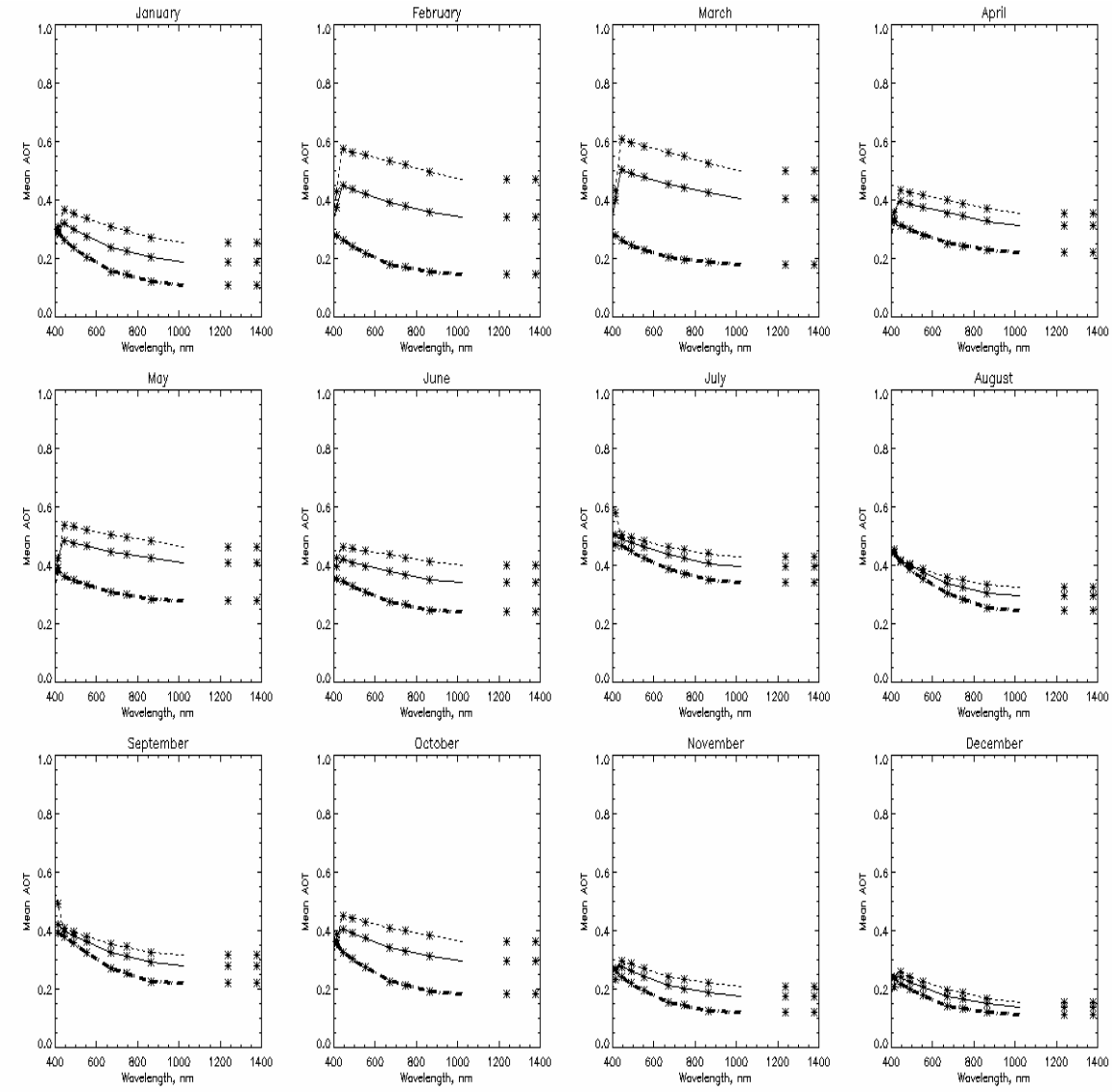

FIGURE 24. INTERPOLATED SPECTRAL DEPENDENCIES OF REGIONAL MONTHLY MEAN AOTS. STARS SHOW THE VIIRS WAVELENGTHS. THE SAHARA, AN AVERAGE FOR BOTH DESERTS AND ARABIA ARE GIVEN AS TOP, MIDDLE AND BOTTOM CURVES RESPECTIVELY.

3.2.6 Error Budget

The accuracy of the algorithm is a function of all the errors affecting the product. The major source of errors in the derived aerosol optical thickness and size parameter are uncertainties in the surface reflectance and in the aerosol model used to generate LUTs for retrieval. For ocean surface, the main uncertainties in the surface reflectance are related to contamination by sunglint and whitecaps. To estimate their impact on the optical thickness, we can add errors separately to the reflectance for each channel according to the procedures used by Kaufman *et al*. (1997) for MODIS aerosol retrievals. Over land, the error is mainly due to unexpected surface properties and to contamination by snow, ice or water. These errors are based on control of the surface reflectance in selecting dark targets. Aerosol model uncertainties primarily affect the LUT values through uncertainties in the aerosol indices of refraction and through the assumption of spherical particles (Mishchenko *et al.*, 1995). These uncertainties may be examined by checking the sensitivity of retrieval products with respect to refractive index (or single scattering albedo) and asymmetry parameter.

Other errors may be introduced indirectly to the final EDR products. These include instrument calibration and stability error, geolocation mapping error and errors in ancillary data. All the errors are discussed in detail in the “VIIRS Error Budget” document *[Y3249]*, which generally suggests accuracy and precision errors of ~0.015 and ~0.014 respectively over ocean and ~0.062 and ~0.038 over land respectively.

3.3 PRACTICAL CONSIDERATIONS

3.3.1 Numerical Computation Considerations

The aerosol retrieval algorithms over land and ocean are based on the LUT technique. The linear interpolation on the LUTs is used to derive optical thickness from grid values on the table. Extrapolation of the LUT is not permitted to ensure reasonable physical meaning. The error introduced from the interpolation is much less than that from the uncertainty in the surface reflectance, aerosol model, and wind speed.

3.3.2 Configuration of Retrievals

To avoid “hard-wiring" specific values into the operational software, a retrieval configuration file can be adopted. The file would store numerical values of adjustable parameters used within the retrievals, such as the thresholds establishing whether a successful retrieval occurs.

3.3.3 Quality Assessment and Diagnostics

We will introduce a quality assurance (QA) flag for VIIRS aerosol products over land and ocean to reflect the quality of aerosol parameters retrieved by our algorithms. The QA flag

will be stored at the same HCS as the as the output of the aerosol optical thickness and aerosol particle size parameter retrievals.

TABLE 12. VIIRS AOT AND APSP EDR QUALITY FLAGS

Byte	VIIRS AOT and APSP EDR Quality Flag	Result	Bits
0	AOT Product Quality	11 = High 10 = Medium 01 = Low 00 = Not retrieved	2
	APSP Product Quality	11 = High 10 = Medium 01 = Low 00 = Not retrieved	2
	Land / Ocean / Not Produced	11 = Not Produced 01 = Ocean 00 = Land	2
	AOT Out of Spec Range	1 = Yes 0 = No	1
	APSP Out of Spec Range	1 = Yes 0 = No	1
1	Cloud Contamination in Cell	1 = Yes 0 = No	1
	Cloud Adjacent to Cell	1 = Yes 0 = No	1
	Cirrus Contamination in Cell	1 = Yes 0 = No	1
	Bad SDR	1 = Yes 0 = No	1
	Sun Glint in Cell	1 = Yes 0 = No	1
	Cloud Shadow in Cell	1 = Yes 0 = No	1
	Snow / Ice in Cell	1 = Yes 0 = No	1

Byte	VIIRS AOT and APSP EDR Quality Flag	Result	Bits
	Fire Detected in Cell	1 = Yes 0 = No	1
2	Low Sun, Degraded, 80 > SZA > 65	1 = Yes 0 = No	1
	Low Sun, Excluded, SZA > 80	1 = Yes 0 = No	1
	Bright Surface in Cell (Land) / Shallow or Turbid Water in Cell (Ocean)	1 = Yes 0 = No	1
	Excluded, Angstrom Exponent for AOT at 550 nm < 0.15	1 = Yes 0 = No	1
	Spare Bit		1
	Spare Bit		1
	Spare Bit		1
	Spare Bit		1

Byte	VIIRS AOT and APSP EDR Quality Flag	Result	Bits
3 (Land)	Land Aerosol Model Index	101 = Urban, Polluted 100 = Urban, Clean 011 = Smoke, Low Absorption 010 = Smoke, High Absorption 001 = Dust	3
	Spare Bit		1
	Spare Bit		1
	Spare Bit		1
	Spare Bit		1
	Spare Bit		1
3 (Ocean)	Small Mode Model	11 = Fine Mode 4 10 = Fine Mode 3 01 = Fine Mode 2 00 = Fine Mode 1	2
	Large Mode Model	100 = Coarse Mode 5 011 = Coarse Mode 4 010 = Coarse Mode 3 001 = Coarse Mode 2 000 = Coarse Mode 1	3
	Spare Bit		1
	Spare Bit		1
	Spare Bit		1
4 (Land)	Spare Bit		1
	Spare Bit		1
	Spare Bit		1
	Spare Bit		1
	Spare Bit		1
	Spare Bit		1
	Spare Bit		1
	Spare Bit		1
4 (Ocean)	Small Mode Fraction	Valid range of 0-100	8

3.3.4 Exception Handling

Aerosol retrieval applicability is tested on the pixel level. If a pixel is found to be unusable or contaminated according to a certain test, the remaining tests are not performed and the pixel is discarded.

3.4 ALGORITHM VALIDATION

The following validation activities are suggested possibilities only. The NPOESS and NPP Calibration/Validation Plans should be consulted for specific validation activities.

3.4.1 Pre-Launch Validation Studies

The pre-launch research algorithm may be verified using AVHRR, SeaWiFS, and simulated VIIRS data. Optical depths derived from 1993 AVHRR data were compared to AeroNet (see the next section for more on AeroNet) sun-photometer observations from the same time period over the eastern United States and Brazil. These results are illustrated in Figures 25 and 26. These preliminary results indicate good agreement, but more studies with larger samples are required to demonstrate that the goals of the measurement accuracy are being met.

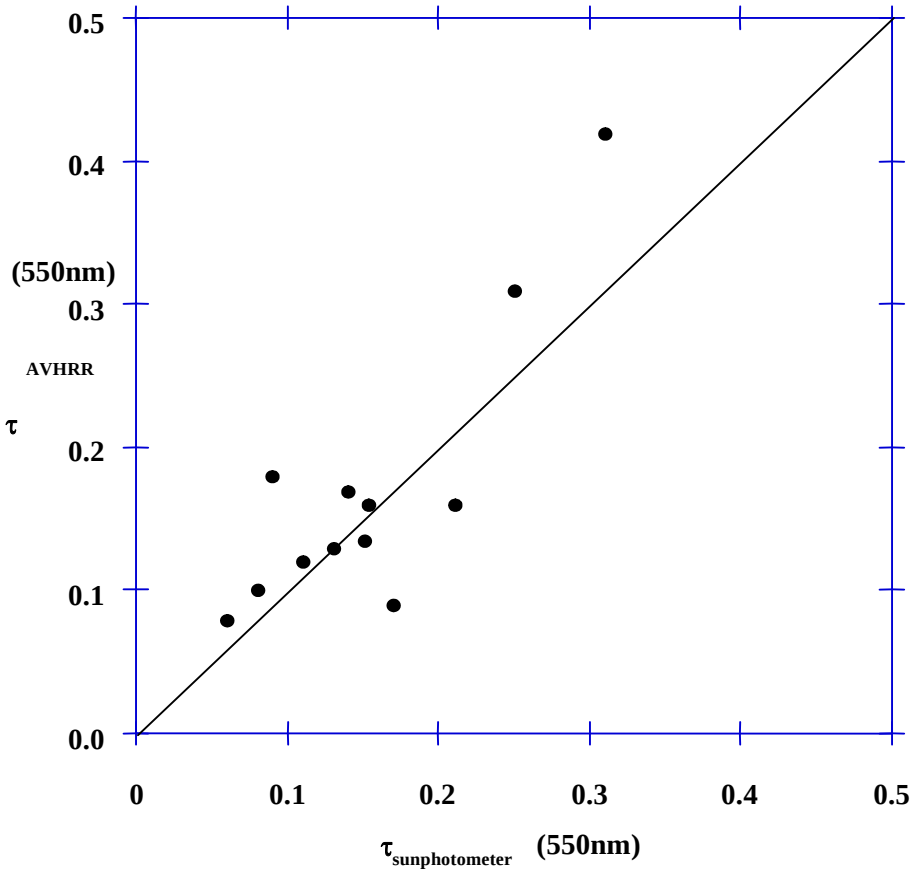

FIGURE 25. COMPARISON OF RETRIEVED OPTICAL DEPTH USING AVHRR DATA AND THE DARK TARGET APPROACH WITH MEASURED OPTICAL DEPTH FROM AERONET IN AUGUST 1993 OVER THE EASTERN UNITED STATES.

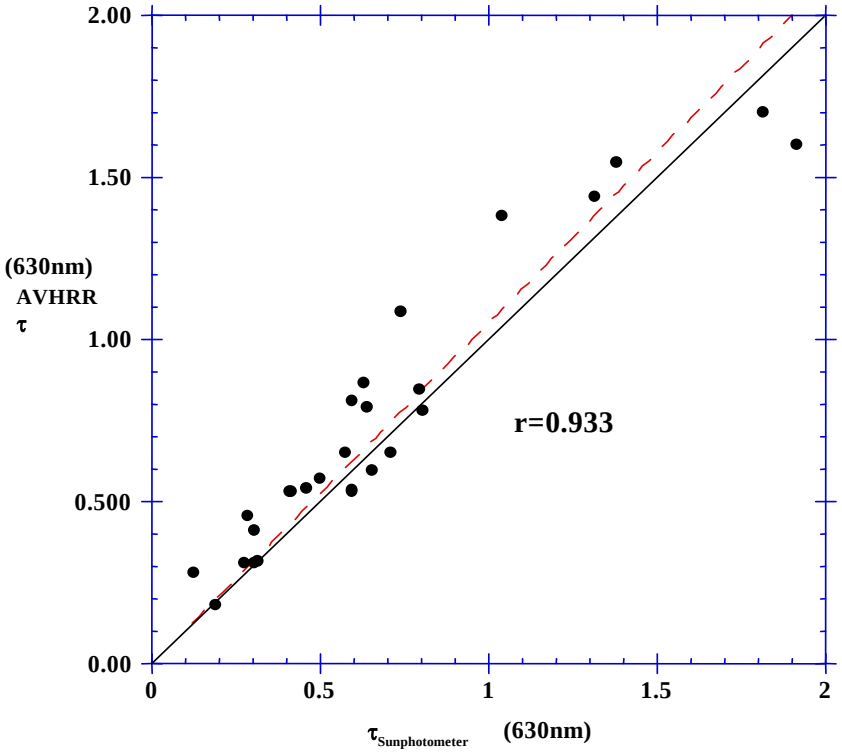

FIGURE 26. COMPARISON OF RETRIEVED OPTICAL DEPTH USING AVHRR DATA AND THE DARK TARGET APPROACH WITH MEASURED OPTICAL DEPTH FROM AERONET IN 1993 OVER BRAZIL.

MODIS Data collected from April 24, 2000 to May 23, 2000 were used to test the aerosol retrieval over land. First, the aerosol optical thickness was derived and the values screened for cloud contaminated cases and unacceptably high spatial variability. The remaining data set was compared to the Level 1.5 (cloud screened) AeroNet data (Holben et al., 1998). Filtering was undertaken again based on temporal variability observed in the AeroNet data and time difference between AeroNet measurements and MODIS retrieval (±30 minutes). Figures 27 and 28 show that the derived optical thickness compares extremely well with the measurements from AeroNet. The error bars on the Y axis represent the standard deviation of the MODIS retrieval. The two black lines are suggestive of the accuracy of the product +/-(□□□□□□□□□□□□□□which is actually much better than the accuracy predicted prior to launch +/-(0.05 + 0.2□□□□

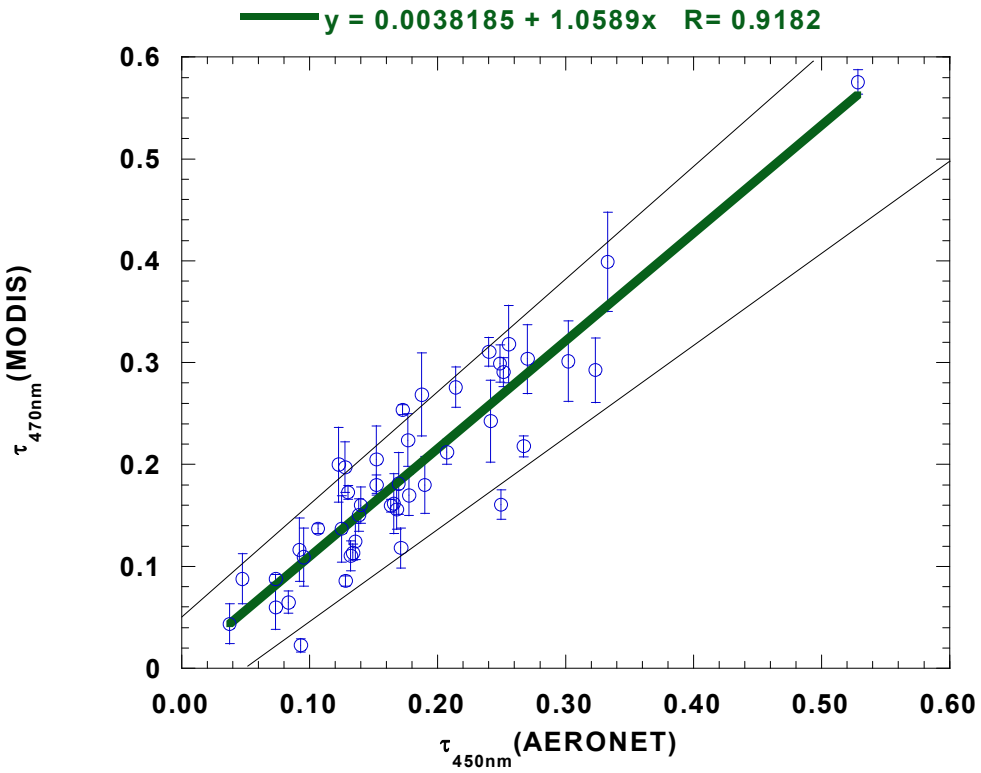

FIGURE 27. COMPARISON OF AEROSOL OPTICAL THICKNESS RETRIEVED BY MODIS BLUE CHANNEL WITH AERONET SUNPHOTOMETER MEASUREMENTS DURING THE APRIL,24,2000 TO JUNE,10,2000 PERIOD.

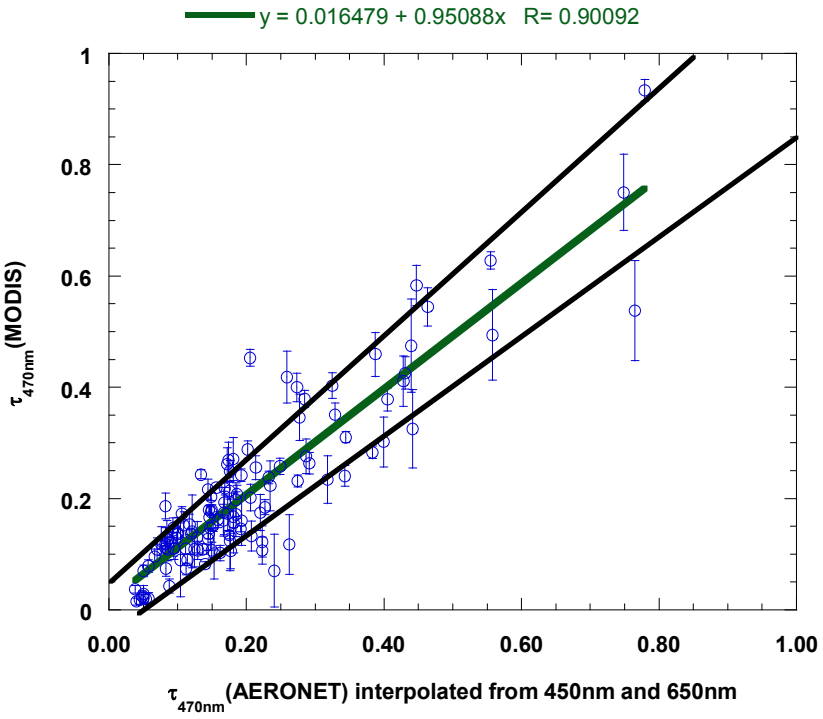

FIGURE 28. COMPARISON OF 1KM OPERATIONAL AEROSOL OPTICAL THICKNESS RETRIEVED BY MODIS BLUE CHANNEL (~120 MATCHES) WITH AERONET SUNPHOTOMETER MEASUREMENTS DURING THE MARCH, APRIL, MAY 2001 PERIOD.

3.4.2 Post-Launch Routine Ground-Based Observations

Post-launch routine ground-based observations can be made using AeroNet, the International Aerosol Lidar Network, and any of the several miscellaneous techniques, including the diffuse/direct method, aureole meters, and polarization measurements.

3.4.2.1 AeroNet

AeroNet (Aerosol Robotic Network) is a network of ground-based sun-photometers established and maintained by Brent Holben of Code 923 of the NASA Goddard Space Flight Center and Tom Eck of Raytheon ITSS. The sun-photometers measure the spectral aerosol optical thickness and sky radiance. Data is sent via a satellite communication link from each remotely located CIMEL sun-photometer to Goddard Space Flight Center from sunrise to sunset, 7 days a week. The data is analyzed to give aerosol optical depths at several wavelengths and is then placed on the Internet with a delay of a few days.

By comparing the AeroNet aerosol optical depths to the VIIRS aerosol optical depths, we can provide ground-truth observations to validate VIIRS. A large number of intercomparisons must be made to see if any systematic differences exist and if there are any trends in these differences. Because of the delay in the availability of the AeroNet observations, it is not anticipated that the validation studies will be part of the operational code; rather, they will be a separate, off-line study. These measurements are expected to be the primary method of validating the VIIRS observations.

3.4.2.2 International Aerosol Lidar Network

The International Aerosol Lidar Network is a confederation of lidar investigators who take tropospheric and stratospheric measurements. These measurements are particularly useful for tracking volcanic dust clouds. They also offer an opportunity to validate the VIIRS aerosol optical depths.

3.4.2.3 Miscellaneous techniques

A number of miscellaneous techniques can be used to derive aerosol optical depths. They include aureole meters, measurements of location of polarization neutral points, and the direct/diffuse method using pyrheliometers and pyranometers. Most of these observations are only made occasionally, but they may offer opportunities for intermittent comparison to the VIIRS aerosol optical thicknesses.

3.4.3 Post-Launch Special Field Experiments

Many of the present satellite observations are augmented by special field campaigns to provide ground-truth data for the satellite-derived measurements. Although the NPOESS project does not yet have formal plans for such experiments, it is anticipated that they will be required for calibration purposes. The VIIRS aerosol optical thickness and size distribution measurements could be validated using sun-photometer and lidar observations. Suspended matter determinations might be checked by Fourier transform interferometer measurements, *in situ* chemical analyses, and dustsondes. The details of these campaigns (timing, location, instrumentation, aircraft use, etc.) will not be determined solely by the aerosol validation requirements, so these experiments will not be further discussed here.

3.4.4 Post-Launch Satellite-Based Intercomparisons

VIIRS-derived aerosol optical depths may be validated by comparing them with aerosol optical depths derived by other satellite sensors, such as MODIS. It is not clear what sensors will be flying contemporaneously with VIIRS after the year 2008. The basic intercomparison technique involves four steps: 1) identification of locations where both

sensors fly over at nearly the same time; 2) extraction of data for storage in an intercomparison archive; 3) analysis of the differences between the measurements; and 4) communication of the results to the appropriate people so that proper corrective actions can be taken if needed. It is possible that the intercomparison procedure could be fully automated and put in the operational code, but it is more likely that it will involve human intervention and judgment to understand the results.

4.0 ASSUMPTIONS AND LIMITATIONS

4.1 ASSUMPTIONS

The following assumptions are made with respect to the aerosol retrievals described in this document:

(1) Aerosol particles are homogeneous spheres.
(2) A horizontally homogeneous atmosphere applies to each horizontal cell size of aerosol products.

4.2 LIMITATIONS

4.2.1 General

Limitations applying to our aerosol retrieval are:

(1) Retrievals will only be specified over regions with dark water or dark vegetation surfaces.
(2) Retrievals will be performed under clear conditions.
(3) Retrievals will only be specified for solar zenith angles less than 70^{o} (i.e., daytime).

4.2.2 Aerosol profile

A detailed analysis of the influence of the aerosol height can be provided over land and ocean. The height or aerosol profile versus molecules or gaseous absorbants is particularly critical when inverting information where substantial absorption by water vapor is present (e.g., AVHRR band 2). The aerosol profile is also critical when inverting signal in the ultra Violet portion of the spectrum (e.g., TOMS) in particular for absorbing aerosol.

For the VIIRS instrument, the band are well chose so the absorption of water vapor is minimal and the inversion over ocean rely on wavelengths equal or greater than 0.850 m, in that case the impact of the height of aerosol given the very weak molecular scattering is probably negligible.

Over land, a more detailed study may be required, but given the fact the shortest wavelength determining the optical depth is around 488nm (412nm and 445nm are used to refine the aerosol model) and that EDR's accuracy are much less constraining at this point we believe such a study does not constitute a high priority. We believe other factors related to surface effect are the most limiting for land aerosol at this point. Moreover, MODIS retrievals over Land using fixed height aerosol (2km), shows that the EDR could be obtained over land with fixed model at required accuracy.

5.0 REFERENCES

Born, M. and E. Wolf (1975). *Principles of Optics*, Fifth Edition, Pergamon Press.

Charlson, R. J., S. E. Schwartz, J. M. Hales, R. D. Cess, J. A. Coackley Jr., J. E. Hansen, and D. J. Hofman (1992). Climate forcing of anthropogenic aerosols. *Science*, 255, 423-430.

Cox, C., and W. Munk (1954). Statistics of the sea surface derived from sun glitter. *J. Mar. Res*., 13, 198-208.

Dubovik, O., B. N. Holben, T. F. Eck, A. Smirnov, Y. J. Kaufman, M. D. King, D. Tanré, and I. Slutsker, 2001, "Variability of absorption and optical properties of key aerosol types observed in worldwide locations", *J. Atmos. Sci.*, 59,590-608.

Eck, T. F., B. N. Holben, J. S. Reid, O. Dubovik, A. Smirnov, N. T. O'Neill, I. Slutsker, and S. Kinne, 1999. Wavelength dependence of the optical depth of biomass burning, urban, and desert dust aerosols. J. Geophys. Res., 104D, 31333-31349.

Ferrare, R. A., R. S. Fraser, and Y. J. Kaufman (1990). Satellite remote sensing of large-scale air pollution: Measurements of forest fires smoke, *J. Geophys. Res.*, 95, 9911-9925.

Geogdzhayev, I. V. and M. I. Mishchenko, 1999. Preliminary Aerosol Climatology for the Period of NOAA-9 Observations (http://gacp.giss.nasa.gov)

Griggs, M. (1975). Measurements of atmospheric aerosol optical thickness using ERTS-1 data, *J. Air pollut. Control Assoc.*, 25, 622-626.

Hansen, J. E., and A. A. Lacis (1990). Sun and dust versus greenhouse gases: An assessment of their relative roles in global climate change. *Nature*, 346, 713-719.

Holben, B.N., T.F. Eck, I. Slutsker, D. Tanré, J.P. Buis, A. Setzer, E.F. Vermote, J.A. Reagan, Y.J. Kaufman, T. Nakajima, F. Lavenue, I. Jankowiak, and A. Smirnov (1998). AeroNet – A federated instrument network and data archive for aerosol characterization, *Remote Sensing of the Environment,* 66:(1) 1-16.

Intergovernmental Panel on Climate Change (IPCC) (1994). Radiative Forcing of Climate Change. Edited by B. Bolin, J. Houghton, and L. G. M. Filho, UNEP, World Meteorol. Organ., Geneva.

Kaufman, Y. J., R. S. Fraser, and R. A. Ferrare (1990). Satellite measurements of large-scale air pollution methods, *J. Geophys. Res.*, 95, 9895-9909.

Kaufman, Y. J., and D. Tanré (1996). Algorithm for Remote Sensing of Troposheric Aerosol from MODIS, *http://eospso.gsfc.nasa.gov/atbd/modistables.html.*

Kaufman, Y. J., D. Tanré, L. A. Remer, E. F. Vermote, A. Chu, and B. N. Holben (1997). Operational remote sensing of tropospheric aerosol over land from EOS moderate resolution imaging spectroradiometer. *J. Geophys. Res*., 102, 16971-16988.

Kaufman, Y. J., A. E. Wald, L. A. Remer, B. Gao, R. Li, and L. Flynn (1997). The MODIS 2.1-μm Channel-Correlation With Visible Reflectance for Use in Remote Sensing of Aerosol*. IEEE Trans. on Geoscience and Remote Sensing*, 35, 1286-1298.

King, M. D., D. M. Byrne, B. M. Herman, and J. A. Reagan (1978). Aerosol size distribution obtained by inversion of optical depth measurements. *J. Atmos. Sci.*, 35, 2153-2167.

Koepke, P. (1984). Effective reflectance of oceanic whitecaps, *Appl. Opt.*, 23, 1816-1823.

Mishchenko, M. I., A. A. Lacis, B. E. Carlson, and L. D. Travis (1995). Nonsphericity of dust-like tropospheric aerosols: Implications for aerosol remote sensing and climate modeling, *Geophys. Res. Letters*, 22, 1077-1080.

Li, R. R., Y. J. Kaufman, B. C. Gao, and C. O. Davis (2003). Remote Sensing of Suspended Sediments and Shallow Coastal Waters, *IEEE Trans. Geosci. Remote Sens.,* 41, 559-566.

Petitcollin F. and Vermote E. F. 2001, Land surface reflectance, emissivity and temperature from MODIS middle and thermal infrared data., accepted in R.S.E.

Remer, L.A. and Y.J. Kaufman, 1998, Dynamic aerosol model: Urban/Industrial aerosol, *Journal of Geophysical Research*, 102, 16849-16859.

Roger J.C and Vermote E. F., 1998, A method to Retrieve the Reflectivity Signature at 3.75μm from AVHRR data, *Remote Sensing of the Environment*, 64:103-114.

Stowe, L. L., A. M. Ignatov, and R. R. Singh (1997). Development, validation, and potential enhancements to the second-generation operational aerosol product at the National Environmental Satellite, Data, and Information Service of the National Oceanic and Atmospheric Administration, *J. Geophys. Res.*, 102, 16,923-16,934.

Tanré, D., M. Herman, and Y. J. Kaufman (1996). Information on aerosol size distribution contained in solar reflected spectral radiances. *J. Geophys. Res*., 101, 19,043-19,060.

Vermote, E., D. Tanré, J.L. Deuzé, M. Herman, and J.J. Morcette, 1997. *6S User Guide* Version 2.

Vermote, E., D. Tanré, J.L. Deuzé, M. Herman, and J.J. Morcette, 1997. *Second Simulation of the Satellite Signal in the Solar Spectrum, 6S: An Overview, IEEE, Trans. On Geo. Remote Sensing, VOL 35, 1997*.

Wen, G., S. Tsay, R. F. Cahalan, and L. Oreopoulos, 1999. Path radiance technique for retrieving aerosol optical thickness over land. *J. Geophys. Res.*, 104D, 31321-31332.